Effect of stress on protein homeostasis mediated by FKBP51 as a possible mechanism underlying stress-related disorders

Dissertation der Fakultät für Biologie
der Ludwig-Maximilians-Universität München

Silvia Martinelli
München, 2019

MAX-PLANCK-INSTITUT
FÜR PSYCHIATRIE

IMPRS
From Biological Structures
to Neural Circuits

Diese Dissertation wurde angefertigt
unter der Leitung von Dr. Elisabeth B. Binder
im Bereich von dem Max Planck Institut für Psychiatrie
an der Ludwig-Maximilians-Universität München

Erstgutachter: PD Dr. Mathias Schmidt
Zweitgutachterin: Prof. Dr. Angelika Böttger

Tag der Abgabe: 25.06.2019
Tag der mündlichen Prüfung: 03.12.2019

Eidesstattliche Erklärung

Ich versichere hiermit an Eides statt, dass die vorgelegte Dissertation von mir selbständig und ohne unerlaubte Hilfe angefertigt ist.

München, den 14.06.2019 Silvia Martinelli

(Unterschrift)

Erklärung

Hiermit erkläre ich, *

☒ dass die Dissertation nicht ganz oder in wesentlichen Teilen einer anderen Prüfungskommission vorgelegt worden ist.

☒ dass ich mich anderweitig einer Doktorprüfung ohne Erfolg **nicht** unterzogen habe.

☐ ~~dass ich mich mit Erfolg der Doktorprüfung im Hauptfach .....~~

~~und in den Nebenfächern .....~~

~~bei der Fakultät für ..... der .....~~

(Hochschule/Universität)

unterzogen habe.

☐ ~~dass ich ohne Erfolg versucht habe, eine Dissertation einzureichen oder mich der Doktorprüfung zu unterziehen.~~

München, den 14.06.2019 Silvia Martinelli

(Unterschrift)

*) Nichtzutreffendes streichen

Table of Contents

Abstract

Homeostasis is a dynamic equilibrium fundamental for a healthy system. A major challenge to homeostasis is environmental stress to which the organism reacts with the stress response. The hypothalamic-pituitary-adrenal (HPA) axis is the main regulator of the stress response that, upon activation, leads to the release of glucocorticoids (GCs). GCs are steroid hormones that exert their function via glucocorticoid receptors (GR). They trigger on one hand the appropriate stress response in the periphery, and, on the other, inhibit the HPA axis itself via negative feedback to restore homeostasis. FK506-binding protein 51 (FKBP51) is a co-chaperone able to modulate the GR, and therefore the HPA axis. Furthermore the expression of *FKBP5*, the gene coding for FKBP51, is induced by GR activation. In the last decade, increasing evidence has unveiled additional roles of FKBP51 in the regulation of several cellular pathways and functions that are independent from its inhibitory role on GR. Among these, FKBP51 has been shown to link stress signaling to macroautophagy, a lytic type of autophagy pathway. Autophagy represents one of the main mechanisms regulating cellular homeostasis and response to stress. For this reason, in the first part of this doctoral thesis, the role of GR-mediated stress was investigated on two further autophagic pathways: 1) the chaperone-mediated autophagy (CMA), a selective type of lytic autophagy, and 2) the secretory autophagy, an unconventional secretory mechanism regulated by autophagy-related proteins and found to be involved in extracellular signaling of immune response. For this aim, an *in vitro* approach was adopted using human and murine cell lines that were treated with dexamethasone (Dex), a synthetic GR agonist.

For the first pathway, biochemical assays indicated that Dex-induced GR activation enhances CMA-mediated degradation of known CMA target proteins and that this process is dependent on FKBP51. Furthermore, the underlying molecular mechanism could be revealed by co-immunoprecipitation that displayed the co-localization of FKBP51, AKT and PHLPP on lysosomes. With a SILAC-based proteomics analysis, the proteome-wide effect of Dex-induced CMA could be observed and novel CMA targets were identified.

For the second pathway, interactome and co-immunoprecipitation analyses revealed the involvement of FKBP51 in the SNARE complex assembly essential for secretory autophagy. Furthermore, treatment with Dex lead to a strengthened interaction between the SNARE proteins and FKBP51, and to an increased secretion of IL1B, a well characterized cargo of

secretory autophagy, as observed with *in vitro* ELISA experiments and *in vivo* hippocampal microdialyses. A global effect of Dex-induced secretory autophagy was finally observed with a secretome analysis.

The second part of my doctoral thesis focused on *FKBP5*/51 transcription variants and protein isoforms. In fact, despite its involvement in many cellular functions and disorders, very little is known about its four transcription variants and two isoforms. Thus, expression and degradation dynamics of FKBP51 isoforms and their differential functions in known molecular pathways were analyzed.

Overall this study highlighted FKBP51 as crucial mediator of the stress response on two autophagic pathways, which might contribute to the regulation of cell and protein homeostasis. Furthermore, this regulatory mechanism might underlie the link of stress to immune and psychiatric disorders.

Zusammenfassung

Homöostase, die Aufrechterhaltung physiologischer Funktionen in einem dynamischen Gleichgewicht, ist Voraussetzung für ein gesundes biologisches System. Eine große Herausforderung für die Homöostase ist Umweltstress. Der Organismus reagiert mit einer Stressreaktion. Hauptregulator der Stressreaktion ist die Hypothalamus-Hypophysen-Nebennieren (HPA) -Achse, die bei Aktivierung zur Freisetzung von Steroidhormonen, den Glukokortikoiden (GCs) führt. Glukokortikoide aktivieren Glukokortikoidrezeptoren (GRs), die einerseits die angemessene Stressreaktion in der Peripherie auslösen und andererseits die HPA-Achse selbst durch negatives Feedback hemmen, um die Homöostase wiederherzustellen. Das FK506-binding protein 51 (FKBP51) ist ein Co-Chaperon, das den GR und damit die HPA-Achse modulieren kann. Darüber hinaus wird die Expression von FKBP5, dem für FKBP51 kodierenden Gen, durch GR-Aktivierung induziert. Zunehmende Erkenntnisse in den letzten zehn Jahren weisen auf weitere Rollen von FKBP51 bei der Regulation mehrerer zellulärer Signalwege und Funktionen, die unabhängig von seiner inhibitorischen Rolle auf den GR sind. So wurde zum Beispiel gezeigt, dass FKBP51 das Stresssignal auf Makroautophagie vermittelt. Makroautophagie stellt eine Form der Autophagie dar, einer der Hauptmechanismen zur Regulierung der zellulären Homöostase und der Reaktion auf Stress. Daher wurde im ersten Teil der vorliegenden Arbeit die Wirkung des GR-vermittelten Stresses durch FKBP51 auf zwei weitere Autophagie-Signalwege untersucht. 1. Auf die Chaperon-vermittelte Autophagie (CMA), eine selektive Art der lytischen Autophagie und 2. Auf die sekretorische Autophagie, einen unkonventionellen sekretorischen Mechanismus, der an der extrazellulären Signalübertragung der Immunantwort beteiligt ist. Es wurde ein in vitro-Ansatz mit menschlichen und murinen Zelllinien verwendet, die mit Dexamethason, einem synthetischen GR-Agonisten behandelt wurden.

Für den ersten Signalweg zeigten biochemische Assays, dass Dexamethason-induzierte GR-Aktivierung den CMA-vermittelten Abbau bekannter CMA-Zielproteine verstärkt und dass dieser Prozess durch FKBP51 vermittelt wird. Darüber hinaus konnte der zugrunde liegende molekulare Mechanismus durch Co-Immunopräzipitation aufgedeckt werden, die eine Co-Lokalisierung von FKBP51, AKT und PHLPP auf Lysosomen ergab. Mit einer SILAC-

basierten Proteomics-Analyse konnte der proteomweite Effekt von Dexamethason-induziertem CMA beobachtet und neuartige CMA-Ziele gefunden werden.

Für den zweiten Signalweg zeigten Interaktom- und Co-Immunpräzipitationsanalysen, dass FKBP51 an der SNARE-Komplexanordnung sowohl beteiligt, als auch Voraussetzung für dessen Bildung ist, die wiederum für die sekretorische Autophagie essentiell ist. Die Behandlung mit Dexamethason führte nicht nur zu einer verstärkten Wechselwirkung zwischen den SNARE-Proteinen und FKBP51, sondern auch zu einer erhöhten Sekretion von IL1B. Dies konnte anhand von ELISA-Experimenten in vitro und Mikrodialysen in vivo charakterisiert werden. Ein globaler Effekt der Dexamethason-induzierten sekretorischen Autophagie wurde schließlich mit einer Sekretomanalyse beobachtet.

Der zweite Teil meiner Doktorarbeit befasst sich mit FKBP51-Transkriptionsvarianten und Isoformen des Proteins. Obwohl es eines der am meisten untersuchten Gene im Bereich der Psychiatrie darstellt und an zahlreichen zellulären Funktionen beteiligt ist, ist nur wenig über seine vier Transkriptionsvarianten und zwei Isoformen bekannt. Daher wurden die Expressions- und Degradationsdynamik der Isoformen und ihre unterschiedlichen Funktionen auf FKBP51 regulierte Signalwege charakterisiert.

Insgesamt verdeutlicht die vorliegende Arbeit die entscheidende Rolle von FKBP51 als Mediator der GR-vermittelten Stressreaktion auf zwei Signalwege der Autophagie, die CMA und die sekretorische Autophagie, und damit möglicherweise dessen zentrale Bedeutung im Regulationsmechanismus der Proteinhomöostase bei der Stressreaktion. Weiterhin markieren diese Mechanismen mögliche molekulare Grundlagen von stressbedingten immunologischen und psychiatrischen Störungen.

1. Introduction

1.1. Homeostasis and stress

All living organisms strive to maintain homeostasis, a dynamic equilibrium fundamental for a healthy system. The concept of homeostasis was first defined by Walter Bradford Cannon in the beginning of the 19th century, who wrote: “the blood and other fluids surrounding cells constitute the internal environment with which occur direct exchanges of each cell, and this must always be kept with parameters suitable for cell function, regardless of changes that may be occurring in the external environment.” (Cannon, 1929). Such changes in the external environment can be real or potential threats defined as stressors, and the pursuit to maintain homeostasis as described by Cannon triggers a response, called stress response. In the last decades, research unraveled the complex mechanism regulating the stress response, starting by the definition of a stress system that comprises various brain structures. These structures integrate different stressors and activate appropriate stress responses that, through physiological and behavioral mechanisms, are able to restore homeostasis and promote adaptation (Joëls and Baram, 2009; de Kloet et al., 2005). Additionally, the concept of homeostasis itself has evolved into allostasis, allostatic load and allostatic overload, to define more precisely the “equilibrium” needed in different circumstances. Homeostasis is hence set at different points in dependence of the stress load (Dallman, 2003). Upon perception of a stressor, the stress hormone system is activated. It involves different structures of the central nervous system (CNS) that communicate within the CNS and to the periphery. Two phases of the stress response can be distinguished: an initial immediate and fast systemic response carried out by the sympathetic adrenomedullar system (SAM) that leads to an activation of short-lasting responses such as increased alertness, vigilance and appraisal, typical of the “fight-or-flight” response (Cannon, 1915), and a slower hormonal response. This slower mechanism involves the hypothalamic pituitary adrenal (HPA) axis and results in the release of glucocorticoids (GCs), which cause an amplified and protracted long-lasting response. In this work I will focus on this latter stress response mediated by the HPA axis, and, unless otherwise specified, I will define as stress every input that leads to activation of the GC receptors (GR; described further on).

1.1.1. The HPA axis

In the presence of a stressor, the HPA axis is activated. Brain regions receiving stimuli affecting homeostasis activate the initiators of the axis: the hypophysiotropic neurons, localized in the paraventricular nucleus (PVN) of the hypothalamus. These neurons synthesize and secrete the corticotropin-releasing hormone (CRH), the first neuromodulator and crucial regulator of the axis. Through the hypophyseal portal vessels, CRH is transported to the anterior pituitary gland. Here it binds to the CRH receptor 1 (CRHR1), stimulating the release of the adrenocorticotropic hormone (ACTH) out of the CNS into systemic circulation. The principal target of ACTH is the melanocortin type 2 receptor (MC2-R) on the adrenal cortex. The activation of these receptors promotes the synthesis of GCs, the end effector of the axis, and their release in the bloodstream (Simpson et al., 1988). The most abundant circulating GC hormone in humans is cortisol (CORT; corticosterone in mice). At basal levels, most of the circulating CORT (>90%) is bound to carrier proteins, in particular to corticosteroid binding globulin (CBG), to which it has the highest affinity. The bioavailability (unbound CORT) increases upon stress-induced increase of CORT levels, as the CBG buffer capacity reaches saturation. Its lipophilic nature allows CORT to pass the blood brain barrier (BBB) and cell membranes without needing further carriers, virtually reaching every cell in the body. Its activity, however, is exerted only in cells expressing specific nuclear receptors: the glucocorticoid- (GR) and the mineralocorticoid receptor (MR). MRs are occupied to a much greater extent than GR due to their 10 fold increased affinity to CORT (Reul and de Kloet, 1985), resulting in an almost saturation of the MR at basal levels of cortisol. On the contrary, GRs are significantly occupied only during an increase of CORT levels during peaks of the circadian cycle or with acute stress (Reul and de Kloet, 1985; Spencer et al., 1993), assuming a more dynamic role in the stress response. The differential function of the two GC receptors is also dependent on their distribution pattern within different tissues. In the brain, MRs are expressed predominantly in limbic areas such as hippocampus, lateral septum and central amygdala, while GR is ubiquitously expressed (Mifsud and Reul, 2018). Activation of MRs and GRs by GCs leads to the activation of an adaptive stress response that involves many diverse physiological processes including immune, cognitive and metabolic ones. These cause changes in physiology and behavior directed to counteract the stress stimulus. In addition to generating an adequate stress

response, activation of GRs induces a rapid repression of genes that encode for mediators of the HPA axis, such as CRH and ACTH (Russell et al., 2010; Watts, 2005). This negative feedback is a regulatory mechanism, crucial for terminating the stress response and restoring the correct homeostasis after the end of a threat (fig. I a). In fact, an imbalance between activation and inhibition of the stress response can lead to the development of pathological states. Disruption of normal HPA function, termed allostatic load, is a hallmark of somatic and neuropsychiatric diseases, such as metabolic dysfunction, major depression disorder (MDD), anxiety and posttraumatic stress disorder (PTSD) (Gotlib et al., 2008; de Kloet et al., 2006; Macfarlane et al., 2008; Pariante and Lightman, 2008; Rosmond, 2003; Shea et al., 2005). A mechanism that increases the risk for disrupting the HPA function and developing psychiatric disorders is the exposure to early life adversities. In fact, the stress response is shaped by genetics and environment; hence early life phases are particularly critical because the brain is more vulnerable to external stimuli. Early life adversities have been found to cause a long-term impact on the circuitry responsible for emotional and cognitive functions, and are found to be associated with increased vulnerability to develop psychiatric disorders later in life (Chrousos, 2009; Heim and Nemeroff, 2002; Juruena, 2014; Krugers et al., 2017; Lippmann et al., 2007; Lucassen et al., 2013; Lupien et al., 2009).

At the cellular level, in the absence of ligand, GR and MR are primarily localized in the cytoplasm in an inactive state as part of a multiprotein complex that includes the chaperone heat-shock protein 90 (HSP90) and a number of co-chaperones and molecules. The co-chaperones define the maturation state of the complex that determines the binding capability of the GR and MR. In the mature state, these nuclear receptors (GR and MR) are bound to HSP90 together with the co-chaperones Cyclophilin 40 (Cyp40), Protein Phosphatase 5 (PP5), FK506 binding protein 51 (FKBP51) and the co-chaperone molecule p23 (Sanchez, 2012). However, upon binding of CORT, FKBP51 is replaced by its closest homologue FKBP52. FKBP52, unlike FKBP51, promotes nuclear receptors translocation into the nucleus through binding to the dynamitin subunit of the dynactin transport machinery (Galigniana et al., 2004; Harrell et al., 2004; Wochnik et al., 2005). This switch allows the translocation of GR and MR into the nucleus where they homo- and heterodimerize and bind to a palindromic 15 DNA base pair consensus sequence, known as GC response element (GRE), enhancing or repressing the transcription of numerous GC-responsive genes (Mifsud and Reul, 2016; Nicolaides et al., 2014). FKBP51 and FKBP52 exert, therefore,

respectively an inhibiting and activating function on the GR and MR. Interestingly, the gene coding for FKBP51, FKBP5, is one of the GC-responsive genes, whose expression is enhanced upon GR and MR activation (Jääskeläinen et al., 2011). This regulation results in an ultra-short negative feedback on the receptors at the cellular level, and, by extension, on the HPA axis (Denny et al., 2000; Zannas and Binder, 2014). Given the different dynamics of GR and MR, in this work I will only focus on the GR, assuming a lesser impact of the MR in the analyzed processes.

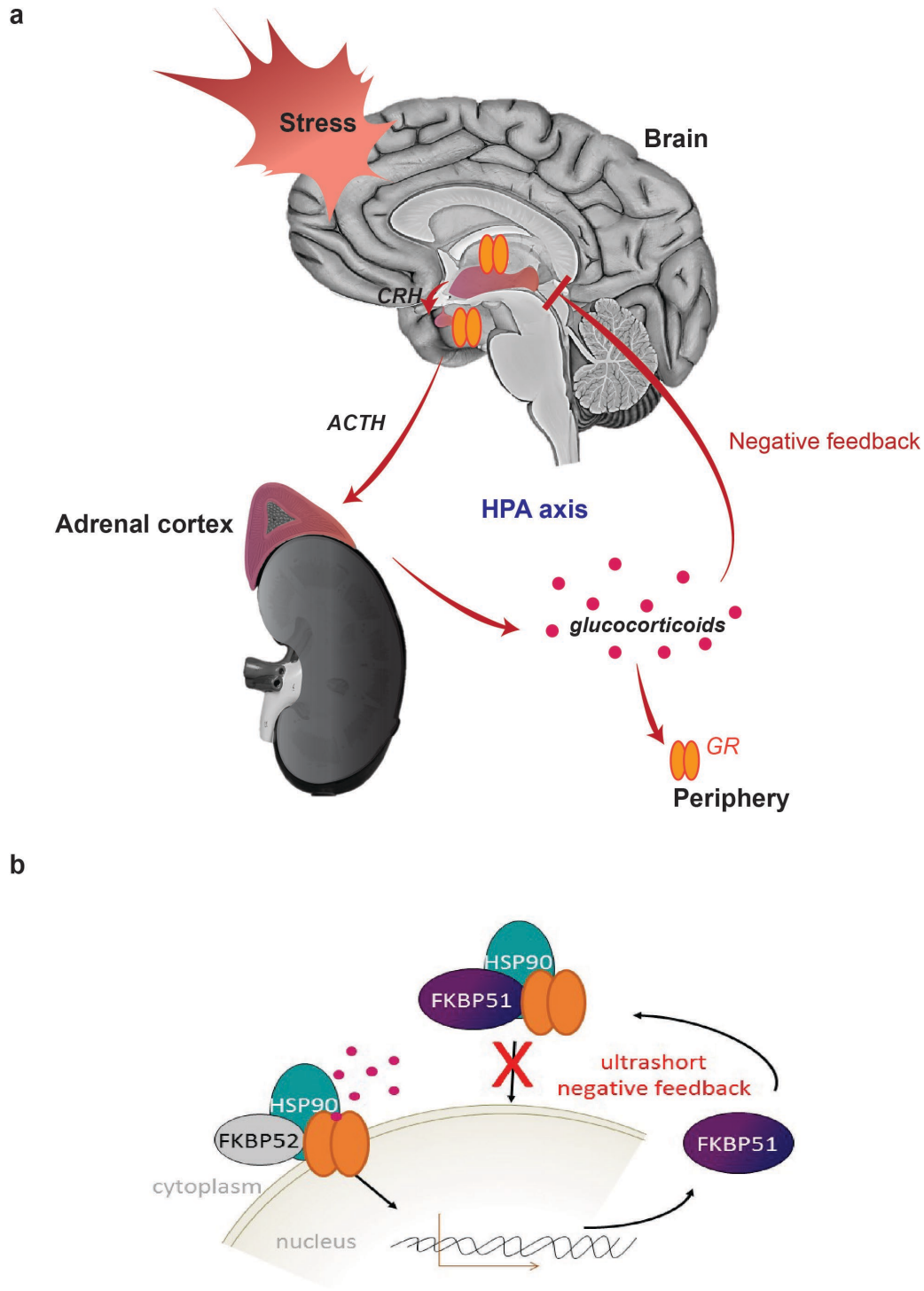

Figure I – Regulation of stress response. **a)** HPA axis: an environmental stressor perceived by different brain structures stimulates hypophysiotropic neurons in the PVN leading to the secretion of CRH into the hypophyseal portal vessels. These transport CRH to its receptor in the pituitary gland where secretion of ACTH is triggered. ACTH exits the CNS and binds MC2-R on the adrenal cortex, leading to the secretion of GCs. GCs bind to GRs and MRs triggering, on one hand, a stress response in the periphery, and on the other exerting a negative feedback of the HPA axis itself. **b)** At the cellular level, inactive GR is part of a multi-protein complex including HSP90 and FKBP51, localized in the cytoplasm. Upon CORT binding, FKBP51 is replaced by FKBP52 that allows translocation into the nucleus and activation of its transcription function. Among the genes regulated by GR is *FKBP5* itself, which expression is increased, leading to an ultra-short negative feedback of GR activity.

1.2. FKBP51: a co-chaperone for stress modulation

FKBP51 is an immunophilin, member of the FK506 binding proteins (FKBPs) (Schreiber, 1991; Trandinh et al., 1992). At least 15 FKBPs have been identified in humans and the suffix designates the approximate molecular mass of these proteins (Somarelli et al., 2008) that are ubiquitously found in almost all organisms and subcellular compartments (Romano et al., 2011). FKBP51´s inhibitory effect on GR was initially discovered in New World monkeys, which have very high circulating GC levels but do not present any associated symptomatology that would occur for example in humans. The explanation to this was given by the concurrent inherently high levels of FKBP51 that confer GR resistance (Scammell et al., 2001). As mentioned before, the gene coding for FKBP51, *FKBP5*, is regulated by GR itself, leading to an ultra-short negative feedback of the GR and, by extension, of the HPA axis (fig. I b). As a modulator of the stress response, it appears clear that a correct regulation of *FKBP5* expression levels are of crucial importance.

1.2.1. Genetic and epigenetic regulatory mechanisms

The transcription of *FKBP5* is mediated via GREs that are distributed in the regions from upstream of the promoter to introns 2, 5 and 7 of the gene (Paakinaho et al., 2010). GRs binding to GREs allow the formation of three-dimensional (3D) chromatin loops connecting the transcription start site (TSS) and RNA polymerase II (Jääskeläinen et al., 2011). In this way, GCs can affect *FKBP5*'s transcription; gene expression is enhanced compared to the basal state (Klengel et al., 2013). At the genetic level, Binder and colleagues discovered an association of the intronic single nucleotide polymorphism (SNP) of *FKBP5*, rs1360780, with increased intracellular FKBP51 protein levels. This association was also paralleled with increased response to antidepressants and recurrence of depressive episodes. Furthermore, only within the TT genotype population, *FKBP5* mRNA levels had a significant direct correlation with plasma cortisol levels of the individuals (Binder et al., 2004). The rs1360780 polymorphism is part of a haplotype, commonly tagged by rs3800373, rs9296158, or rs1360780, that spans the entire gene and contains up to 18 SNPs in strong linkage disequilibrium in Caucasians. Different studies found this haplotype to be associated with increased *FKBP5* expression and increased vulnerability to stress-related psychiatric disorders (Binder et al., 2008; de Castro-Catala et al., 2017; Zannas et al., 2016). Klengel *et*

al. deciphered the underlying mechanism linking the polymorphism to *FKBP5* expression. They showed that the previously described 3D chromatin loop is allele-dependent. In fact, the sequence containing the T allele forms a TATA box with stronger binding affinity to the TATA box binding protein (TBP), compared to the C containing genotype, as revealed by chromatin immunoprecipitation experiments (ChIP) (Klengel et al., 2013). Polymorphisms can also be a variable in genetically intrinsic patterns of epigenetic modifications both indirectly, by influencing the effect of the environment on methylation marks, and directly, by disrupting CpG sequences recognized by methyltransferases. For this reason, Klengel and colleagues further investigated epigenetic changes of *FKBP5* in correlation to its expression levels. CpG sites located in the proximity of the functional GRE in intron 7 of *FKBP5* were analyzed via pyroseqeuncing in bisulfite-treated genomic DNA extracted from peripheral blood cells. Demethylation was observed in association with exposure to childhood abuse, in rs1360780 T allele carriers (both homo- and heterozygous), but not in individuals with the alternate genotype. Furthermore, previous *in vivo* experiments showing DNA demethylation of *Fkbp5* in the murine hippocampus, hypothalamus, and peripheral blood after systemic exposure to GCs (Lee et al., 2010) support that demethylation in humans with early trauma is driven by GR activation. Therefore, environmentally induced DNA methylation changes interact with *FKBP5* polymorphisms resulting in altered expression. Furthermore, *FKBP5* expression can also be altered by environmentally-induced histone modifications. GR activation has been found to increase histone H3 acetylation and histone H3-lysine 4 trimethylation in the *FKBP5* gene, enhancing its expression (Paakinaho et al., 2010). Despite robust findings indicating that GR activation leads to *FKBP5* disinhibition and demethylation, numerous studies demonstrate that this regulation is dependent on the species and the developmental stage. Methylation analyses performed in a human fetal hippocampal progenitor cell line stimulated with a synthetic GR agonist dexamethasone (Dex) revealed that only when cells were treated in their proliferation and differentiation phase, and not once the cells had differentiated, *FKBP5* methylation levels were decreased, supporting the evidence that regulation of epigenetic changes is specific to developmental stages. The same study showed, furthermore, that these demethylations were stable after differentiation even if the exposure to GC was terminated (Klengel et al., 2013). However, this lasting effect was not seen in a different study conducted by Lee et al., where *Fkbp5*

demethylations observed in different mouse tissues were not maintained upon withdrawal of GR agonists (Lee et al., 2010), suggesting a species-specificity.

Overall these studies provide evidence that *FKBP5* expression is regulated by both genetic and epigenetic mechanisms and that an increased *FKBP5* expression is associated with a more dynamic phenotype (increased susceptibility, but also increased response to antidepressant; Binder et al. 2004), dependent on the developmental stage and the species.

1.2.2. *FKBP5* disinhibition and dysregulation of the stress response

As a modulator of the stress axis, dysregulation of *FKBP5* expression has potentially analogous effects to dysregulation of the axis itself. In fact, numerous studies have shown correlations between *FKBP5* genotype and altered neuroendocrine endophenotypes. The rs1360780 haplotype was found to be correlated with suppressed negative feedback of the stress axis accompanied by prolonged cortisol release (Ising et al., 2008). Furthermore, increased cortisol levels were found in T-allele carriers after Trier social stress test (TSST) in correlation with childhood trauma exposure, indicating long-term alterations of neuroendocrine regulation associated with *FKBP5* genotype (Buchmann et al., 2014). Genetic and epigenetic characteristics leading to an increased expression of *FKBP5* have also been linked to both psychiatric and somatic disorders.

Psychiatric disorders

Its central role in the regulation of the stress axis makes *FKBP5* the perfect candidate for mediating gene-environment interactions underlying mood and anxiety disorders. Klengel and colleagues identified the mechanism underlying the correlation between *FKBP5* polymorphisms and its expression levels connected to modulation of the GR response and regulation of the stress axis (Klengel et al., 2013). Furthermore, these findings suggest that an impaired return to baseline of stress-induced cortisol levels is the basis of an increased vulnerability to develop stress-related psychiatric disorders. To date, the strongest association so far has been found via clinical studies between *FKBP5* disinhibition and PTSD. The presence of the T genotype in the rs1360780 polymorphism is predictive of PTSD development after childhood trauma (Binder et al., 2008). A recent meta-analysis corroborated this association by finding a significant genetic effect of the rs1360780 haplotype in interaction with trauma exposure on the development of PTSD (Hawn et al., 2019). A different study analyzing the *FKBP5* SNP rs9296158 found that PTSD patients

carrying the T allele showed GR super-sensitivity, while hypocortisolism was observed in patients with the CC genotype (Mehta et al., 2011). In line with these findings, enhanced GR sensitivity was also found in whole blood from PTSD patients in correlation with decreased *FKBP5* levels (Yehuda et al., 2009). It was also suggested that *FKBP5* affects over-consolidation or impaired extinction of traumatic memories, both characteristics of PTSD (Binder, 2009; Gillespie and Ressler, 2005; Pitman and Delahanty, 2005; Rothbaum and Davis, 2003). Also, *post mortem* studies revealed enhanced *FKBP5* expression in cortical regions of PTSD patients compared to healthy controls (Young et al., 2015). *FKBP5* haplotypes have furthermore been associated with mood disorders such as depression (Binder et al., 2004; Höhne et al., 2015) and bipolar disorder (BD) (Willour et al., 2009). These results were supported by *post mortem* brain analyses of cortical and hippocampal region samples, where increased *FKBP5* mRNA levels were found in subjects with MDD and BD (Chen et al., 2013; Darby et al., 2016; Mamdani et al., 2015; Sinclair et al., 2013; Tatro et al., 2009). This evidence, together with the data from PTSD subjects, suggests that elevated *FKBP5* expression in specific brain regions might contribute to psychiatric disorders (Matosin et al., 2018).

Somatic disorders

Disinhibition of *FKBP5* has also been found in correlation with non-psychiatric disorders such as Alzheimer´s disease both in *post mortem* (Braak and Braak, 1991) and animal studies (de Calignon et al., 2010, 2012; Lasagna-Reeves et al., 2012; SantaCruz et al., 2005). As mentioned previously, dysregulation of the stress axis has been associated with metabolic disorders. Indeed, type 2 diabetes, which is considered a stress-related pathophysiology, has been associated with the high induction *FKBP5* SNPs (Pereira et al., 2014) that also correlate with enhanced insulin resistance and elevated serum triglycerides (Fichna et al., 2018). Hyperexpression of FKBP51 has also been reported in different human cancers such as leukemias, gliomas, breast and prostate cancers, and is associated with apoptosis resistance and enhanced proliferation in gliomas (Romano et al., 2011).

1.2.3. FKBP51 as a drug target

Due to its involvement in several disorders, spanning from psychiatric diseases to cancer, FKBP51 has attracted interest from different scientific fields as a possible target for drug design. An important information deriving from animal studies is that *Fkbp5* knock out (KO)

mice are viable and do not present pathological alterations that would indicate a possible target-related toxicity for FKBP51 drugs (Schmidt et al., 2012). However, in order to evaluate the safety and efficacy of FKBP51 as a drug target, its overall expression pattern and functions need to be considered. From the literature, FKBP51 would be expected to have an effect on GR response, energy metabolism and chronic pain (Balsevich et al., 2017; Maiarù et al., 2016, 2018). *FKBP5*/51 is increasingly being recognized as biomarker for tumor progression and is therefore seen as possible target for therapy. A reduction of prostate cancer cell proliferation has already been shown as a consequence of FKBP51 inhibition with the immunosuppressive drug FK506 (Schmidt et al., 2012), and also rapamycin, another FKBP ligand, has been reported to have anti-tumor activity (Avellino et al., 2005; Romano et al., 2004).

From a technical point of view, the high similarity to other FKBPs has represented the major difficulty so far in the process of ligand design. The first molecule designs were based on the known inhibitors rapamycin and FK506; however, these drugs cross-reacted with other FKBPs and resulted mainly in an immunosuppressive effect. The search for an FKBP51-specific, non-immunosuppressive ligand faced a selectivity issue between the homologues FKBP51 and FKBP52 (Blackburn and Walkinshaw, 2011). In 2015 Gaali and colleagues developed a series of ligands with a 10'000-fold increased affinity for FKBP51 over FKBP52. These ligands are termed Selective Antagonist of FKBP51 by induced fit (SAFit), and include two main molecules: 1) SAFit1, with better solubility and slightly better off-target profile, preferred for in vitro studies, and 2) SAFit2, with much better pharmacokinetic properties and the current gold standard for *in vivo* studies (Gaali et al., 2015). To date, SAFit ligands are the most selective and effective ligands published, nevertheless further optimization is required to improve the physicochemical properties in order to be suitably used in the CNS (Wager et al., 2010). In fact, SAFit1 and SAFit2 present too high molecular weights (748 and 803 g/mol, compared to 426 g/mol for 90% of CNS drugs) and too low ligand efficiencies (LE = 0.21 and 0.19, compared to 0.37 for 90% of CNS drugs) (Gaali et al., 2016). Furthermore, in addition to optimizing the chemical and pharmacokinetic characteristics of the drug, increased knowledge on the target itself is necessary to develop an optimal drug. A deeper understanding of the numerous functions of FKBP51 are necessary in order to achieve a more precise targeting design.

1.2.4. Mechanistic studies

Given the central role of *FKBP5* in stress response and its correlation with diverse diseases, animal and *in vitro* approaches were used to deepen the understanding of FKBP51´s functions. A study by Scharf *et al*. in 2011 demonstrated a significant induction of *Fkbp5* by GCs in a brain region-specific manner (Scharf et al., 2011). The use of *Fkbp5* KO animals allowed to decipher numerous physiological and behavioral mechanisms. Despite *Fkbp5* KO mice not displaying major phenotypic differences (under basal conditions) compared to their wild type (WT) counterparts, Touma *et al*., observed significantly increased stress-coping behavior after exposure to acute stress (Touma et al., 2011). In line with these findings, Hartmann *et al*. reported prolonged swimming activity of *Fkbp5* KO mice compared to WT in the forced swim test, a paradigm to assess stress coping behavior, indicating a higher resilience to stress. Interestingly, the same study reported physiological differences between KO and WT mice, independently of the experimental condition (stressed vs. non-stressed), observing reduced thymus and adrenal gland weights as well as lower body weight in the KO mice. Furthermore, under chronic stress conditions, *Fkbp5* KO mice displayed significantly lower CORT levels compared to WT. These differences can be connected with the predicted higher GR activity, reduced HPA axis activity and increased negative feedback in the KOs compared to the WTs (Hartmann et al., 2012). Using tail suspension and forced swim test, O´Leary *et al*., found that *Fkbp5* KO mice displayed improved stress coping behavior, associated with significantly reduced CORT release compared to WT after stress (O'Leary et al., 2011). Analogously, using a different strategy, Attwood and colleagues, reported that prevention of *Fkbp5* upregulation, following stress exposure, decreased anxiety-related behavior (Attwood et al., 2011). These studies independently demonstrate a direct correlation of *Fkbp5* reduction with antidepressive-like and pro-resilience behaviors. Murine models also corroborated the role of *Fkbp5* in metabolic disorders. An upregulation of *Fkbp5* has been reported in mice both as consequence of a high fat diet (Balsevich et al., 2014), and after a 24h food deprivation period (Guarnieri et al., 2012). Furthermore, *Fkbp5* depletion was revealed to protect against high fat diet-induced weight gain and hepatic steatosis (Cho et al., 2001; Stechschulte et al., 2016). A more recent study showed that loss of Fkbp51 in mice markedly improves metabolism, in particular glucose tolerance in both control and high fat diet conditions (Balsevich et al., 2017).

At the cellular level, FKBP51 has been found to regulate a plethora of intracellular pathways that have been characterized by cellular and biochemical studies. In an HSP90 interactome study, Taipale and colleagues identified an unexpectedly vast and diverse repertoire of FKBP51 interactors. FKBP51 was found to bind to kinases, Argonaut proteins, transcription factors, and subunits of the minichromosome maintenance (MCM) protein complex (Taipale et al., 2014). Furthermore, several studies evidenced the role of FKBP51 in the regulation of numerous pathways involved in physiology and disease (Table 1). This growing body of evidence presents FKBP51 as a central hub of various cellular pathways, independently of its role in GR inhibition. These studies, together with the knowledge that FKBP51´s expression is enhanced by stress, make this protein a stress mediator, or "switch", for a plethora of cellular functions.

Pathway	Exerted effect	FKBP51 interactor	Related disease	Study
GC signalling	Inhibited GR activity via HSP90 interaction	HSP90	Stress-related disorders	(Sanchez, 2012)
Androgen signalling	Enhanced transcriptional activation of AR	HSP90	Prostate cancer, resistance to anti-cancer therapies	(Ni et al., 2010; Periyasamy et al., 2010)
Progesterone signalling	Inhibited PR (progesterone receptor) activity	HSP90		(Barent et al., 1998)
NFAT	Enhanced NFAT-regulated gene expression	CaN	inflammation	(Li et al., 2002)
NF-kB	Enhanced NF-kB-mediated transcription via inhibition of the NF-kB inhibitor IkB	IKK, TRAF2	Inflammation, cardiovascular diseases , cancer, resistance to anti-cancer therapies	(Bouwmeester et al., 2004; Romano et al., 2015a)
JAK/STAT	Induced apoptotic resistance to cytokine deprivation via STAT hyperactivation	Hypothesized JAK2	cancer	(Komura et al., 2003)
Rho-ROCK signaling	Enhanced cell motility and invasion of cancer cells via upregulation of RhoA activity and enhanced Rho-ROCK signaling.	DLC1, DLC2	cancer	(Takaoka et al., 2017)
CDK4	Stabilized CDK4 levels and kinase function	CDK4	cancer	(Jirawatnotai et al., 2014)
mTOR	Inhibited mTOR catalytic activity triggered by rapamycin	mTOR (in complex with rapamycin)	Cancer, autophagy	(Hausch et al., 2013)
Macroautophagy	Enhanced macroautophagy activation	AKT1, PHLPP, Beclin1		(Gassen et al., 2014)
GSK3B signalling	Increased effect of antidepressants and lithium via GSK3B inhibition	CDK5, GSK3B		(Gassen et al., 2016)
DNA methylation	Decreased DNA methylation via inhibition of DNMT1	DNMT1, CDK5		(Gassen et al., 2015a)
Microtubules polymerization	Enhanced microtubule polymerization via tau dephosphorylation	Tau, PP5	Alzheimers disease	(Jinwal et al., 2010)
AKT2-AS160 signaling	Dephosphorylated and consequently inactivated AKT2 and AS160	AKT2, AS160, PHLPP	Type 2 dyabetes	(Balsevich et al., 2017)
miRNA maturation	Enhanced AGO2 transcription and facilitade RISC assembly	AGO2		(Martinez et al., 2013)
store-operated calcium entry current (ISOC)	Inhibited ISOC via PP5-mediated dephosphorylation	PP5		(Hamilton et al., 2018)

Table 1 – Literature review of FKBP51-regulated cellular pathways. List of pathways that are regulated by FKBP51, the effects exerted by FKBP51 on each pathway, the main interactors of FKBP51 for each pathway, possible implications in disease and study reference.

1.2.5. Regulation of autophagy

A particularly interesting function in which FKBP51 exerts its "switch" role is macroautophagy, a cellular mechanism able to maintain homeostasis and manage stress responses. Autophagy, of which macroautophagy is a subtype, is an important quality control process in physiological and pathological states (Mizushima and Komatsu, 2011; Mizushima et al., 2008). It maintains energy and nutrient supplies during starvation or absence of growth factors (Galluzzi et al, 2014), prevents accumulation of protein aggregates, controls organelle quality and quantity in the cell, and has antimicrobial and other immune functions (Randow & Youle, 2014; Rubinsztein et al, 2015; Sica et al, 2015; Khaminets et al, 2016). The regulation of macroautophagy by FKBP51 can be considered an additional regulatory process of the stress-response at the cellular level. In the presence of a stressor (GR activation), *FKBP5* expression is increased and enhances macroautophagy activation via interaction with the kinase AKT and the macroautophagy initiatoir Beclin 1 (Gassen et al., 2015b), restoring cellular and protein homeostasis after stress. Besides macroautophagy, there are other autophagy pathways governed by autophagy-related (ATG) proteins, and they can be distinguished into two main types: 1) lytic autophagy: proteins, microbes and damaged organelles recycled and degraded to respectively maintain cellular homeostasis in accordance to energy availability and ensure cellular health and functionality; 2) secretory autophagy: the cytoplasmic cargo is secreted into the extracellular matrix either for signaling purposes or as a disposal mechanism. Recent studies suggest that secretory autophagy plays an important role in extracellular signaling of immune response (Cadwell et al., 2008; Ushio et al., 2011; Michaud et al., 2011; Deretic et al, 2013). Nevertheless, the exact mechanisms controlling secretory autophagy are still under investigation. Depending whether the selection of the material to be degraded is targeted or unspecific, lytic autophagy can be further subdivided into selective and non-selective. To the second one belong micro- and macro-autophagy. In microautophagy, the lysosomal membrane is invaginated and differentiated into the autophagic tube enclosing random portions of the cytosol for degradation (Li et al., 2012). Conversely, in macroautophagy, the first and most studied type of autophagy, non-selective substrates are first sequestered into double-membrane vesicles termed autopahgosomes. These are then fused with lysosomes, forming autolysosomes, where the content is degraded (Klionsky, 2005). However, macroautophagy

can also be highly specific in terms of type of engulfed organelle, resulting in selective organellophagy (mitophagy, ribophagy, etc.). This specificity is promoted by the initiating stimulus that causes a specific homeostatic perturbation, increasing the availability of distinct autophagic substrates, in opposition to a general stress stimulus that demands non-specific autophagic regulation (Okamoto, 2014). A more selective kind of autophagy is the chaperone-mediated autophagy (CMA). Here, only single proteins, recognized by a KFERQ or KFERQ-like motif in the amino acid sequence are targeted and transported to the lysosomal lumen by the heat shock-cognate chaperone 70 (HSC70) (Alfaro et al., 2019). Although each autophagic pathway has specific regulators, ATG proteins are a common denominator of all types of autophagy and their involvement defines autophagy as such. All these autophagic processes are activated in response to different stimuli and stressors, and represent a fundamental mechanism that not only maintains a correct proteostasis but also preserves the homeostasis of the whole organism. So far, only cellular stressors such as starvation and oxidative stress have been analyzed as trigger for most of these autophagic pathways. The evidence collected from the study by Gassen *et al*. shed some light on the link between environmental stress and autophagy, unveiling this as a possible mechanism regulating the stress response at the cellular level. The effect of GCs on other autophagic pathways, however, remains unknown.

1.2.6. Splicing variants and protein isoforms: the unexplored *FKBP5*

Despite being among the most investigated genes in psychiatric research, there remains a major lack of knowledge regarding the splicing variants and protein isoforms of *FKBP5*/51. To date, four transcription variants (variant 1-4) of the human *FKBP5* have been annotated, coding for two different isoforms (isoform 1 and 2) of the protein FKBP51. Thus far, only a few studies carried out by the lab of M.F. Romano at the University of Naples, Italy, have investigated isoform 2 in association to the development of melanoma and glioma (D'Arrigo et al., 2017; Romano et al., 2015b). A reason for the lack of distinction between the isoforms in the literature might be the fact that in mice, from which a large body of current knowledge on *FKBP5*/51 comes, only one isoform of FKBP51 is annotated. In humans, transcription variant 1 (ENST00000357266.8) differs in the 5' UTR from variants 2 (ENST00000536438.5) and 3

(ENST00000539068.5) and all three code for the 475 amino acid (aa) long isoform 1 (Q13451-1), while variant 4 (ENST00000542713.1) corresponds to a much shorter transcript and codes for the "truncated" isoform 2 (Q13451-2) of 268 aa (fig. II). Gene expression data (www.genesapiens.org) indicate that *FKBP5* is ubiquitously expressed with particularly high expression levels in bone marrow myeloid cells, muscle and adipose tissue. The little information available on the expression of the different transcription variants indicates that variant 4 is less expressed than variant 1, but slightly more than variants 2 and 3 in most of the human tissues. In the brain, the expression of variant 1 and 4 is the lowest among all the tissues, while variants 2 and 3 are undetectable (www.gtexportal.org). Therefore, we can assume that in all experiments conducted without distinguishing between the different variants, the overall expression levels mirror mainly the ones of variant 1.

At the protein level, FKBP51 isoform 1 has two N-terminal FK506-binding (FK) domains and three tetratricopeptide repeat (TPR) motifs at the C-terminus. Isoform 2 of FKBP51 coincides with isoform 1 for the first 222 aa, corresponding to the FK domains. The sequence ranging from aa 223 to its C-terminus (aa 268) is unique and, so far, uncharacterized. Missing the rest of isoform 1's C-terminal region, isoform 2, therefore, lacks the TPR motifs (fig. II b). The first FK domain, FK 1, is the binding site of the immunosuppressive drug FK506, from which the protein gets its name. FK1 also exerts a peptidyl-prolyl *cis-trans* isomerase (PPIase) or rotamase activity (Schiene and Fischer, 2000), characteristic of all immunophilins. The pocket in FK1 is also the binding site for another drug, rapamycin. This drug, in complex with FKBP51, exerts immunosuppressive and anticancer effects, mediated via the selective inhibition of the mechanistic target of rapamycin (mTOR) (Sabatini, 2006). Downstream, adjacent to FK1, is the second FK domain, FK2, that is presumably derived from a duplication event of the FK1 domain and shares 32% sequence homology with it (Cioffi et al., 2011), but lacks measurable rotamase activity (Sinars et al., 2003) and does not bind FK506. Instead, it might have cooperative functions with the TPR motifs (Sinars et al., 2003). The TPR motifs at the C-terminus promote protein-protein interactions (Russell et al., 1999), in particular with chaperone proteins such as HSP90 and heat shock protein 70 (HSP70) (Dornan and Walkinshaw, 2003). Furthermore, Li *et al*. showed that the TPR motifs are also responsible for the interaction with the serine-threonine phosphatase calcineurin (CaN). This phosphatase activates nuclear transcription

factors of activated T lymphocytes (NFAT), responsible for the expression of interleukin-2 (IL2) and several T cell specific activators, regulating thereby the clonal expansion of T cells after stimulation by an antigen (Li et al., 2002). These domain-dependent roles suggest differential functions for the two isoforms, whose investigation would be of particular interest due to the scarce literature regarding their distinctive roles.

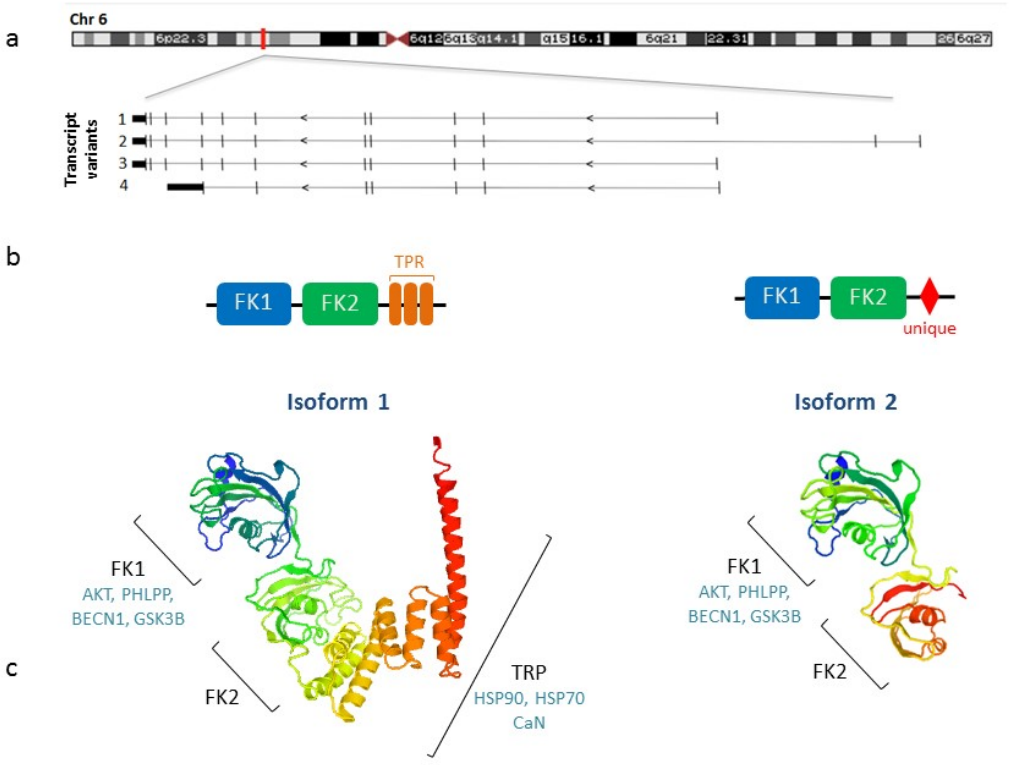

Figure II – FKBP51 splicing variants and isoforms. a) Schematic view of the *FKBP5* locus on human chromosome 6 and the four splicing variants of the gene. **b)** Schematic view of FKBP51 isoform 1 and 2 protein structures. **c)** 3D structure models generated with the swiss model repositoty server of the expasy portal (https://swissmodel.expasy.org/). Domains are indicated in black and experimentally validated domain-associated binding partners in blue.

2. Rationale and aims

The overarching aim of this work is to deepen the understanding of how FKBP51 modulates the effect of stress to trigger a cellular response able to promote and restore homeostasis.

In the first part of my work, I will investigate the regulatory role of FKBP51 in autophagy, as this is a cellular mechanism able to maintain homeostasis and manage stress responses. In particular I will focus on a selective type of autophagy, the chaperone-mediated autophagy, to understand the effect of stress on selective protein homeostasis (proteostasis), and on secretory autophagy, a non-lytic, autophagic mechanism that has been linked to immune response, but whose role is still unclear.

The second part of this work is dedicated to a better characterization of FKBP51. Despite being vastly investigated both at the genetic and protein level, there is a lack of knowledge regarding its splicing variants and isoforms. Given its vast involvement in the regulation of a plethora of cellular functions, a better understanding of possible differential roles of FKBP51 isoforms and their dynamics, might contribute not only to a deeper understanding of FKBP51's functions, but also enhance the possibility for a more precise targeted drug design.

3. Materials and Methods

3.1. Study design

To answer my research questions, different approaches were used. Most of the investigation was conducted *in vitro*, using different cell lines, accordingly to the aim of the experiment.

To assess the role of stress in chaperone-mediated autophagy (CMA), we used pulse chase assays that allowed us to quantify the net degradation of selected proteins excluding the new synthesis. The involvement of FKBP51 was determined with the use of CRISPR-Cas9-generated FKBP51 KO cells. Successively, the molecular interactions of the CMA-regulating complex was elucidated via lysosome extraction followed by immunoprecipitation (IP) of key proteins. A proteome wide effect of stress-triggered CMA was then assessed via pulse-SILAC mass spectrometry through which the extent of stress-triggered CMA could be analyzed and novel targets could be detected.

To investigate the possible role of FKBP51 in other and novel cellular pathways we analyzed its interactor partners. Spectrometry analysis, was used to find the novel interactor of FKBP51 Sec22b that led to the investigation of the role of FKBP51 in the secretory autophagy pathway. The regulatory complex of the pathway was further tested via IP. To examine the functional effect of stress and FKBP51 on secretory autophagy, different secreted target proteins were analyzed via ELISA and hippocampal microdyalisis *in vitro* and *in vivo* respectively. Lastly, the global effect of GC on secretory autophagy was observed and novel secreted proteins were detected via quantitative secretome analysis.

Given the plethora of functions of FKBP51, the need to a better characterization of the different isoforms led to a basal characterization in HeLa cells of Dex responsiveness of the different transcription variants via qPCR. Furthermore degradation dynamics of the two isoforms of FKBP51 was analyzed via pulse chase assay. FKBP51 KO cell model was generated via CRISPR-Cas9 to better analyze the role of the different isoforms. Differential intracellular localization of the two GFP-tagged FKBP51 isoforms was observed with epifluorescence microscopy. The differential role of the two isoforms in different pathways known to be regulated by FKBP51 was examined via WB analyses of downstream targets regulated by overexpression of the different isoforms.

3.2. Methods

3.2.1. Cell culture

The human cell lines HeLa and SY-SY5Y were cultured at 37°C, 6% CO2 in Dulbecco's Modified Eagle Medium (DMEM) high glucose with GlutaMAX (Thermo Fisher, 31331-028), supplemented with 10% fetal bovine serum (Thermo Fisher, 10270-106) and 1% antibiotic-antimycotic (Thermo Fisher, 15240-062).

The murine microglia cell line SIM-A9 was cultured at 37°C, 6% CO_2 in Dulbecco's Modified Eagle Medium (DMEM) high glucose with GlutaMAX (Thermo Fisher, 10566016), supplemented with 10% fetal bovine serum (Thermo Fisher, 10270-106), 5% horse serum (Thermo Fisher, 16050-122) and 1% antibiotic-antimycotic (Thermo Fisher, 15240-062).

3.2.2. Transfections

Jurkat cells (2×10^6; suspension cells), or with 1x trypsin-EDTA (gibco, 15400-054) detached HeLa, SH-SY5Y or SIM-A9 cells (2×10^6) were resuspended in 100 µl of transfection buffer [50 mM Hepes (pH 7.3), 90 mM NaCl, 5 mM KCl, and 0.15 mM $CaCl_2$]. Up to 2 µg of plasmid DNA was added to the cell suspension, and electroporation was carried out using the Amaxa 2B-Nucleofector system (Lonza). Cells were replated at a density of 105 cells/cm^2.

For the intracellular localization experiments, Hela cells were transfected with Lipofectamine 3000 transfection reagent (Thermo Fisher, L3000001) according to the supplier's protocol.

3.2.3. Western Blot Analysis

Protein extracts were obtained by lysing cells in 62.5 mM Tris, 2% SDS, and 10% sucrose, upplemented with protease (Sigma, P2714) and phosphatase (Roche, 04906837001) inhibitor cocktails. Samples were sonicated and heated at 95 °C for 5 min. Proteins were separated by SDS-PAGE and electro-transferred onto nitrocellulose membranes. Blots were placed in Tris-buffered saline solution supplemented with 0.05% Tween (Sigma, P2287) (TBS-T) and 5% non-fat milk for 1 hour at room temperature and then incubated with primary antibody (diluted in TBS-T) overnight at 4 °C. Subsequently, blots were washed and probed with the respective

horseradish-peroxidase- or fluorophore-conjugated secondary antibody for 1 hour at room temperature. The immuno-reactive bands were visualized either using ECL detection reagent (Millipore, WBKL0500) or directly by excitation of the respective fluorophore. Recording of the band intensities was performed with the ChemiDoc MP system from Bio-Rad.

3.2.3.1. Quantification of Protein Data

All protein data were normalized to Actin or GAPDH, which was detected on the same blot. In the case of AKT phosphorylation, the ratio of pAKTS473 to total AKT was calculated. Similarly, the direct ration of LC3BII over LC3BI is also provided, as well as the ratio over Actin.

3.2.4. Real time quantitative polymerase chain reaction (RT-qPCR)

Total RNA was isolated from HeLa cells with the RNeasy mini kit (Qiagen, 74104) following the manufacturer's protocols. Reverse transcription was performed using SuperScript II reverse transcriptase (Thermo Fisher, 18064014). Subsequently, the cDNA was amplified in triplicates with the LightCycler 480 Instrument II (Roche, Mannheim, Germany) using primers from IDT and TaqMan™ Fast Advanced Master Mix (Thermo Fisher, 4444964).

3.2.5. CRISPR-Cas9 KO generation

Generation of SIM-A9 *Atg5* KO cell line: using Lipofectamine 3000 transfection reagent (Thermo Fisher Scientific, L3000001), cells were transfected with CRISPR-Cas9 Atg5 plasmid. 48 hours after transfection 2 µg/ml of puromycin (InvivoGen, ant-pr-1) was added to the medium. After 36 hours the medium was changed and single clones were manually picked and replated in single wells for expansion. KO clones were selected via western blot analyses.

Generation of *FKBP5* KO HeLa cell line: using Lipofectamine 3000 transfection reagent (Thermo Fisher, L3000001), cells were transfected with a pool of three CRISPR/Cas9 plasmids containing gRNA targeting human *FKBP5* and a GFP reporter (Santa Cruz, sc-401560). 48 hours post transfection, cells were FACS sorted for GFP as single cells into a 96-well plate using BD FACS ARIA III) in FACS medium [PBS, 0.5% BSA Fraction V, 2 mM EDTA, 20mM Glucose, and 100 U/mL Penicillin-Streptomycin]. Single clones were expanded and western blotting was used to validate the knockouts.

For the generation of *FKBP5* KO SH-SY5Y cell line, cells were co-transfected with a pool of three CRISPR/Cas9 plasmids containing gRNA targeting human *FKBP5* and a GFP reporter (Santa Cruz, sc-401560) together with a homology directed repair plasmid (sc-401560-HDR) consisting of 3 plasmids, each containing a homology-directed DNA repair (HDR) template corresponding to the cut sites generated by the FKBP51 CRISPR/Cas9 KO Plasmid (sc-401560). 48 hours after transfection, medium was changed to 2 µg/ml puromycin-containing medium. After 36 hours single clones were manually picked and replated in single wells for expansion. KO clones were selected via western blot analyses.

3.2.6. Lysosome extraction

Cells were cultured in serum deprived medium for 72 hours prior to the experiment in order to enhance CMA. Dex or vehicle were added to the media 24 hours prior to the experiment. 2 x 10^8 SH-SY5Y cells were used for each condition. Lysosomes were extracted following manufacturer instructions with the lysosomal isolation kit (Sigma, LYSISO1). Briefly, cells were washed with PBS and homogenized in the extraction buffer provided with the kit. 200 µl were kept as whole cell lysate. After centrifugation, the crude lysosomal fraction was separated by density gradient centrifugation (150,000×g for 4 hours) on a multi-step OptiPrep gradient. All fractions were tested for LAMP2A by western blotting and for each condition, the fraction containing LAMP2A was used for further analysis as the lysosomal fraction.

3.2.7. Co-immunoprecipitation

In case of FLAG- or GFP-tag immunoprecipitation, cells were cultured for 3 days after transfection. Cells were lysed in CoIP buffer [20 mM tris-HCl (pH 8.0), 100 mM NaCl, 1 mM EDTA, and 0.5% Igepal complemented with protease inhibitor cocktail (Sigma)] for 20 min at 4 °C with constant mixing. The lysates were cleared by centrifugation, and the protein concentration was determined and adjusted (1.2 mg/ml); 1 ml of lysate was incubated with 2.5 µg of FLAG or GFP antibody overnight at 4 °C with constant rotating. Subsequently, 20 µl of bovine serum albumin–blocked protein G Dynabeads (Invitrogen, 100-03D) were added to the lysate-antibody mix followed by a 3 hour incubation at 4 °C. Beads were washed three times with PBS, and bound proteins were eluted with 100 µl of 1 × FLAG peptide solution (100 to 200 ug × ml−1, Sigma F3290) in PBS for 30 min at 4 °C. In case of precipitation of GFP tag, elution

was performed by adding 60 µl of Laemmli sample buffer and by incubation at 95 °C for 5 min. 5 to 15 µg of the input lysates or 2.5 to 5 µl of the immunoprecipitates were separated by SDS–polyacrylamide gel electrophoresis (PAGE) and analyzed by western blotting. When quantifying co-immunoprecipitated proteins, their signals were normalized to input protein and to the precipitated interactor protein.

3.2.8. Subcellular fractionation

Subcellular fractionation was performed according to Suzuki *et al.,* 2010 with little modifications. Briefly, 48 hours after transfection, $1x10^6$ cells were harvested on ice with a plastic scraper and centrifuged for 30 sec with a mini centrifuge. After the supernatant was discarded, pellets were resuspended in 200 µl REAP buffer [0.1% NP40/PBS] and triturated 5x with a p1000 micropipette. 50 µl of the lysate were removed as "whole cell lysate" and 16 µl of 4 × Laemmli sample buffer were added to it. The remaining (150 µl) material was centrifuged for 30 sec and 75 µl of the supernatant was removed as the "cytosolic fraction". 25 µl of 4 × Laemmli sample buffer was added to this fraction. After the remaining supernatant was removed, the pellet was resuspended in 100 µl of ice-cold REAP buffer and centrifuged as above for 30 sec and the supernatant was discarded. The pellet was resuspended in 75 µl of 1 × Laemmli sample buffer and designated as "nuclear fraction". All samples were boiled at 95 °C for 5 min and stored at -20 °C.

3.2.9. Reporter gene assays

Reporter gene experiments were performed in 96-well plates. 2×10^6 cells were transfected with 1 ug TCF/LEF-Luc, 100 ng pCMV-Gaussia-Luc, and, in case of simultaneous overexpression experiment, 1ug pRK5-FKBP51v1/v4-plasmid. Dex treatment was for 4 hours. To determine Firefly luciferase activity, cells were lysed in 50 µl passive lysis buffer [0.1 M K2HPO4/KH2PO4 pH 7.8, 0.2% Triton X-100]; 50 µl of luciferase reaction buffer [33 mM K2HPO4/KH2PO4, pH 7.8, 1.7 mM ATP, 3.3 mM MgCl2 and 13 mM luciferin] to a fraction of 10 µl of cell lysate were added and luminometric readings were performed with an automatic counter (Tristar from Berthold, Wildbad, Germany). Activity of the secretory Gaussia luciferase38 was measured after addition of 50 µl of substrate/buffer [1.1 M NaCl, 2.2 mM EDTA, 0.22 M KPO4 pH 5.1, 0.44 mg ml-1 bovine serum albumin, and 0.5 mg ml − 1 coelenterazine].

3.2.10. Immunocytochemistry

Cells were cultured on cover glasses (Paul Marienfeld, 0117530). When ready to be processed, cells were fixed with 4% PFA/PBS for 10 min at room temperature, permeabilized with 0.3% Triton X-100/ PBS for 5 min at room temperature and blocked with blocking solution [3% bovine serum albumin, 10% donkey serum in 0,1% Tween20 PBS] for 1 hour at room temperature. Cells were then incubated with primary antibodies diluted in blocking solution overnight at 4 °C and with the appropriate fluorophore-coupled secondary antibodies diluted in blocking solution for 1 hour at room temperature. Cells were counterstained with DAPI (Sigma D9542) diluted in PBS-T for 5 min and then mounted on imaging slides with Aqua-Polymount (Polyscience, 18606).

3.2.11. Pulse chase assay

48 hours after transfection with halotag (HT)-tagged plasmids, cells were labeled with HT fluorescent ligands (HaloTag R110Direct Ligand, Promega) for 24 hours after which the fluorescent ligand was washed off (chase) for the indicated amounts of time. Cells were harvested, proteins extracted minimizing light exposure and western blots were performed. Fluorescence was successively measured on membrane with the ChemiDoc MP system from Bio-Rad.

3.2.12. ELISA

The Il1b solid-phase sandwich ELISA (enzyme-linked immunosorbent assay) (Thermo Fisher, # BMS6002) was performed according to the manufacturer protocol. Briefly, microwells were coated with mouse anti-Il1b antibody followed by a first incubation with biotin-coupled anti mouse antibody, a second incubation with streptavidin-HRP and a final incubation with the SIM-A9 culture medium. Amounts of Il1b were detected with a plate reader (iMARK, Bio-Rad) at 450 nm.

3.2.13. *In vivo* brain microdialysis in mice

Microdialyses were performed by the in-house analytics and mass spectrometry core facility as in Anderzhanova et al., 2013, Kao et al, 2015 and Yen et al., 2015.

Briefly, stereotaxic implantation of microdialysis probe guide cannula was performed 7 days before the probe implantation and, respectively, 8 days before the start of an experiment. One day before the actual experiment, microdialysis probes were inserted and connected to the perfusion lines. All perfusion line connections were secured via wired-mediated attachment of the metal peg and swivel. The shape of the perfusion lines was tailored to minimize both inlet and outlet total volumes (this reduces the back pressure and lag time). From the moment of insertion, the probe was continuously perfused with sterile Ringer's solution (Biooscientific, USA) at a flow rate of 0.3 µl/min with high precision perfusion pump (Harvard Apparatus, USA). On the experimental day, microdialysis fractions (30 min) were constantly collected into Protein LoBind tubes (Eppendorf, Germany) at a perfusion rate of 0.4 µl/min. During collection time, tubes were kept on ice at 4 °C. After collection of two baseline samples animals were transferred to the fear conditioning chamber (ENV-407, ENV-307A; MED Associates, 7 St Albans, VT, USA connected to constant electric flow generator (ENV-414; MED Associates) and a foot shock (1.5 mA x 1 sec x 2) was delivered. After this procedure mice were returned to the microdialysis cage were two post-footshock samples were collected. To examine an effect of ULK1 inhibitor MRT 68921 on stress-evoked changes in extracellular content of proteins the drug was injected intraperitoneally (i.p.) in a dose of 5.0 mg/kg and in a volume 10 ml/kg four hours before the moment of foot shock (the drug was prepared freshly dissolving a stock solution [60%EthOH/40% DMSO mixture] with saline in proportion 1:20). Once collected, samples were stored at −80 °C prior to analysis. After completing the microdialysis procedure, mice were anaesthetized with isoflurane (3-4 % v/v in air), the microdialysis probe were removed, the animals were sacrificed via cervical dislocation (under anaesthesia) and brains were collected. 40 µm brain sections were stained with cresyl violet (Carl Roth GmbH, Germany) and probe placement was verified under a microscope using Paxinos and Franklin (2001) mouse atlas. If probe placement was found to be out of the targeted region of interest, the respective samples were excluded from the study.

3.2.14. CMA proteomics analyses

Liquid chromatography and mass spectrometry (LC-MS/MS) analysis and peptide and protein identification and quantification were performed by the proteomics and mass spectrometry core facility of the Max Planck Institute of Biochemistry (Martinsried, Germany).

3.2.14.1. (LC-MS/MS)

Peptides were separated by liquid chromatography performed on an EASY-nano-LC (Thermo Fisher Scientific) coupled with a nanoelectrospray-source to a Q Exactive™ HF Hybrid Quadrupol-Orbitrap mass spectrometer (Thermo Fisher Scientific). LyseC digested Peptides were solved in buffer A [H_2O with 0.1% formic acid] and separated with an isocratic gradient 30% buffer B [80% acetonitrile with 0.1% formic acid] for 120 min followed by a column wash step and re-equilibration at a flow rate of 250 nl/min. Precursor ions were measured at a resolution of 60'000 (scan range: 300-1750 *m/z*) and a target value of 3e6 ions. The 15 most intense ions from each MS scan were isolated, fragmented, and measured with a resolution of 15'000 (scan range: 200-2000 m/z) and a target value of 1e5.

3.2.14.2. Peptide and Protein identification and quantification

The MaxQuant software (version 1.5.3.34) was used for the analysis of raw files, and peak lists were searched against the human UniProt FASTA reference proteomes and a common contaminants database by the Andromeda search engine. Cysteine carbamidomethylation was used as a fixed modification, and methionine oxidation and protein N-terminal acetylation as variable modifications. Lysin/C was specified as the proteolytic enzyme and up to four missed cleavage sites were allowed. The FDR was set to 1%.

3.2.14.3. Data analysis

Only the light isotope signal was used for analysis. The Perseus software suite (v. 1.6.0.9) was used to filter out contaminants, reverse hits and protein groups, which were only identified by site. Only protein groups that were detected in at least two out of the three replicates in at least one condition were considered for the analysis.

The filtered data was log normalized and missing values were imputed according to the normal distributed imputation algorithm implemented in the Perseus framework. Default values were used (width: 0.3; down shift: 1.8). To find the significantly regulated protein groups a volcano plot analysis was performed using the default settings (s0= 0.1; FDR= 0.05). The results were exported for further enrichment analyses performed on the reactome platform (www.reactome.org).

3.2.15. Interactome analyses

Interactome analyses were performed in-house by the C. Turck lab as part of a collaboration.

3.2.15.1. Sample preparation

HEK cells were transfected with a FLAG tagged FKBP51 expressing plasmid or a FLAG expressing control vector. 48 hours after transfection, a FLAG IP was performed on all the samples and the eluted proteins were separated by SDS gel electrophoresis. Separated proteins were stained with Coomassie staining solution for 20 min and destained over night with Coomassie destaining solution. Each gel lane was cut into 16 approximately 2.5 mm slices per biological replicate and these further cut into smaller gel pieces.

3.2.15.2. In-gel-trypsin digestion and peptide extraction

The gel pieces were covered with 100µl of 25 mM Na4HCO3/50% ACN in order to destain the gel pieces completely and mixed for 10 min at room temperature. The supernatant was discarded and this step was repeated twice. Proteins inside the gel pieces are reduced with 75 µl 1x DTT/25 mM NH_4HCO_3 mixed at 56 °C for 30 min in the dark. The supernatant was discarded and 100µl IAM were added for alkylation to the gel pieces and mixed for 30 min at room temperature. The supernatant was discarded and the gel pieces washed twice with 100µl 25 mM Na_4HCO_3/50% ACN and mixed for 10 min at room temperature. The supernatant was discarded and gel pieces were dried for approximately 20 min at room temperature. Proteins were digested with 50 µl trypsin solution [5 ng/µl trypsin/25 mM NH_4HCO_3] over night at 37 °C. Peptides were extracted from the gel pieces by mixing them in 50 µl of 2% FA/50% ACN for 20 min at 37 °C and subsequently sonicating them for 5 min. The supernatant contained the peptides. This step was repeated twice with 50 µL of 1% FA/50% ACN.

3.2.15.3. LC MS/MS

Tryptic peptides were then dissolved in 0.1% FA and analyzed with a nanoflow HPLC-2D system (Eksigent, Dublin, CA, USA) coupled online to an LTQ-Orbitrap XL^{TM} mass spectrometer. Samples were on-line desalted for 10 min with 0.1% FA at 3 µl/min (Zorbax-C18 (5 µm) guard column, 300 µm × 5 mm; Agilent Technologies, Santa Clara, CA, USA) and separated via RP-C18 (3 µm) chromatography (in-house packed Pico-frit column, 75 µm × 15 cm, New Objective, Woburn, MA, USA). Peptides were eluted with a gradient of 95% ACN/0.1% HCOOH from 10%

to 45% over 93 min at a flow rate of 200 nl/min. Column effluents were directly infused into the mass spectrometer via a nanoelectrospray ion source (Thermo Fisher Scientific). The mass spectrometer was operated in positive mode applying a data-dependent scan switch between MS and MS/MS acquisition. Full scans were recorded in the Orbitrap mass analyzer (profile mode, m/z 380–1600, resolution R = 60000 at m/z 400). The MS/MS analyses of the five most intense peptide ions for each scan were recorded in the LTQ mass analyzer in centroid mode. The peptides were then identified with Mascot Daemon (Matrix Sciences London, http://www.matrixscience.com/daemon.html). Proteins were considered with a score ≥ 50 and ≥ 2 peptide matches and searched within the Swiss-Prot database FDR ≤ 0.05.

3.2.16. Secretome analyses

LC-MS/MS analysis and peptide and Protein identification and quantification were performed by the Bernhard Küster lab of the Technical University Munich (TUM) as part of a collaboration.

3.2.16.1. Sample preparation

All samples were prepared in triplicates. For each replicate 2 x 150 mm culture dishes, containing each 20 ml of medium, were used. WT and Atg5 KO SIM-A9 cells were cultured in methionine-free medium [DMEM, high glucose, no glutamine, no methionine, no cystine (Thermo Fisher, 21013024), 2 mM L-Glutamine (Thermo Fisher, 25030081), 1 mM sodium pyruvate (Thermo Fisher, 11360070), 0.2 mM L-Cysteine (Sigma, C7352), 10% dialyzed FBS (Thermo Fisher, 30067334), 1% Antibiotic-Antimycotic (Thermo Fisher, 15240-062)] for 30 min (12 hours and 30 min before supernatant collection). After 30 min, medium was changed to AHA enriched medium [methionine-free medium with 20 µM Click-IT™ AHA (L-Azidohomoalanine) (Thermo Fisher, C10102)] to lable newly synthetysed proteins. After 6 hours, cells were treated with 100 nM Dex or vehicle at a dilution of 1:10’000 (6 hours before supernatant collection). After 3 hours (3 hours before supernatant collection), all media were refreshed in order to analyze proteins that were secreted only during the last 3 hour time window. After 3 hours, supernatants were collected and centrifuged at 1000 x g for 5 min. EDTA-free proteinase inhibitor cocktail (Sigma, S8830) was added and supernatants were frozen at -20°C. The next day, supernatants were thawed on ice and concentrated with Amicon

Ultra 15 centrifugal filters, Ultracell 3K (Millipore, UFC900324) at 4000 x g at 4 °C for 5 hours. The concentrated samples were transferred into new 1.5 ml tubes (Sigma, Z606340). For the enrichment and digestion of AHA-labeled proteins, the Click-iT™ Protein Enrichment Kit (Thermo Fisher Scientific) was used according to the instructions of the supplier. Resulting peptides were further desalted by using 0.1 % formic acid in 50 % acetonitrile in the micro-column format (three discs, Ø 1.5 mm, C18 material, 3M Empore per micro-column were used). After drying in a centrifugal evaporator, the samples were stored at -20 °C until LC-MS/MS analysis.

3.2.16.2. LC-MS/MS

LC-MS/MS measurement of peptides in eluates was performed using a nanoLC UltiMate 3000 (Thermo Fisher Scientific) coupled to a quadrupole-Orbitrap Q Exactive HF-X mass spectrometer (Thermo Fisher Scientific). Peptides separated on an Acclaim PepMap analytical column (0.1 mm x 15 cm, C18, 2 µM, 100 Å; Thermo Fisher Scientific) using a 60 min linear gradient from 3-28 % solvent B [0.1 % formic acid, 5 % DMSO in acetonitrile] in solvent A [0. 1% formic acid, 5 % DMSO in water] at a flow rate of 10 µL/min. The mass spectrometer was operated in data dependent acquisition and positive ionization mode. MS1 spectra were acquired over a range of 360-1300 m/z at a resolution of 60’000 in the Orbitrap by applying an automatic gain control (AGC) of 3e6 or maximum injection time of 50 ms. Up to 12 peptide precursors were selected for fragmentation by higher energy collision-induced dissociation (HCD; 1.3 m/z isolation window, AGC value of 1e5, maximum injection time of 22 ms) using 28 % normalized collision energy (NCE) and analyzed at a resolution of 15’000 in the Orbitrap.

3.2.16.3. Peptide and Protein identification and quantification

Peptide and protein identification and quantification was performed using MaxQuant (version 1.6.0.16) by searching the tandem MS data against all murine canonical and isoform protein sequences as annotated in the Swissprot reference database (25175 entries, downloaded 13.07.2018) using the embedded search engine Andromeda. Carbamidomethylated cysteine was set as fixed modification and oxidation of methionine and N-terminal protein acetylation as variable modification. Trypsin/P was specified as the

proteolytic enzyme and up to two missed cleavage sites were allowed. Precursor tolerance was set to 4.5 ppm and fragment ion tolerance to 20 ppm. The minimum peptide length was set to seven and all data were adjusted to 1 % PSM and 1 % protein FDR. Intensity-based absolute quantification (iBAQ) was enabled within MaxQuant.

3.2.16.4. Data analysis

The Perseus software suite (v. 1.6.2.3) was used to filter out contaminants, reverse hits and protein groups, which were only identified by site. Only protein groups that were detected in at least two out of the three replicates in at least one condition were considered for the analysis.

The filtered data was log normalized and missing values were imputed according to the normal distributed imputation algorithm implemented in the Perseus framework. Default values were used (width: 0.3; down shift: 1.8). To find the significantly regulated protein groups a volcano plot analysis was performed with a difference of s0 =0.1 and a false discovery rate (FDR) of 0.05. The results were exported for further enrichment analyses performed on the reactome platform (www.reactome.org).

3.2.17. Statystical analyses

Except for the proteomics data, all statistical analyses were performed with GraphPad Prism 8. Analyses of paired measurements (time course, dose-response curve) between two groups were performed using the Sidak's multiple comparisons test. Analyses of paired measurements between three or more groups were performed using the Turkey's multiple comparison test. Unpaired analyses were performed pairwise using the Mann-Whitney test.

3.3. Materials

3.3.1. Antibodies

The following primary antibodies were used for western blot: Beclin1 (1:1000, Cell Signaling, #3495), ATG12 (1:1000, Cell Signaling, #2010), LC3B-II/I (1:1000, Cell Signaling, #2775), FLAG (1:7000, Rockland, 600-401-383), FKBP51 (1:1000, Bethyl, A301-430A), AKT (1:1000, Cell

Signaling, #4691), pAKT (Ser473 1:1000, Cell Signaling, #4058 and #9275), Actin (1:5000, Santa Cruz Biotechnology, sc-1616), GAPDH (1:8000, Millipore CB1001), TRIM16 (1:1'000, Bethyl A301-160A), IL1B (1:50, Cell Signalling, #12242), Cathepsin D (for Mouse) (1:50, Abcam, ABCAAB6313-100), SNAP29 (1:1000, Sigma, SAB1408650), SNAP23 (1:1000, Sigma, SAB2102251), STX3 (1:1000, Sigma, SAB2701366), STX4 (1:1000, Cell Signalling. #2400), GAL8 (1:1'000, Santa Cruz, sc-28254), GAL3 (1:1'000, Santa Cruz, sc-32790), SEC22B (1:1000, Abcam, ab181076)

3.3.2. Plasmids

FKBP51-FLAG as described in Wochnik et al. 2004.

The following expression vectors were purchased from Promega: NUP155-pFN21A, #FHC01121, SNCA-pFN21A #FHC02635, FKBP5-pFN21A #FHC02776, GAPDH-pFN21A #FHC02698, MEF2D-pFN21A #FHC00981, Halotaq-pFN21AB8354 #FHC02776, pFN21A HaloTag CMV Flexi Vector #9PIG282.

GFP-Sec22b and Trim16-FLAG were kind gifts by Dr. Vojo Deretic (University of New Mexico).

HT-FKBP51 isoform 2 expressing plasmid was generated by enzymatic cloning of the coding sequence (ENST00000542713.1) into the pFN21A HaloTag CMV Flexi Vector.

FKBP51 CRISPR/ Cas9 KO Plasmid (h), Santa Cruz #sc-401560; pSpCas9 BB-2A-Puro (PX459). V2.0 vector containing Atg5-targeting gRNA (Atg5 [house mouse] CRISPR gRNA 2: TATCCCCTTTAGAATATATC) purchased from GenScript.

3.3.3. RT-qPCR primers

FKBP5 transcripts 1-3 (Exon 11-12), IDT Hs.PT.58.813038:

forward primer: AAAAGGCCAAGGAGCACAAC

reverse primer: TTGAGGAGGGGCCGAGTTC

FKBP5 (all transcripts Exon 5-6), IDT Hs.PT.58.20523859

forward primer: GAACCATTTGTCTTTAGTCTTGGC

reverse primer: CGAGGGAATTTTAGGGAGACTG

FKBP5 variant 4 (Exon 8-10b), IDT Hs.PT.58.26844122:

forward primer: GAGAAGACCACGACATTCCA

reverse primer: AGCCTGCTCCAATTTTTCTTTG

YWHAZ (Exon 9-10), IDT Hs.PT.58.4154200:

forward primer: GTCATACAAAGACAGCACGCTA

reverse primer: CCTTCTCCTGCTTCAGCTTC

4. Results

4.1. Stress enhances chaperone-mediated autophagy via FKBP51

Target-proteins of chaperone-mediated autophagy (CMA) are identified through a specific sequence by HSC70, and transported directly to the lysosome surface (Chiang et al., 1989). Here, the assembly of the lysosome-associated membrane protein type 2A (LAMP2A) into a multimeric complex translocates the substrate protein into the lysosome lumen where it is degraded by proteases (Bandyopadhyay et al., 2008; Cuervo and Dice, 1996). GFAP and EF1A modulate the complex assembly dynamics of LAMP2A (Bandyopadhyay et al., 2010). CMA is regulated by AKT that inhibits the translocation complex assembly through phosphorylation of GFAP. AKT, in turn, is inhibited by the phosphatase PHLPP or activated by mTORC2. With regard to the discovered role of FKBP51 on scaffolding AKT and PHLPP (Pei et al., 2009), a possible regulatory function of FKBP51 in CMA was hypothesized. Furthermore, since FKBP51 is activated by GR, the impact of GR-mediated stress as enhancer of CMA was investigated.

4.1.1. Stress enhances degradation of known CMA targets

Baseline activity of CMA is very low, but is enhanced in the presence of cellular stressors (hypoxia, starvation, oxidative stress). First, I investigated whether GR activation could trigger CMA. For this purpose, the synthetic GR agonist Dex was used in the neuroblastoma cell line SH-SY5Y. To monitor CMA activity, the degradation of known CMA targets was determined. Pulse-chase assays of the well-established CMA targets MEF2D (Yang et al., 2009), GAPDH (Aniento et al., 1993) and SNCA (Cuervo et al., 2004) were performed. As control, the long living protein NUP155 (Toyama et al., 2013) was analyzed under the same conditions. Furthermore, to control for CMA-mediated degradation only, the essential CMA regulator LAMP2A was knocked down (KD) via siRNA 48 hours prior to the experiment. In parallel, cells were transfected with scramble siRNA as control group. Fluorophore detection on western blot membrane revealed an increased degradation of all three analyzed CMA targets in response to Dex treatment in the control samples (transfected with scramble siRNA). However, knock down

of LAMP2A (KD) eliminated the effect of Dex on protein degradation. No differences between the two KD conditions (vehicle and Dex) and the vehicle control could be observed (fig.1 a, b, c). The negative control protein NUP155 remained unaffected by both Dex treatment and LAMP2A KD, confirming the validity of the experiment (fig. 1 d).

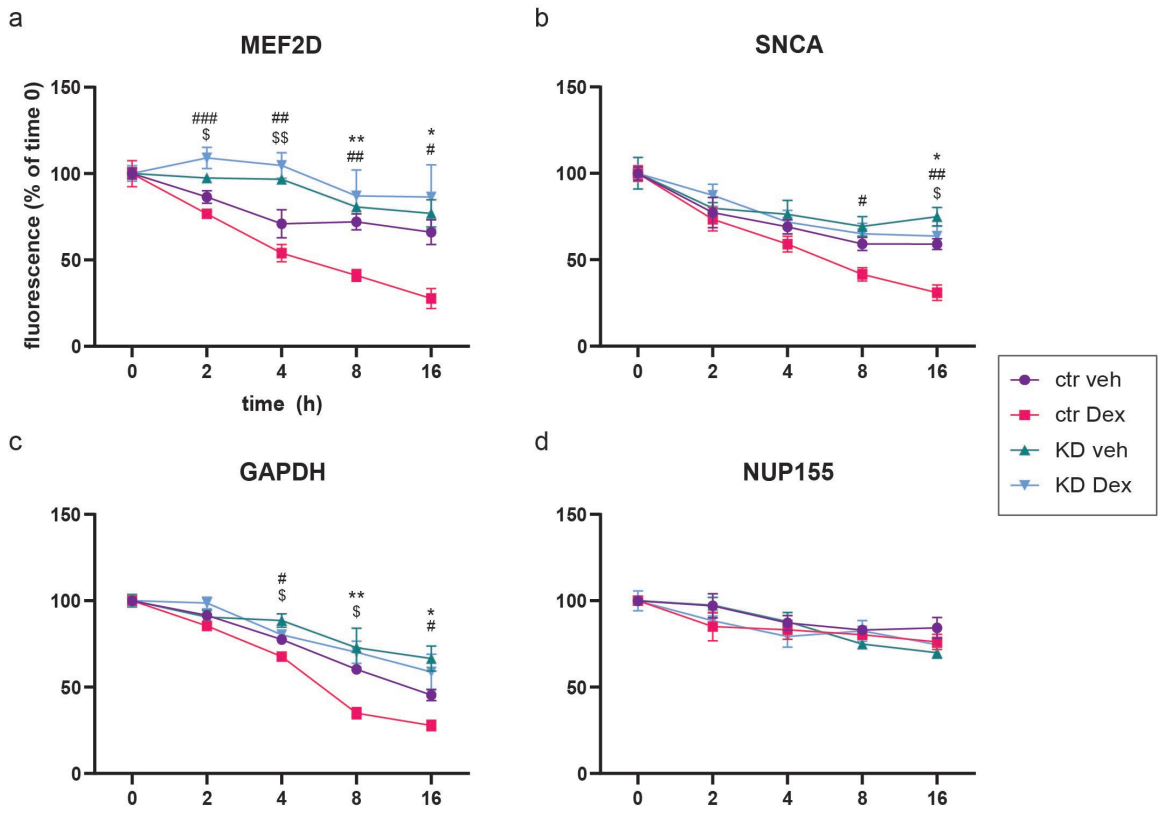

Figure 1 – Effect of stress on degradation of known CMA targets. Fluorophore quantifications of western blots of samples from WT and LAMP2A KD SH-SY5Y cells, transfected with HT-plasmids**,** pulsed with a fluorophore and chased for 2, 4, 8, and 16 hours, during which time cells were treated with 100 nM Dex or vehicle. HT-plasmids were expressing **a)** MEF2D, **b)** SNCA**, c)** GAPDH and **d)** NUP155. *P < 0.05; **P < 0.01; ***P< 0.001. Tukey's multiple comparison test. * refers to ctr veh vs. ctr Dex; # refers to ctr Dex vs. KD veh; $ refers to ctr Dex vs. KD Dex. Not indicated comparisons were not significant.

4.1.2. FKBP51 mediates the effect of stress on CMA

The pulse-chase experiments (fig. 1) revealed that GR activation enhances CMA-dependent degradation. At next, it was tested whether FKBP51 plays a role in mediating this effect. For this purpose, a FKBP51 KO SH-SY5Y cell line was generated via CRIPSR-Cas9. WT or FKBP51 KO

cells underwent treatment with Dex or vehicle followed by pulse-chase experiments with the known CMA target proteins (fig. 2), as described above. The results confirmed a stimulatory effect of Dex on the degradation of the CMA targets MEF2D, SNCA and GAPDH in WT cells. Interestingly, lack of FKBP51 resulted in the loss of the effect of Dex on target protein degradation, analogously as seen for the LAMP2A KD condition (fig. 2 a, b, c). The negative control NUP155 remained unaffected both by Dex and loss of FKBP51 (fig. 2 d).

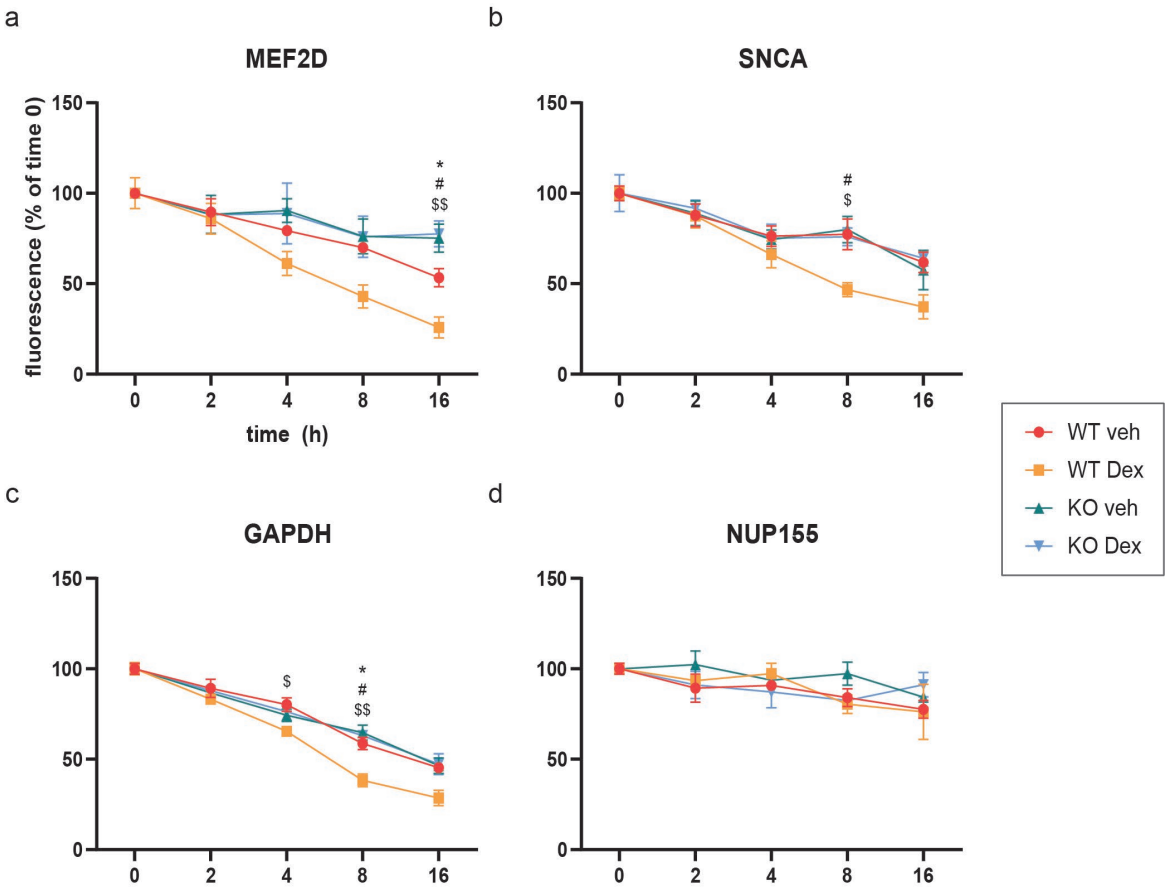

Figure 2 – Effect of stress on degradation of known CMA targets. Fluorophore quantifications of western blots of samples from WT and FKBP51 KO SH-SY5Y cells, transfected with HT-plasmids, pulsed with a fluorophore and chased for 2, 4, 8, and 16 hours, during which time cells were treated with 100 nM Dex or vehicle. HT-plasmids were expressing **a**) MEF2D, **b)** SNCA, **c)** GAPDH and **d)** NUP155. *P < 0.05; **P < 0.01. Tukey's multiple comparison test. * refers to WT veh vs. WT Dex; # refers to WT Dex vs. KO veh; $ refers to WT Dex vs. KO Dex. Not indicated comparisons were not significant.

4.1.3. FKBP51 scaffolds lysosomal AKT and PHLPP

These findings, indicating that FKBP51 plays an important role in CMA-dependent protein degradation, raised the question whether the hypothesis holds true that FKBP51 mediates AKT (de-) phosphorylation, crucial for proper CMA function.

To test this hypothesis, lysosomes were purified from WT and FKBP51 KO SH-SY5Y cells that were cultured in serum-deprived medium for 72 hours in order to enhance CMA. Lysosome purification was determined by western blot quantifications of the main subcellular markers (fig. 3 a-c). A clear enrichment for lysosomal marker LAMP2A was obtained in the lysosomal fraction (Lys) compared to the whole cell lysate (WCL). In line with that, a distinctively decreased signal of the nuclear marker histone H3 was observed in the lysosomal fraction compared to the whole cell lysate, while the mitochondrial marker apoptosis-inducing factor (AIF) appeared unchanged, suggesting a mild mitochondrial contamination in the lysosomal fraction. The main CMA players were analyzed in the lysosomal fraction and compared between WT and FKBP51 KO (fig. 3 d). Interestingly, even though total AKT is increased in the absence of FKBP51, its phosphorylation levels (pAKT) are decreased compared to WT. In addition, levels of PHLPP are slightly decreased in the lysosomal fraction lacking FKBP51. This is in line with the hypothesized scaffolding role of FKBP51. Furthermore, Rapamycin-insensitive companion of mTOR (RICTOR), a protein associated with mTOR and only present in lysosomes capable to perform CMA (Arias et al., 2015), was interestingly found at lower levels in lysosomes of FKBP51 KO samples.

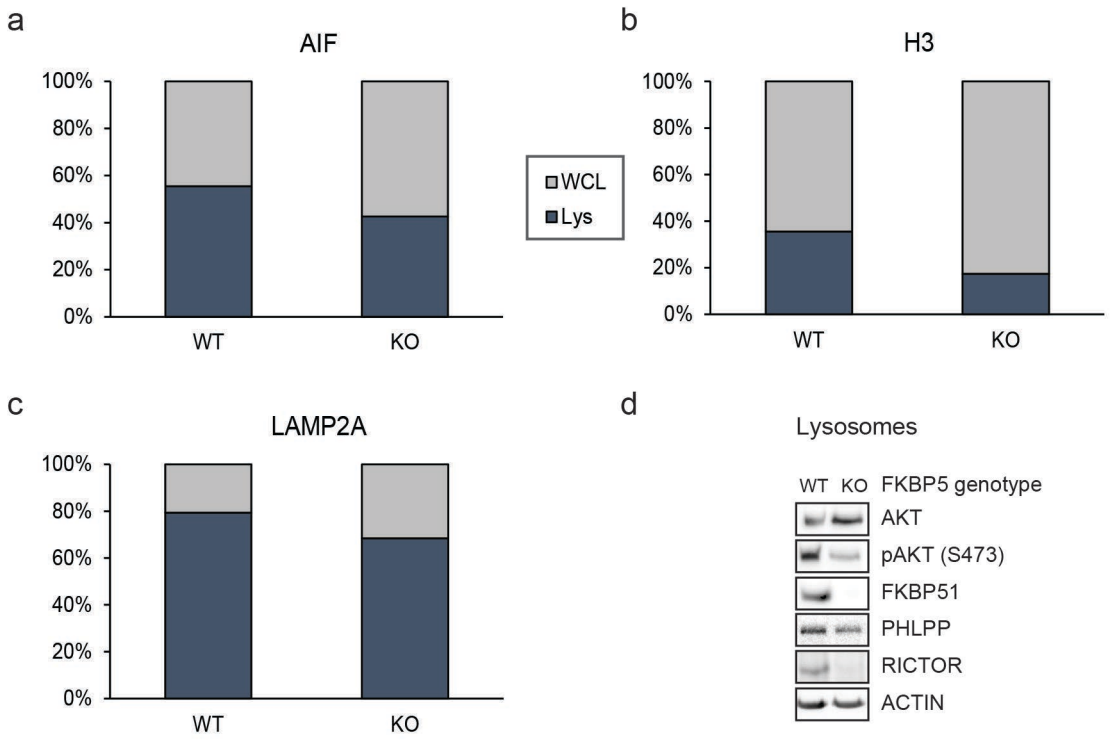

Figure 3 – Validation of lysosome extraction. Western blots of lysosome extracts (Lys) and whole cell lysates (WCL) from WT and FKBP51 KO SH-SY5Y cells cultured in serum-deprived medium for 72 hours. **a)** Quantification of lysosomal marker LAMP2A. **b)** Quantification of nuclear marker histone H3. **c)** Quantification of mitochondrial marker AIF. Western blot of known and hypothesized CMA modulators (AKT, pAKT, FKBP51, RICTOR) and normalizing control actin.

To further test the interactions underlying possible CMA mechanisms, a co-immunoprecipitation (co-IP) of AKT was performed in lysosome extracts and inputs as control, and analyzed for the main interactors via western blot. Results confirmed an interaction between AKT, PHLPP and FKBP51 on lysosomes, and that this interaction is strictly dependent on FKBP51 (absent in FKBP51 KO) (fig. 4).

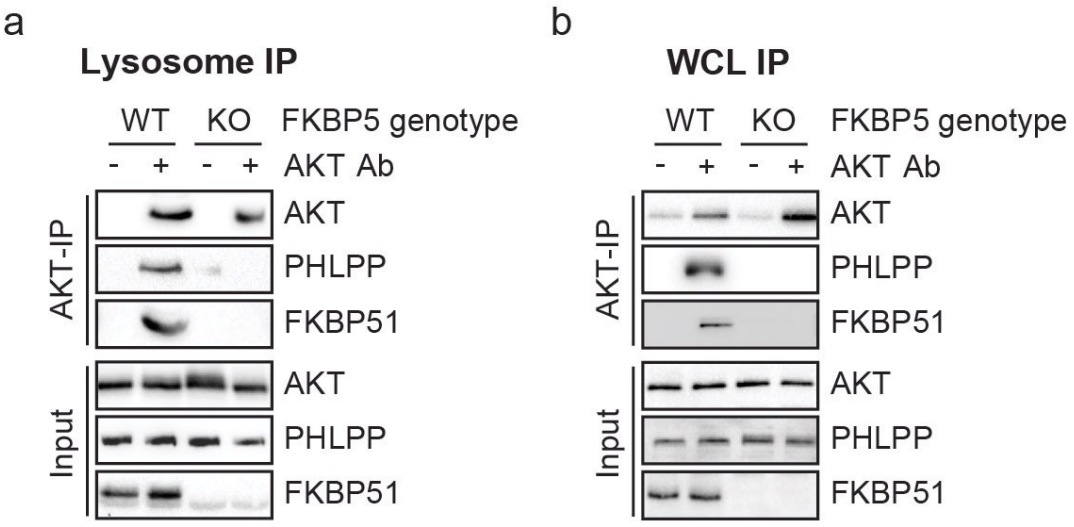

Figure 4 – AKT co-IP on lysosome extracts and whole cell lysates. Immunoprecipitation of AKT followed by Western blotting for AKT, PHLPP, FKBP51, in lysosome extracts (Lysosome IP) and whole cell lysates (WCL) of SH-SY5Y cells cultured in serum-deprived medium for 72 hours.

4.1.4. Proteome wide effect of stress on CMA and identification of novel targets

Having proven that stress (Dex) enhances CMA-dependent degradation of selected targets, and having clarified the underlying mechanism, a proteome-wide, endogenous effect of stress on CMA was explored. I performed a 6 hour stable isotope labeling by amino acids in cell culture (SILAC), during which cells were incubated with 5x concentrated heavy isotope lysines (Lys 8) that replaced the natural light isotope lysines (Lys0) in newly synthetyzed proteins (fig. 5). This allowed the selective identification of degraded proteins during a 6 hours frame, which is indicative for active CMA.

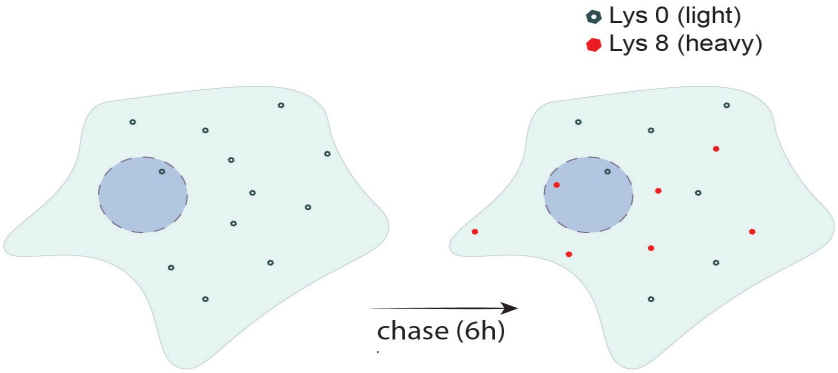

Figure 5 – Schematic representation of inversed pulsed SILAC. Natural light lysine isotope (Lys 0) is replaced by heavy lysine isotope (Lys8) added at a 5x concentration for 6 hours to the medium, competing with Lys 0 and causing its chsase.

An 8 hour Dex treatment was used as a stressor and was applied two hours before the heavy isotope labelling period in order to activate the CMA machinery. To control for specific degradation through CMA, the experiment was performed in cells knocked down for LAMP2A (KD), the key regulator of CMA. For this purpose, SH-SY5Y cells were transfected with siRNA targeting LAMP2A or scramble siRNA, 48 hours prior to the experiment. Samples were processed and analyzed via mass spectrometry. For SILAC quantification of the analyzed peptides, only the light isotope signal was considered. This allowed to observe the protein degradation, excluding novel protein synthesis. 6826 proteins were detected, and, after filtering, 5653 proteins were left for analysis. Volcano plot analyses were performed pairwise comparing the samples as indicated in figure 6. A strong effect of Dex was visible in the WT group (WT veh vs. Dex), with 4865 differentially regulated proteins, the vast majority of which was significantly degraded upon Dex treatment compared to vehicle (4850 vs. 15) (fig. 6 a). This large effect disappeared in the absence of LAMP2A, suggesting that the Dex-induced protein degradation is mediated by CMA (fig. 6 b). In the KD group (KD veh vs. Dex) a trend could be observed. These results were confirmed by complementary comparisons of WT vs. KD in vehicle or Dex treated conditions. Again, a significant effect was only seen in the Dex-treated condition, with 4172 degraded proteins in WT cells, and only 9 in LAMP2A KD cells (fig. 6 c). This result confirmed that Dex triggers CMA-dependent protein degradation. Interestingly, no effect was observed in the vehicle treated condition, suggesting that Dex stimulation is essential to enhance CMA (fig. 6 d).

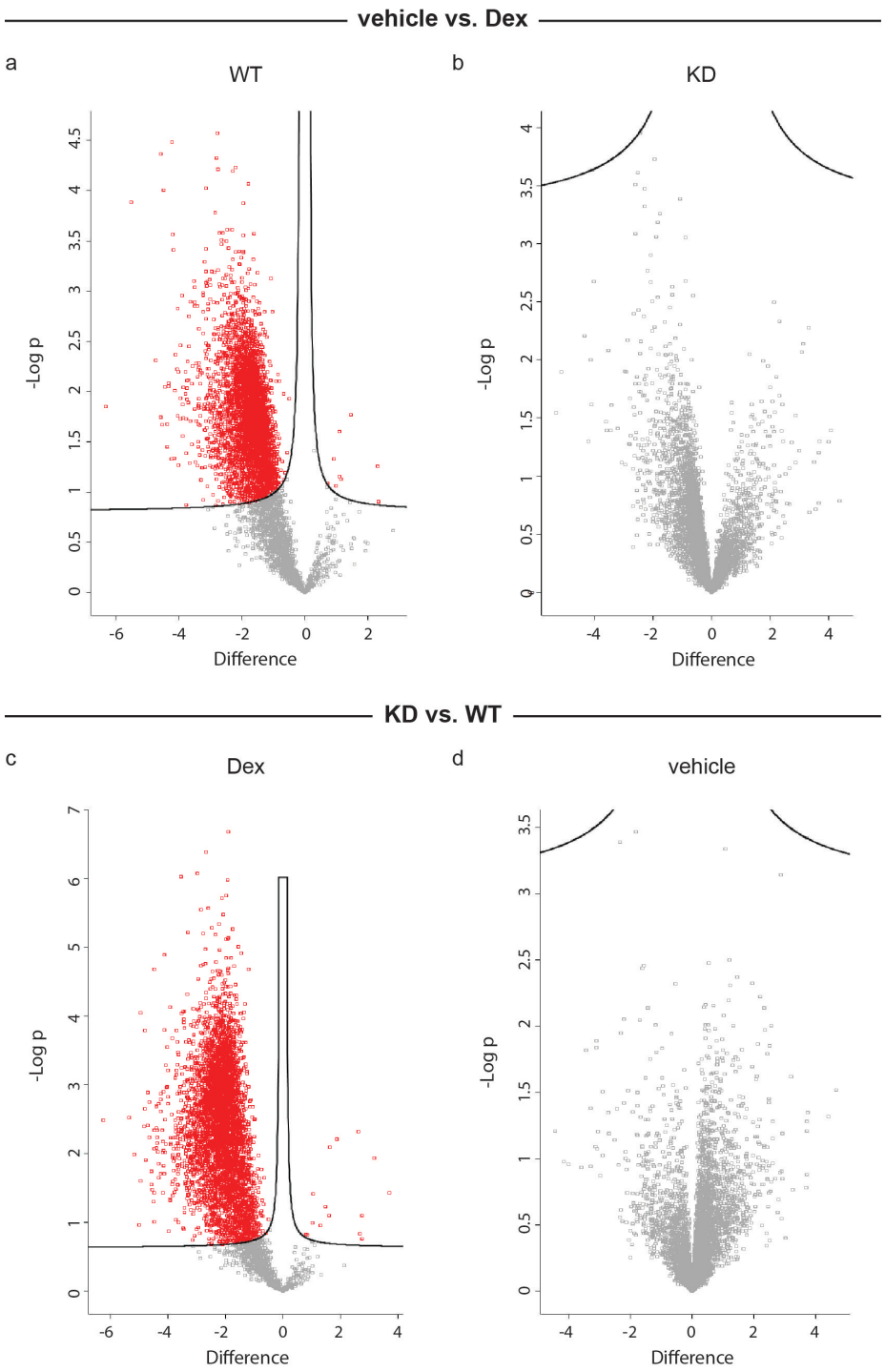

Figure 6 – Volcano plots of light isotope proteins detected via mass spectrometry analysis. a) Comparison between WT SH-SY5Y treated with vehicle or 100 nM Dex for 8 hours. **b)** Comparison between FKBP51 KO SH-SY5Y treated with vehicle or 100 nM Dex for 8 hours. **c)** Comparison between 8-hour 100 nM Dex treated WT and FKBP51 SH-SY5Y cells. **d)** Comparison between 8-hour vehicle treated WT and FKBP51 SH-SY5Y cells. Significantly regulated proteins are represented in red. FDR = 0.01, s0 = 0.1

Given a slight discrepancy in number of regulated proteins by Dex (WT vehicle vs. Dex) and by Dex-triggered CMA (WT Dex vs. KD Dex), a comparison between the degraded proteins resulting from the two groups was performed. Results displayed in the Venn diagram show that more than 80% of the proteins are present in both lists, meaning that these 3898 proteins are degraded via CMA only in response to Dex (fig. 7).

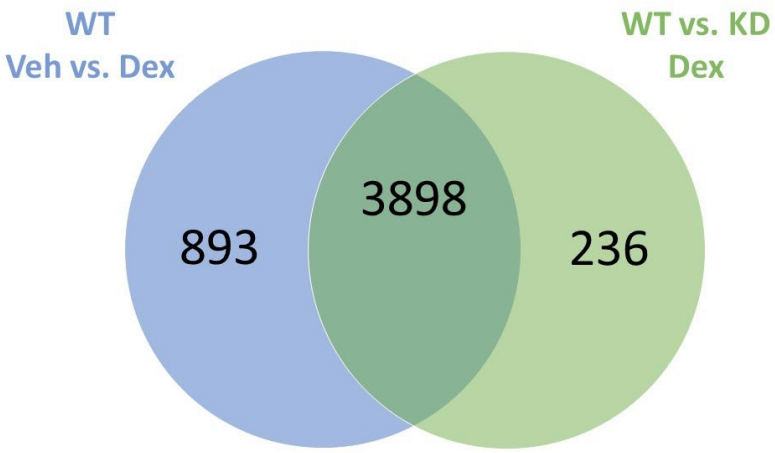

Figure 7 Venn diagram. Comparison between significantly regulated proteins by CMA under 100 nM Dex and vehicle (veh) conditions in SH-SY5Y resulting from volcano plots.

A functional enrichment analysis (https://reactome.org/) was performed on the group of proteins downregulated by Dex via CMA (3898 proteins). Results showed that regulated proteins were enriched in a variety of different cellular functions (fig. 8). Enrichment in cell cycle, DNA repair, metabolism of RNA, organelle biogenesis and maintenance, and metabolism of proteins are very interesting considering that autophagy has the main function of regulating homeostasis via these mechanisms that are the most energy consuming within the cell. This finding indicates that not only cellular stressors, but also GR activation can induce selective protein degradation.

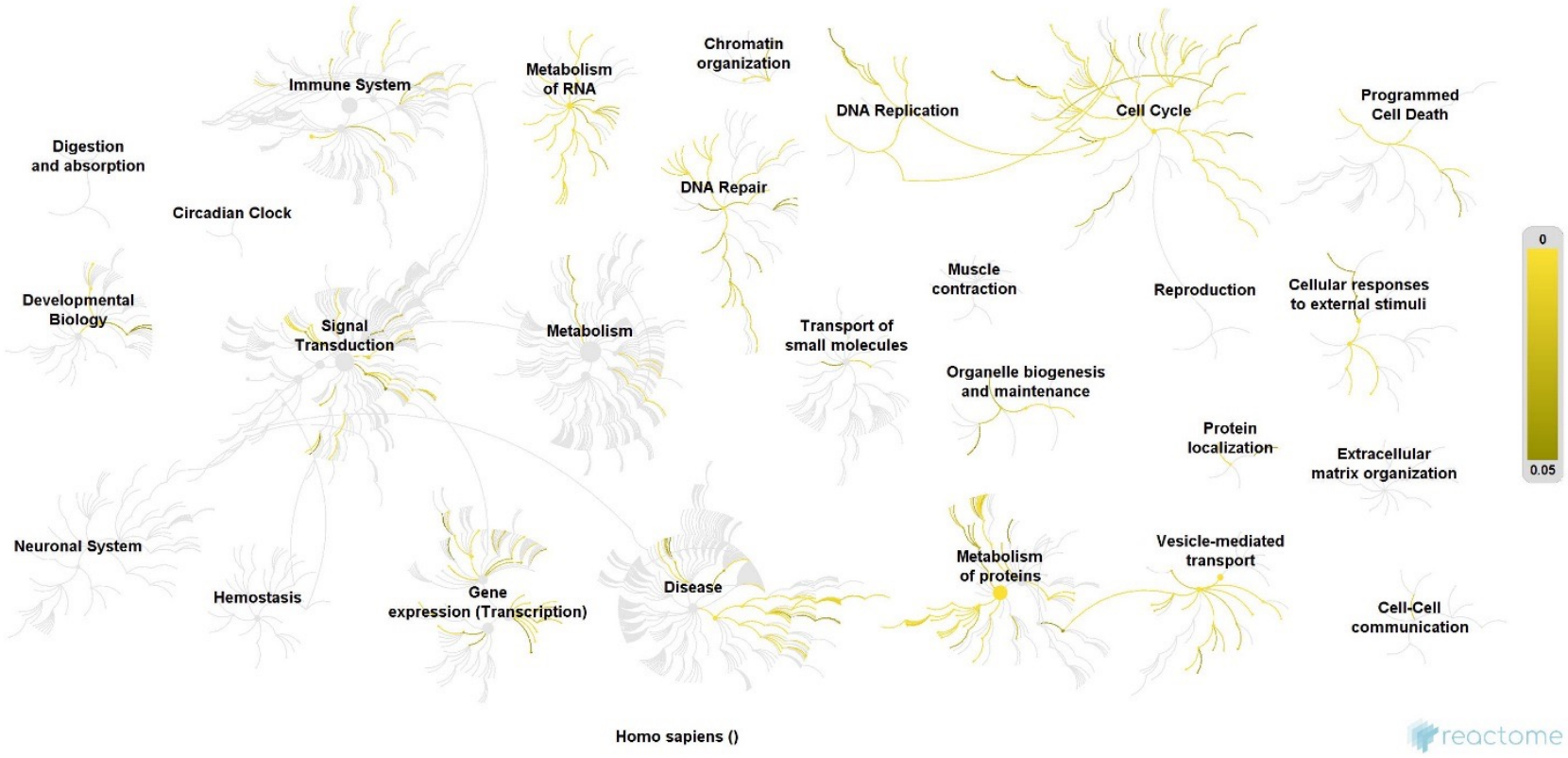

Figure 8 – Functional enrichment analysis. Visual representation of gene onthology enrichment analysis performed with Reactome (https://reactome.org/). Reactome pathways are arranged in hierarchies. Each center is the root of one toplevel pathway. In yellow the significantly enriched pathways (scale bar on the right).

Furthermore, many proteins have been found enriched in vesicle-mediated transport that includes pathways involved in neurotransmitter release, synapse formation and neuronal plasticity (fig. 9).

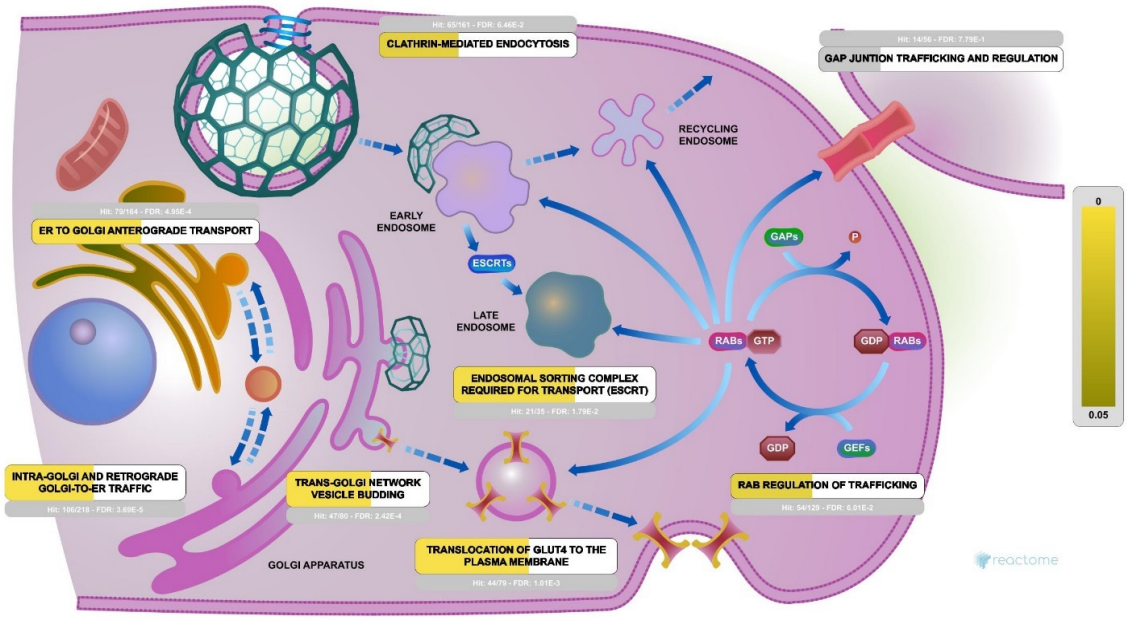

Figure 9 – Visual representation of enriched pathways in vescicle-mediated transport. In yellow the pathways and reactions of vesicle-mediated transport in which input proteins are significantly enriched. Data generated with Reactome (https://reactome.org/). Scale bar on the right.

To deeper investigate this function, enrichment of Dex-triggered, CMA-modulated proteins were analyzed in the neurotransmitter release cycle and a large amount of proteins was found to be significantly enriched in almost every reaction of the pathway (fig. 10).

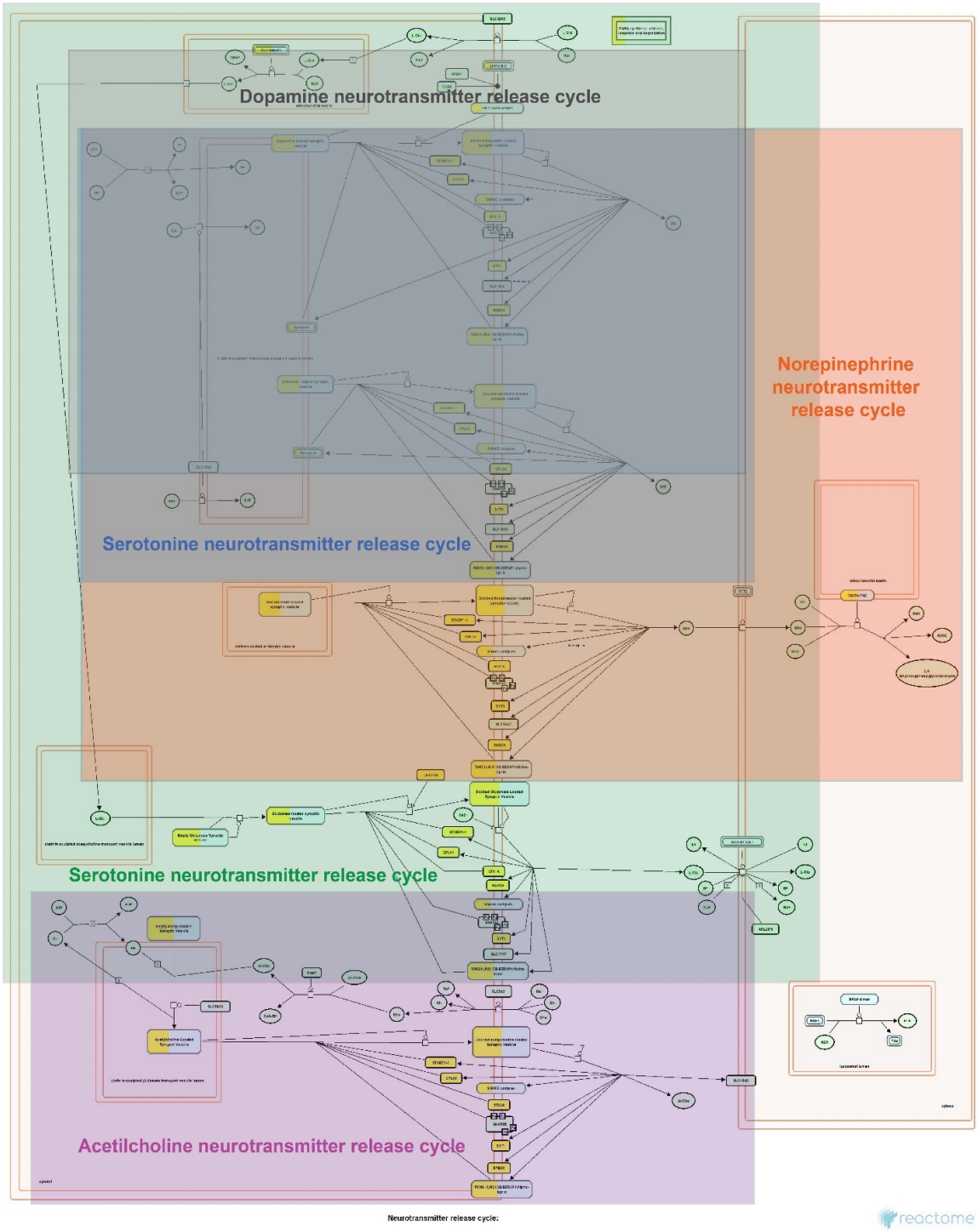

Figure 10 – Visual representation of enriched pathways in neurotransmitter release cycle. In yellow the pathways and reactions in which input proteins are significantly enriched. Data generated with Reactome (https://reactome.org/).

Among the 3898 regulated proteins, one was of particular interest: FKBP51 (fig. 11). Surprisingly, FKBP51 resulted regulated by Dex-triggered CMA in a sort of negative feedback or self-regulating mechanism. Possible implications will be pondered in the discussion section.

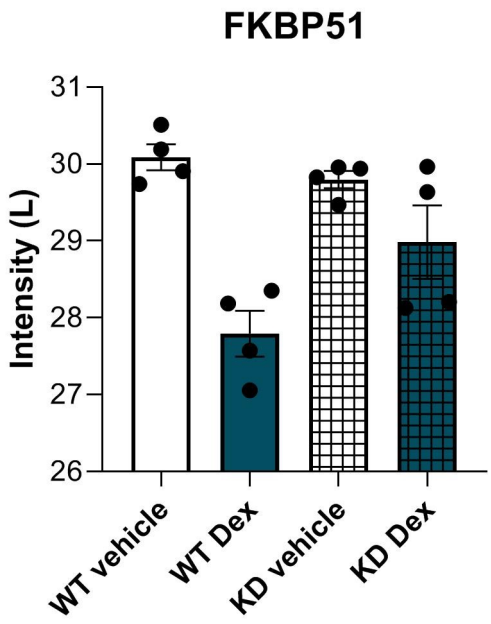

Figure 11 – FKBP51 regulation in mass spectrometry analysis. Graphical display of light isotope (Lys 0) intensity values of FKBP51 from mass spectrometry analysis. Error bars in SEM.

Overall, the SILAC mass spectrometry analysis showed that Dex has a large degradation effect on an unexpectedly extensive fraction of the proteome and that most of this effect is mediated by CMA.

4.2. Stress enhances secretory autophagy in the neuroimmune system

After having seen that FKBP51 mediates the stress effect in CMA via its interaction with AKT and PHLPP, the question that novel binding partners might mediate additional functions was raised. To investigate this hypothesis, novel FKBP51 interactors were searched.

4.2.1. SEC22B links FKBP51 to secretory autophagy

To find novel binding partners of FKBP51, results from an interactome mass spectrometry performed by collaborators were analyzed. The interactome analysis was performed via co-IPs using HEK cells transfected with FLAG-tagged FKBP51 or an empty FLAG-expressing vector as control. In this quantitative-free approach, only FKBP51-FLAG but not FLAG-control interactors were selected for further analysis. These stringent analysis parameters led on one hand to an overrepresentation of false negatives, but, on the other hand, ensured identification of direct, strong and verified FKBP51 interactors.

A resulting list of 29 binding partners was analyzed using the Panther classification system (http://www.pantherdb.org/). Eight different functional protein classes were identified. Among the interacting proteins resulted the vesicle trafficking protein SEC22B (fig. 12).

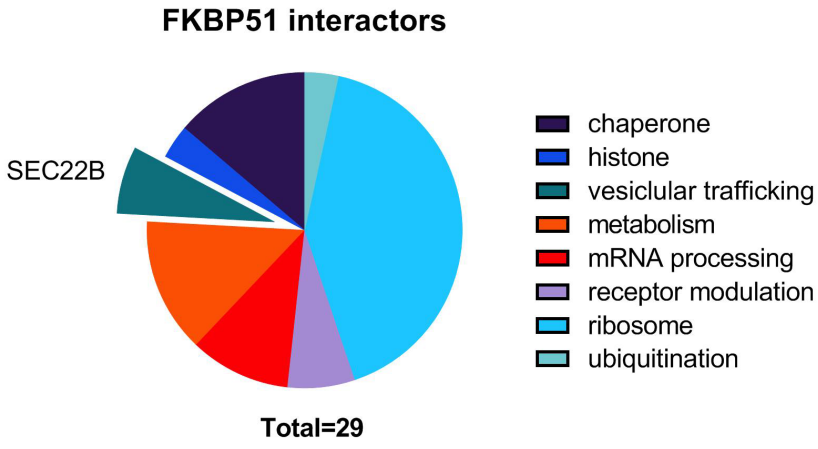

Figure 12 – FKBP51 interactors. Pie-chart representation of FKBP51 interactors identified by mass spectrometry and functional classification.

A study by Kimura and colleagues presented SEC22B as a key molecule in secretory autophagy (fig. 13) (Kimura et al. 2017). Having seen the regulatory role of FKBP51 in other autophagic pathways and its role in mediating stress response and restoring homeostasis, the interaction between FKBP51 and SEC22B appeared of particular interest. Therefore, further investigations were conducted on the interaction between FKBP51 and SEC22B with the hypothesis of a possible regulatory function of FKBP51 in secretory autophagy.

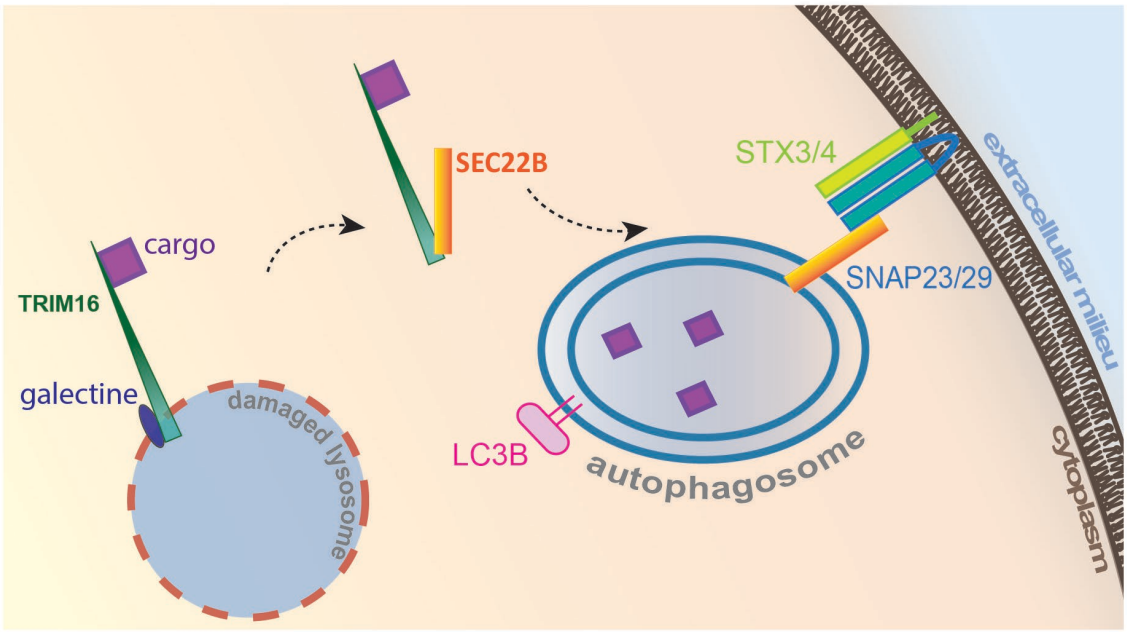

Figure 13 – Schematic overview of the secretory autophagy pathway. Stress-induced lysosomal damage is recognized by galectins, which recruite TRIM16 to the lysosome membrane. TRIM16 binds the secretory autophagy cargo and transfers it to the lumen of LC3B-coated autophagosome, via SEC22B. SEC22B binds then the plasma membrane SNAREs SNAP23/29 and STX3/4, mediating the exocytosis of the autophagosome content.

First, SEC22B and two other putative binding partners from the interactome experiment, RACK1 and UBC12, were validated via co-IP and western blot analyses in the SH-SY5Y cell line (fig. 14). Results confirmed the interaction of FKBP51 with all of them (fig. 14 a). For SEC22B, we further confirmed the interaction with FKBP51 via reciprocal IP (fig. 14 b).

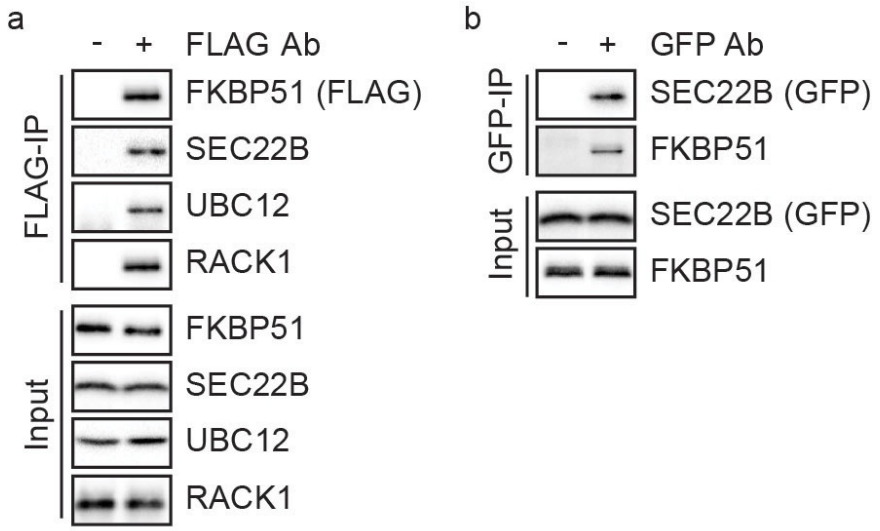

Figure 14 – Validation of FKBP51 interactions with SEC22B, UBC12 and RACK1. a) Immunoprecipitation of the FLAG tag followed by western blotting for FKBP51, SEC22B, UBC12 and RACK1 in SH-SY5Y cells transfected with FLAG-tagged FKBP51 (FLAG-IP) and the input as control. **b)** Immunoprecipitation of the GFP tag followed by western blotting for SEC22B and FKBP51 in SH-SY5Y cells transfected with GFP-tagged SEC22B (GFP-IP) and the corresponding input as control.

Since SEC22B is described to be a key regulator of secretory autophagy, we further examined the interaction of FKBP51 with other major players of this pathway: the secretory autophagy cargo IL1B, its receptor TRIM16, and the autophagosome marker LC3B (fig. 15). Neither IL1B nor LC3B could be identified as FKBP51 interactors by analyzing the co-immunoprecipitate, suggesting that FKBP51 is neither actively part of the transport of cargo proteins, nor it is directly involved in the decoration of autophagic vesicles by LC3B. For TRIM16, a faint band was detected in the eluate, and we confirmed this weak interaction with the inverse co-IP (fig. 15 b).

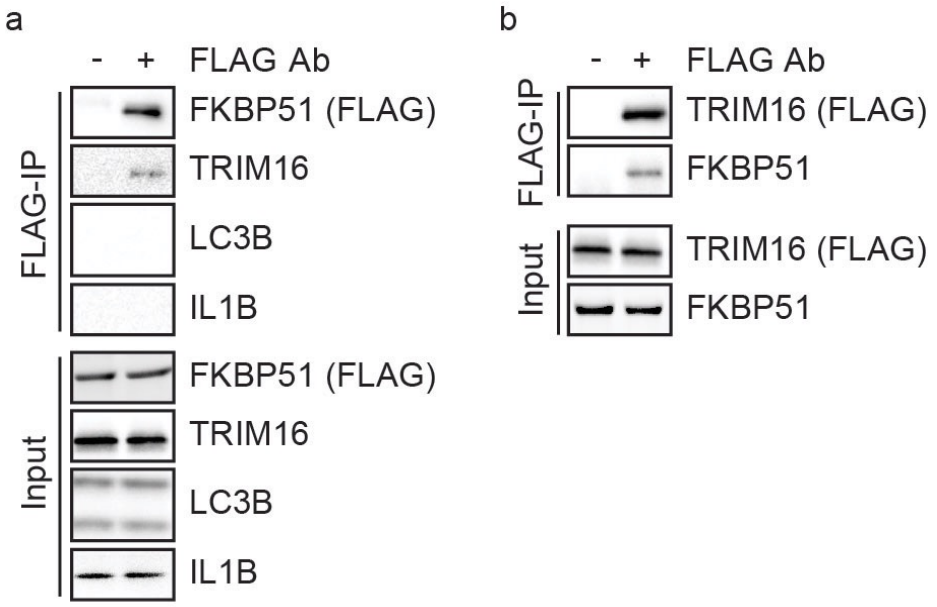

Figure 15 – Identification of novel FKBP51 interactors involved in secretory autophagy. a) Immunoprecipitation of the FLAG tag followed by western blotting for FKBP51, TRIM16, LC3B and IL1B in SH-SY5Y cells transfected with FLAG-tagged FKBP51 (FLAG-IP) and the corresponding input as control. **b)** Immunoprecipitation of the FLAG tag followed by western blotting for TRIM16 and FKBP51 in SH-SY5Y cells transfected with FLAG-tagged TRIM16 (FLAG-IP) and the corresponding input as control.

To further examine the potential role in the secretion dynamic, we analyzed the effect of FKBP51 on the interaction between IL1B and its receptor TRIM16, and between TRIM16 and SEC22B. For this purpose we used the CRISPR-Cas 9-generated FKBP51 KO SH-SY5Y cell line. Co-IP analyses revealed no difference of interaction in the presence and absence of FKBP51 for both interactions (fig. 16).

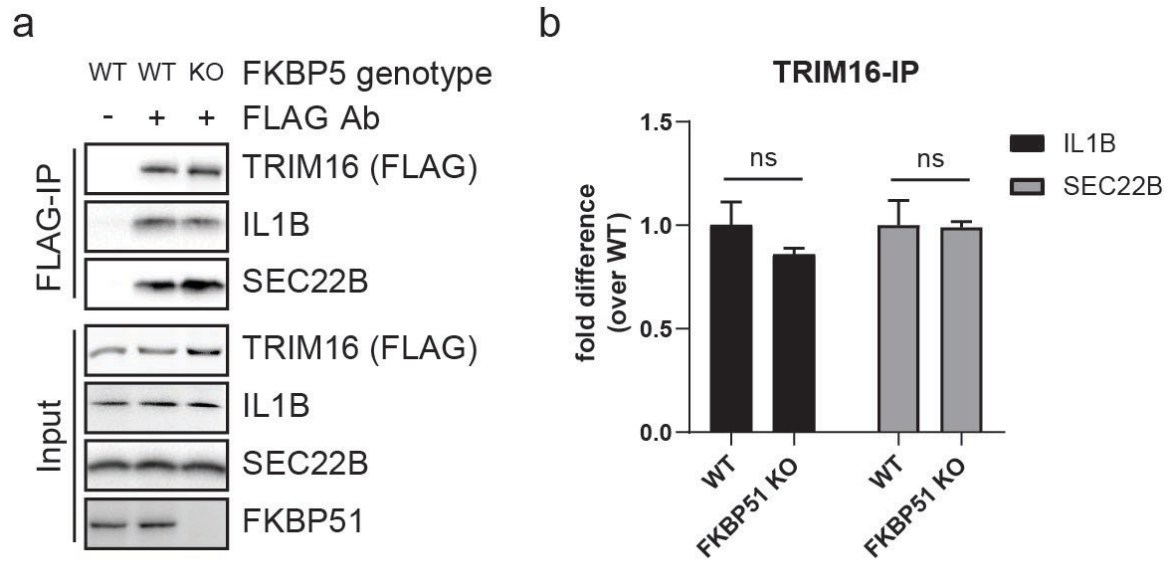

Figure 16 – Effect of FKBP51 on TRIM16-IL1B and TRIM16-SEC22B interactions. a) Immunoprecipitation of the FLAG tag followed by western blotting for IL1B and SEC22B in WT and FKBP51 KO SH-SY5Y cells transfected with FLAG-tagged TRIM16 (FLAG-IP) and the corresponding input as control. Additional western blotting for FKBP51 was performed in the input to confirm the genotype. **b)** Quantification of IL-1B and SEC22B bound to TRIM16 in WT or FKBP51 KO cells. Mann-Whitney test. ns= not significant. Error bars expressed in SEM.

FKBP51 expression is enhanced by GR activation and previous studies showed that it mediates the effect of stress on different pathways and cellular functions. Thus, we investigated weather GR activation had an effect on the interactions between TRIM16 and IL1B or SEC22B by stimulating cells with 100 nM Dex or vehicle for four hours. Co-IP analyses showed that Dex did not affect the interaction between TRIM16 and SEC22B. However, quantifications revealed a suprising decrease of interaction between TRIM16 and the cargo IL1B (fig. 17). Possible reasons behind this observation are presented in the discussion part.

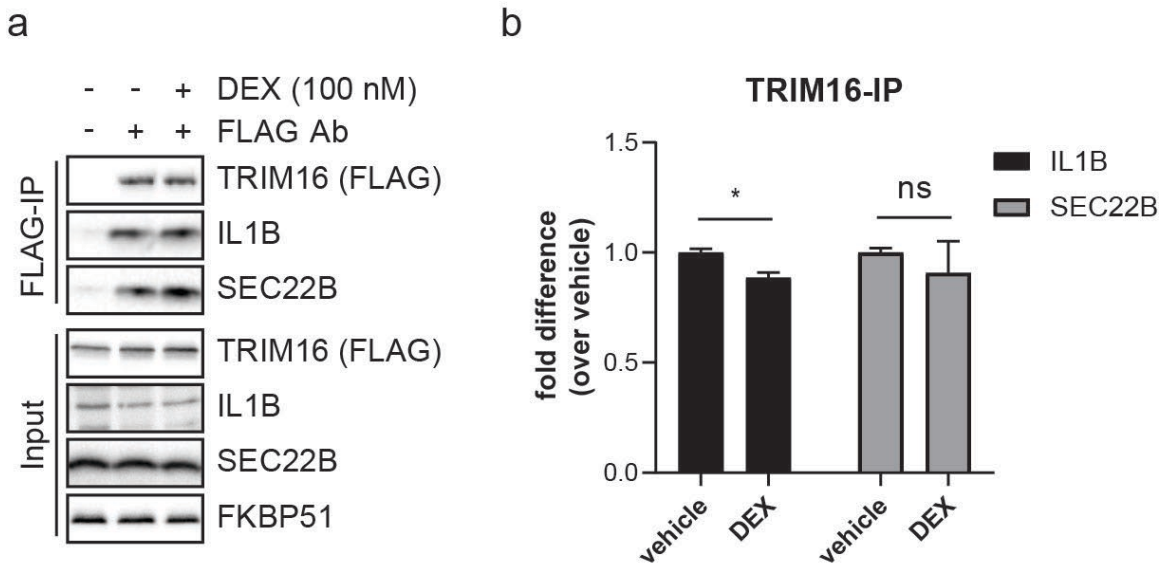

Figure 17 – Effect of dexamethasone on TRIM16-IL1B and TRIM16-SEC22B interactions. a) Immunoprecipitation of the FLAG tag followed by western blotting for TRIM16, IL1B and SEC22B in SH-SY5Y cells transfected with FLAG-tagged TRIM16 (FLAG-IP) and treated with 100 nM dexamethasone or vehicle for 4 hours. Below the corresponding inputs as control. **b)** Quantification of IL-1B and SEC22B bound to TRIM16 in 4 hours vehicle- or 100 nM Dex-treated conditions. Mann-Whitney test; ns= not significant, *P < 0.05. Error bars expressed in SEM.

4.2.2. FKBP51 scaffolds membrane fusion complex

Considering that FKBP51 had no function in the cargo transportation, nor in the sequestration membrane assembly, a possible role in the fusion of vesicles to the plasma membrane was hypothesized. To assess this hypothesis, I first analyzed the association of FKBP51 to other secretory autophagy-related soluble N-ethylmaleimide-sensitive factor attachment protein receptors (SNAREs): the synaptosomal-associated proteins 23 and 29 (SNAP23/29) and the syntaxins 3 and 4 (STX3/4). Via co-IP analyses, strong interactions with SNAP23 and SNAP29 was detected (fig. 18). These are two SNAREs shown to be fundamental for secretory autophagy (Kimura et al., 2017). A signal for STX3 was also detected, while a possible very weak interaction with STX4 could be observed (fig. 18). The weaker interaction could suggest a possible indirect interaction through SNAP23/29 or STX3.

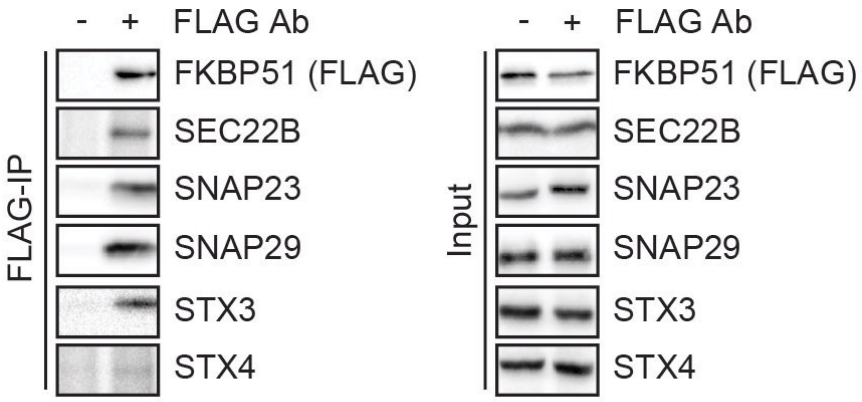

Figure 18 – Interaction of FKBP51 with SNAREs. Immunoprecipitation of the FLAG tag followed by western blotting for FKBP51, SEC22B, SNAP23, SNAP29, STX3 AND STX4 in SH-SY5Y cells transfected with FLAG-tagged FKBP51 (FLAG-IP) and the corresponding input as control.

Kimura and colleagues demonstrated that SEC22B interacts with STX3/4 and SNAP23/29 to form SNARE-fusion complexes (Kimura et al., 2017). Since I found that FKBP51 binds to all these SNAREs, I investigated whether it plays a role in the SNARE complexes assembly. For this purpose a co-IP of SEC22B in WT and FKBP51 KO cells was performed. Furthermore, knowing the stress-mediating effect of FKBP51 described previously, I investigated whether GR activation affects the SNARE complex assembly via FKBP51 by analyzing the interactions between SEC22B and SNAP23/29 or STX3/4 after stimulation with Dex or vehicle (fig. 19).

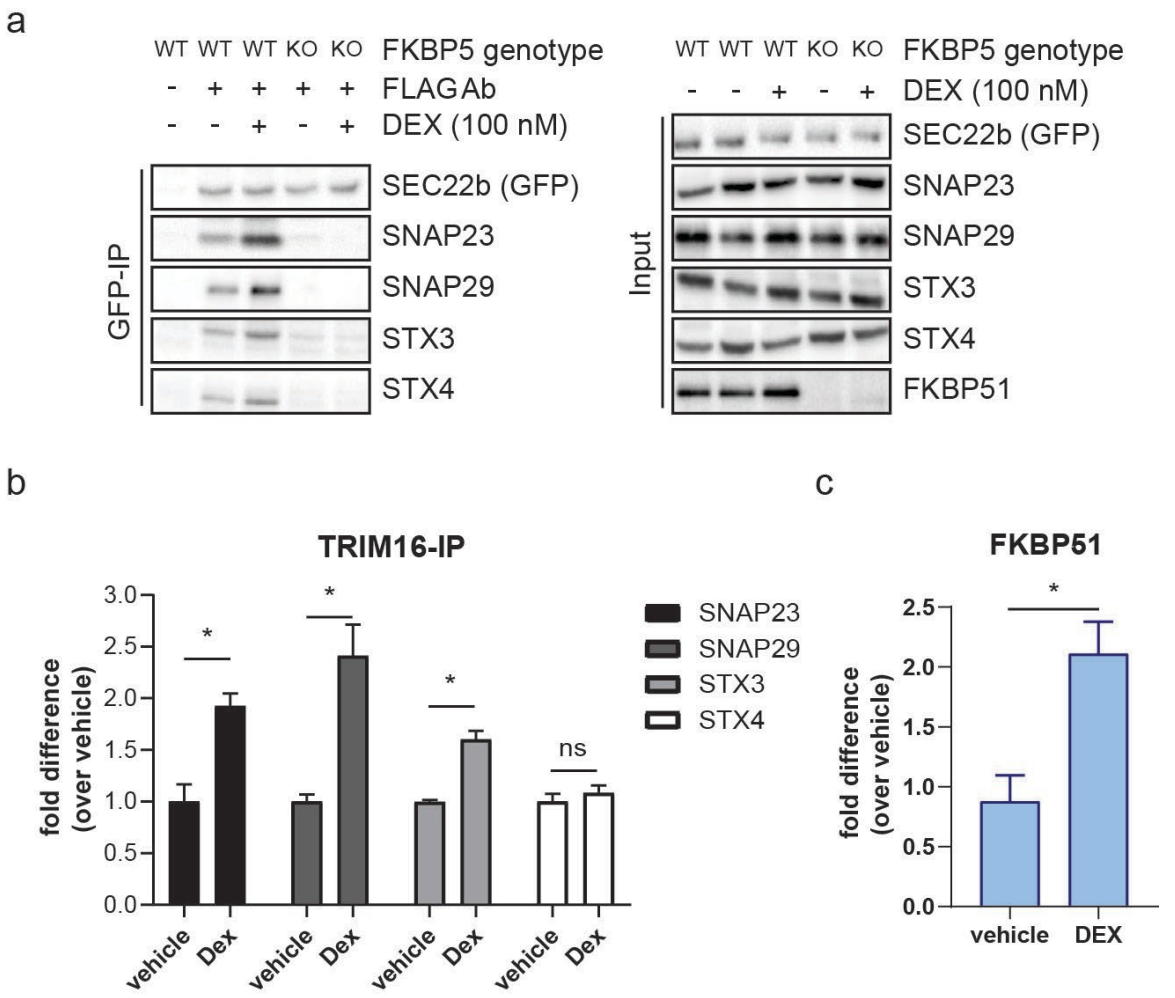

Figure 19 – Effect of FKBP51 and Dex on SNARE complex asembly. a) Immunoprecipitation of the GFP tag followed by western blotting for SEC22B, SNAP23, SNAP29, STX3 and STX4 in WT and FKBP51 KO SH-SY5Y cells transfected with GFP-tagged SEC22B (GFP-IP) and the input as control. **b)** Quantifications of SNAP23, SNAP29, STX3 and STX4 bound to TRIM16, expressed as fold change over vehicle. **c)** Quantification of input FKBP51 of samples treated for 4 hours with vehicle or 100 nM Dex. Mann-Whitney test; ns= not significant, *P< 0.05. Error bars expressed in SEM.

Western blot analyses of the co-IPs showed a strengthened interaction upon Dex stimulation in WT cells. Contrarily, the absence of FKBP51 caused a total impairment of interaction both in vehicle and Dex stimulated conditions, proving that GR activation enhances SNARE complex formation in an FKBP51-dependent manner (fig. 19).

4.2.3. Stress affects lysosomal integrity and triggers secretory autophagy

Having confirmed that Dex affects the assembly of the complex underlying secretory autophagy via FKBP51, other mechanisms leading to secretion were further investigated. Kimura and colleagues showed that secretory autophagy is initiated when lysosomes lose their integrity (Kimura et al., 2017). Based on this phenomenon, lysosomal integrity was analyzed to investigate whether Dex triggers secretory autophagy via the same mechanism.

Galectin-3 (GAL3) and galectin-8 (GAL8) are established markers of damaged endomembranes (Paz et al., 2010; Thurston et al., 2012). Thus, expression levels of these two markers were analyzed in response to Dex stimulation. Quantifications of western blot analyses showed a significant increase in GAL8 protein levels in response to Dex, and a trend in increase of GAL3, suggesting an enhanced lysosomal damage (fig. 20).

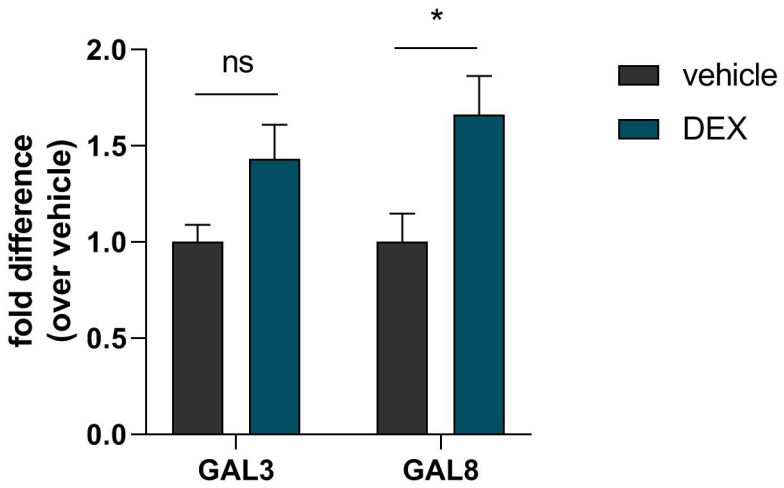

Figure 20 Effect of Dex on GAL3/8 expression. Quantification of western blot analyses for GAL3 and GAL8 normalized on ACTIN from WT SH-SY5Y cells treated with 100nM Dex or vehicle for 4 hours. Mann-Whitney test; ns= not significant, *P < 0.05, error bars expressed in SEM.

To further clarify the molecular mechanism possibly linking lysosomal damage and secretory autophagy, the interaction of GAL3/GAL8 and FKBP51 was tested via co-IP in response to Dex. Interestingly, GAL8 presented a strong interaction to FKBP51 after Dex stimulation, compared to basal levels, while GAL3 did not seem to directly interact with FKBP51 (fig. 20). Using a mutated, TPR domain-lacking form of FKBP51, a decrease in GAL8 binding could be seen,

suggesting that this interaction is at least partially mediated by the TPR domain, and, thus, by HSP90 (fig. 21).

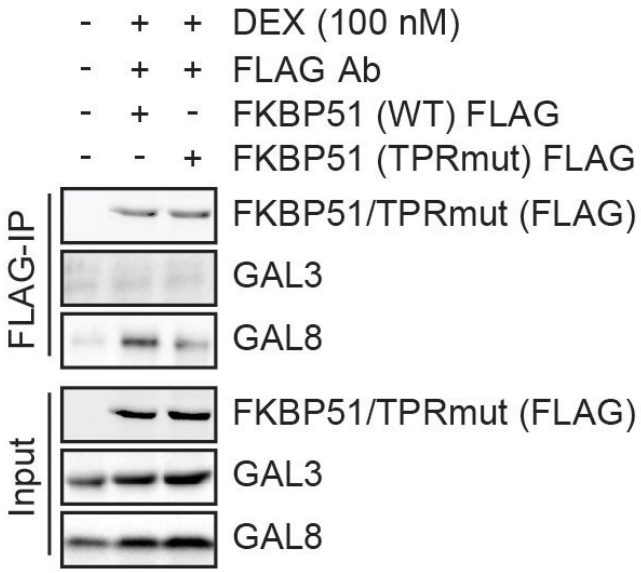

Figure 21 – Interaction of FKBP51 with GAL3/8. Immunoprecipitation of the FLAG tag followed by western blotting for GAL3 and GAL8 SH-SY5Y cells transfected with FLAG-tagged FKBP51 WT or FLAG-tagged FKBP51 lacking the TPR domain (FLAG-IP) and the input as control.

To directly assess lysosomal damage, a tandem fluorescent-tagged Galectin-3 (tfGal3) was used. It is a construct that monitors the pH in (damaged) lysosomes by expressing GFP and RFP. Both RFP and GFP are stable at a neutral pH, but GFP is rapidly degraded in the acidic environment of intact lysosomes, while RFP remains intact (Maejima et al. 2013) (fig. 22).

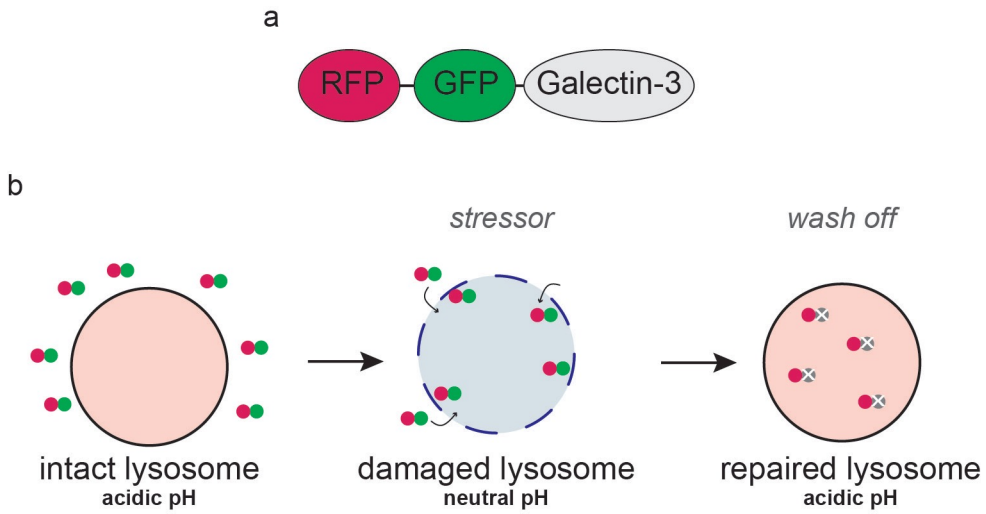

Figure 22 – Stucture and function of fluorescence-tagged Galectin-3 (tfGal3). a) Diagram of the structure of tfGal3 construct. **b)** Schematic representation of the fate of tfGal3 recruited to damaged lysosomes. (Figure adapted from Maejima et al., 2013)

After transient transfection with tfGal3, cells were subjected to various treatments for four hours and washed off for different durations as shown in figure 23. Leu-Leu-O-Me (LLOMe) and bafilomycin (Baf) were used as positive validations of the assay, as described by Meajima and colleagues (Maejima et al. 2013). LLOMe is a lysosome damaging and inflammasome activating substance, while Baf is an inhibitor of the vacuolar ATPase that controls pH in the lysosome. Through this mechanism, Baf prevents the acidification of lysosomes (Yoshimori et al. 1991). Using fluorescence microscopy, RFP and GFP fluorescent puncta were counted and the percentage of GFP^+ puncta over the total RFP^+ puncta was calculated. As expected, a significant reduction in GFP^+ puncta after LLOMe treatment was detected, indicating severe loss of lysosomal integrity. The assay could also be validated by Baf that reverted the effect of LLOMe (fig. 23 a). Interestingly, Dex caused a significant decrease in GFP^+ puncta with higher concentrations (30 nM and 300 nM), particularly noticeable with the 24 hours wash off, indicating lysosomal damage (fig. 23 b). This effect could also be rescued by co-application of Baf (fig. 23 b). These results indicate that high concentrations of Dex induce lysosomal damage.

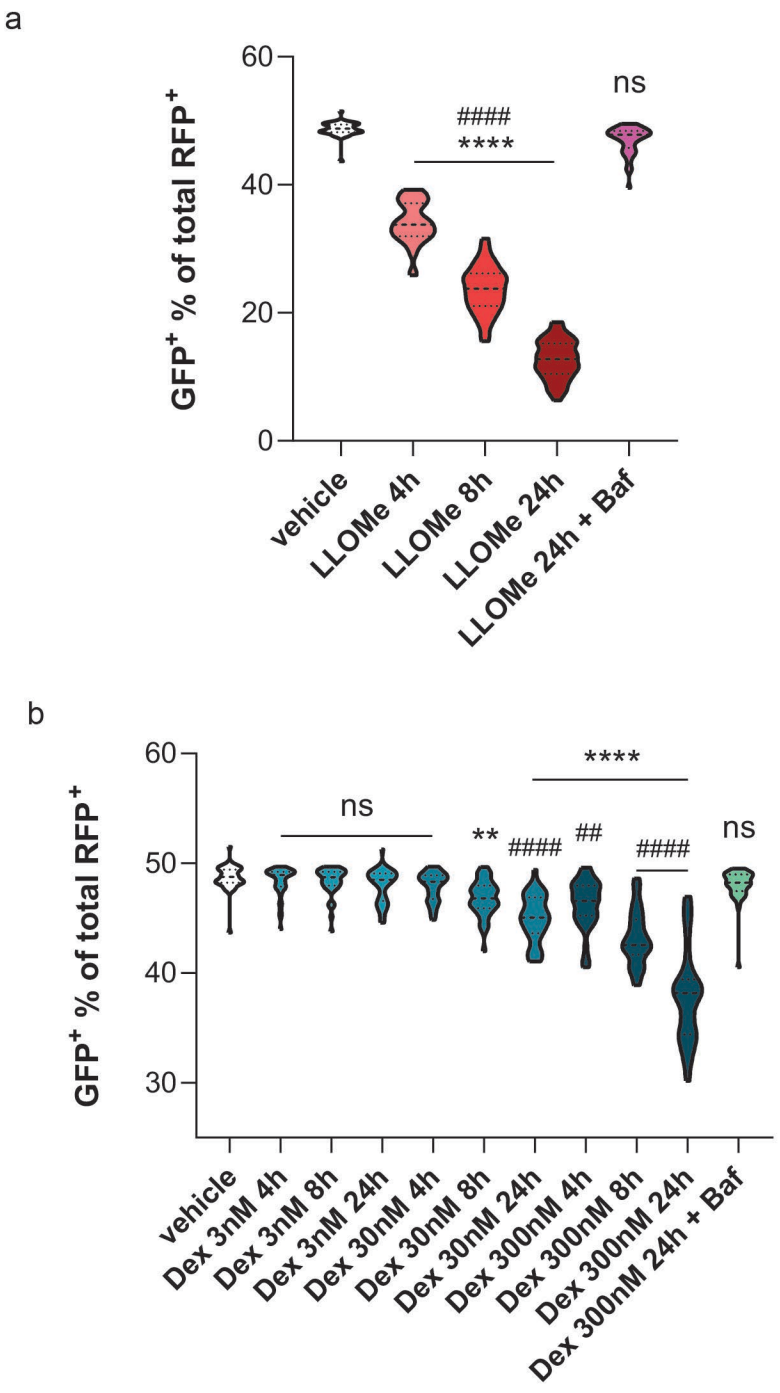

Figure 23 – Quantifications of lysosomal damage via tfGal3 assay. a) Quantification of GFP$^+$ puncta expressed in percentage of total RFP$^+$ puncta in SH-SY5Y cells transfected with tfGal3 construct and treated with 1 mM LLOMe for 3 hours, followed by 4 , 8 and 24 hours wash off, and with 1 mM LLOMe + Baf for 3 hours followed by 24 hours wash off. **b)** Quantification of GFP$^+$ puncta expressed in percentage of total RFP$^+$ puncta in SH-SY5Y cells transfected with tfGal3 construct and treated with 3 nM, 30 nM and 300 nM, each for 3 hours, followed by 4, 8 and 24 hours wash off and with 300nM Dex + Baf for 3 hours followed by 24 hours wash off. *P < 0.05; **P < 0.01; ***P < 0.001; ****P < 0.0001. Tukey's multiple comparison test. * indicate comparisons to vehicle; # indicate comparisons to treatment + Baf.

4.2.4. Dex affects autophagy-dependent Il1b secretion via Fkbp51 in microglia

The evidences collected so far point to the direction that stress affects lysosomal integrity and modulates the assembly of membrane fusion complex via FKBP51 in SH-SY5Y cells. This proposed mechanism is of particular interest in a neuroimmune environment. In fact, several studies revealed how secretory autophagy plays an important role in the extracellular signaling of immune response (Cadwell et al., 2008; Ushio et al., 2011; Michaud et al., 2011; Deretic et al, 2013). Thus, interaction of Fkbp51 with proteins of the membrane fusion machinery was analyzed in a murine microglia cell line, SIM-A9, via co-IP. As observed in SH-SY5Y cells, Fkbp51 was found to strongly interact with the SNAREs Sec22b, Snap23 and Snap29, while a weaker interactions were detected with Stx3 and Stx4 (fig. 24).

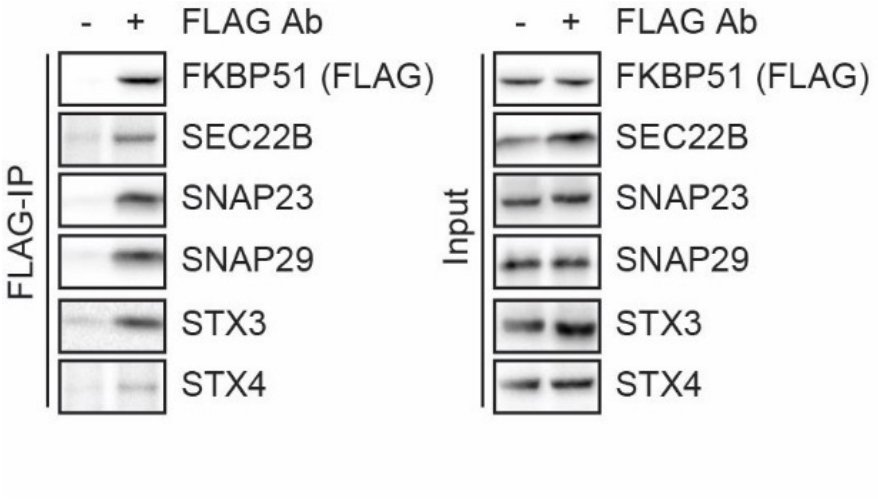

Figure 24 – Interaction of FKBP51 with SNAREs. Immunoprecipitation of the FLAG tag followed by western blotting for Fkbp51, Sec22B, Snap23, Snap29, Stx3 AND Stx4 in SIM-A9 cells transfected with FLAG-tagged FKBP51 (FLAG-IP) and the corresponding input as control.

To further analyze the functional role of Fkbp51 in the membrane fusion machinery, Il1b, a known cargo of secretory autophagy was analyzed via enzyme-linked Immunosorbent assay (ELISA). To validate the assay, cells were first treated with LLOMe, known to trigger Il1b secretion (Ito et al. 2015). ELISA quantifications revealed a large increase of Il1b already after 4 hours (fig. 25 a). Secreted Il1b was measured upon Dex treatment, as indicated in figure 25 b.

Interestingly, a strong increase of Il1b levels could be observed with 30 nM and 300 nM of Dex stimulation(fig. 25 b), the same concentrations that resulted causing lysosomal damage in SH-SY5Y cells. This result evidenced that Dex, analogously to LLOMe, induces Il1b secretion in microglia. To assess whether the underlying mechanism is autophagy-, *i. e.* secretory autophagy-, dependent, an Atg5 KO SIM-A9 cell line was generated via CRISPR-Cas9. Atg5 is an essential regulator in secretory autophagy (Kimura et al. 2017), and loss of this protein ultimately leads to an impairment of this unconventional mechanism of protein secretion. The ELISA experiment was repeated in a Atg5 KO line and results showed a drastic reduction of secreted Il1b levels in Atg5 KO cells, compared to WT, upon Dex treatment (fig. 25 c), demonstrating that the Dex effect on secretory autophagy is tightly linked to Atg5-mediated signaling. Given that Fkbp51 plays a central role in SNARE complex assembly, the effect of Fkbp51 overexpression was examined. SIM-A9 cells were transfected with an Fkbp51-expressing plasmid or control vector. After 24 hours, media were changed and 24 hours later media containing secreted proteins were collected and analyzed via ELISA. Overexpression of Fkbp51 resulted in a significantly increased secretion of Il1b compared to control (fig. 25 d). This result confirms that Fkbp51 mediates the effect of stress on Il1b secretion.

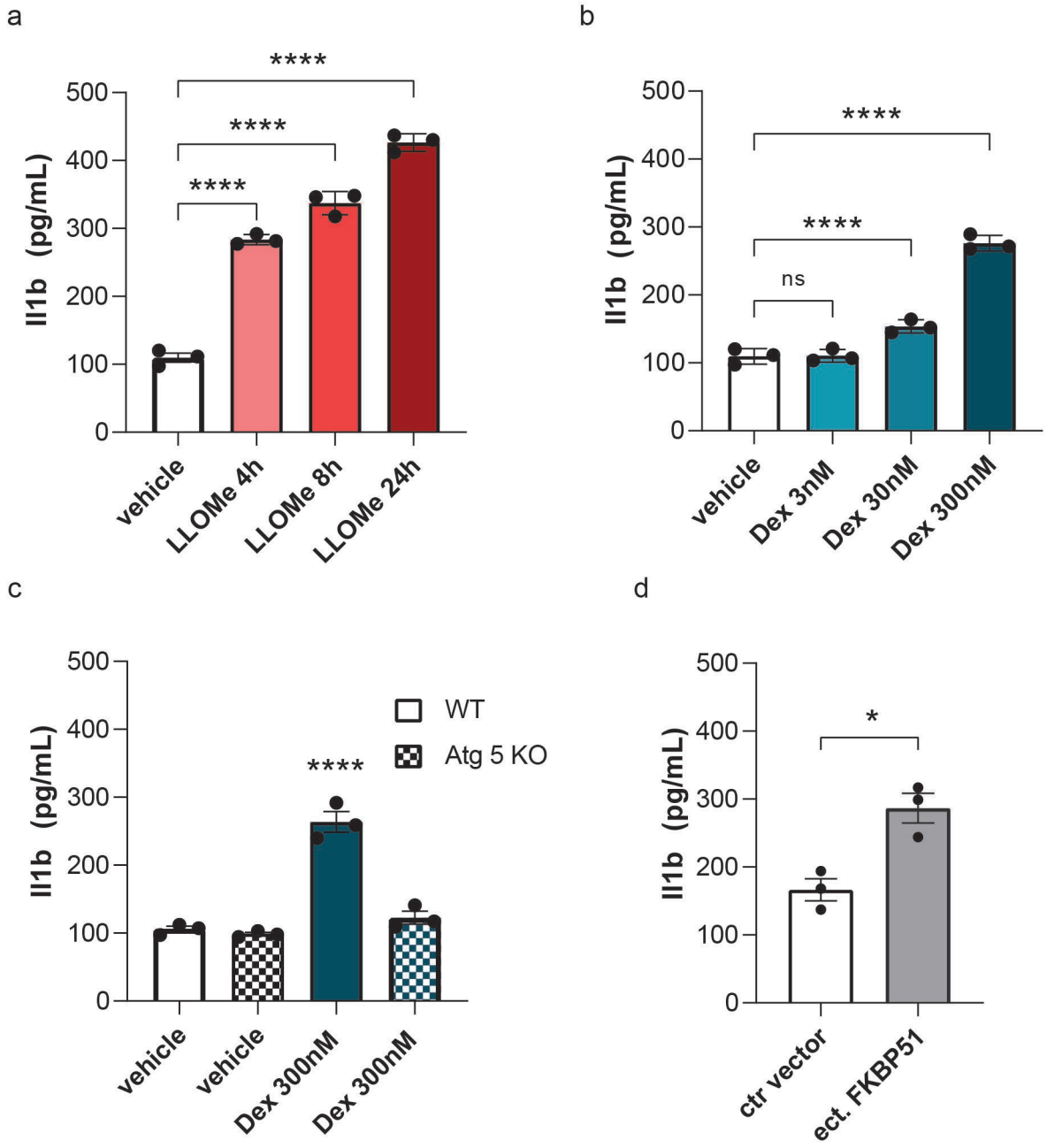

Figure 25 – Quantification of IL1B via ELISA assy. Il1b from supernatants was measured via ELISA after SIM-A9 cells were treated as follow **a**) LLOMe for 4, 8 and 24 hours or vehicle for 24 hours. **b)** 3nM, 30nM and 300nM or vehicle for 4 hours. **c)** 300nM Dex or vehicle for 4 hours in WT and Atg5 KO SIM-A9 cells. **d)** transfected with FKBP51 expressing plasmid or control vector. *P < 0.05; ***P< 0.001; ****P< 0.0001. Tukey's multiple comparison test was used for a, b and c; Mann-Whitney test was used for d. Significances in c are referred to comparison of Dex 300nM with each of the other conditions. Error bars expressed in SEM.

To control that the release of Il1b was due to active secretion and not unspecific leakage, amounts of lactate dehydrogenase (LDH) were measured in the medium of SIMA9-cells. LDH is a soluble cytosolic enzyme present in most eukaryotic cells, which is released into the culture medium upon damage of the plasma membrane. In line with data previously described by Kimura and colleagues (Kimura et al. 2017), levels of LDH were significantly increased in culture medium of SIM-A9 cells upon LLOMe treatment (fig. 26 a). Conversely, despite a visible trend, both Dex and overexpression of FKBP51, did not result in a significant release of LDH compared to controls (fig. 26 b, c). These results suggest that the enhanced release of Il1b described previously is due to an active mechanism rather than an unspecific cytotoxic effect.

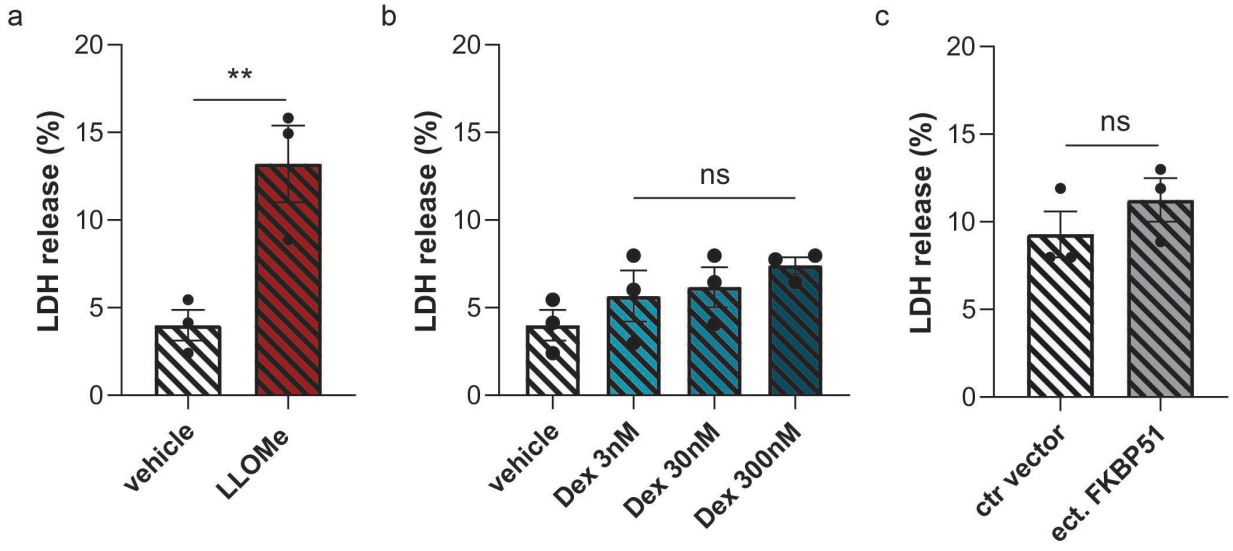

Figure 26 Quantification of secreted lactate dehydrogenase (LDH). LDH from supernatants was measured after SIM-A9 cells were treated as follow **a)** LLOMe or vehicle for 4 hours **b)** 3 nM, 30 nM and 300 nM Dex or vehicle for 4 hours. **c)** transfected with FKBP51 expressing plasmid or control vector. ns = not significant, *P < 0.01; Mann-Whitney test for Dex treatment and Tukey's multiple comparison test for LLOMe treatment and FKBP51 overexpression. Significances are referred to comparisons with vehicle or control vector. Error bars expressed in SEM.

4.2.5. Proteome-wide effect of Dex on secretory autophagy

The data obtained so far give rise to the conclusion that the molecular machinery necessary for secretory autophagy is present in microglia cells. Furthermore, GR activation causes an Fkbp51-dependent increase of Il1b secretion. To assess a global effect of stress on secretory autophagy, and to detect possible novel cargo proteins, a secretome wide analysis was performed.

A sophisticated approach, based on the method established by Eichelbaum and colleagues (Eichelbaum et al. 2012), was used to identify secreted proteins in a proteome-wide manner. Newly synthesized proteins were metabolically labeled for 12 hours and enriched to avoid abundant fetal bovine serum (FBS) proteins contained in the medium to be included in the secretome. To ensure that secretion of the analyzed proteins was autophagy dependent, microglial Atg5 KO cells were used. SIM-A9 WT or Atg5 KO were treated with Dex or vehicle for 6 hours. Culture media were collected, from which secreted proteins were enriched and analyzed by mass spectrometry. The resulting secretome consisted of 862 detected proteins that were filtered, leaving 710 proteins for analysis. Volcano plot analyses were first performed comparing pairwise the four groups (fig 27 a, b, c, d). Unexpectedly, only two proteins resulted significantly regulated by Dex in WT cells and no protein was significantly regulated by Dex in Atg5 KO cells. Despite this result, a trend of increased proteins in the vehicle-treated sample was clearly visible in the WT condition. This modest but evident effect disappeared in the absence of Atg5 suggesting that there is a slight effect of Dex on secretory autophagy. Interestingly, a much greater effect was observed when comparing WT and Atg5 KO conditions. In both vehicle and Dex treated samples, a large number of proteins was significantly decreased in the absence of Atg5 (499 and 560 respectively) (fig. 27 c, d).

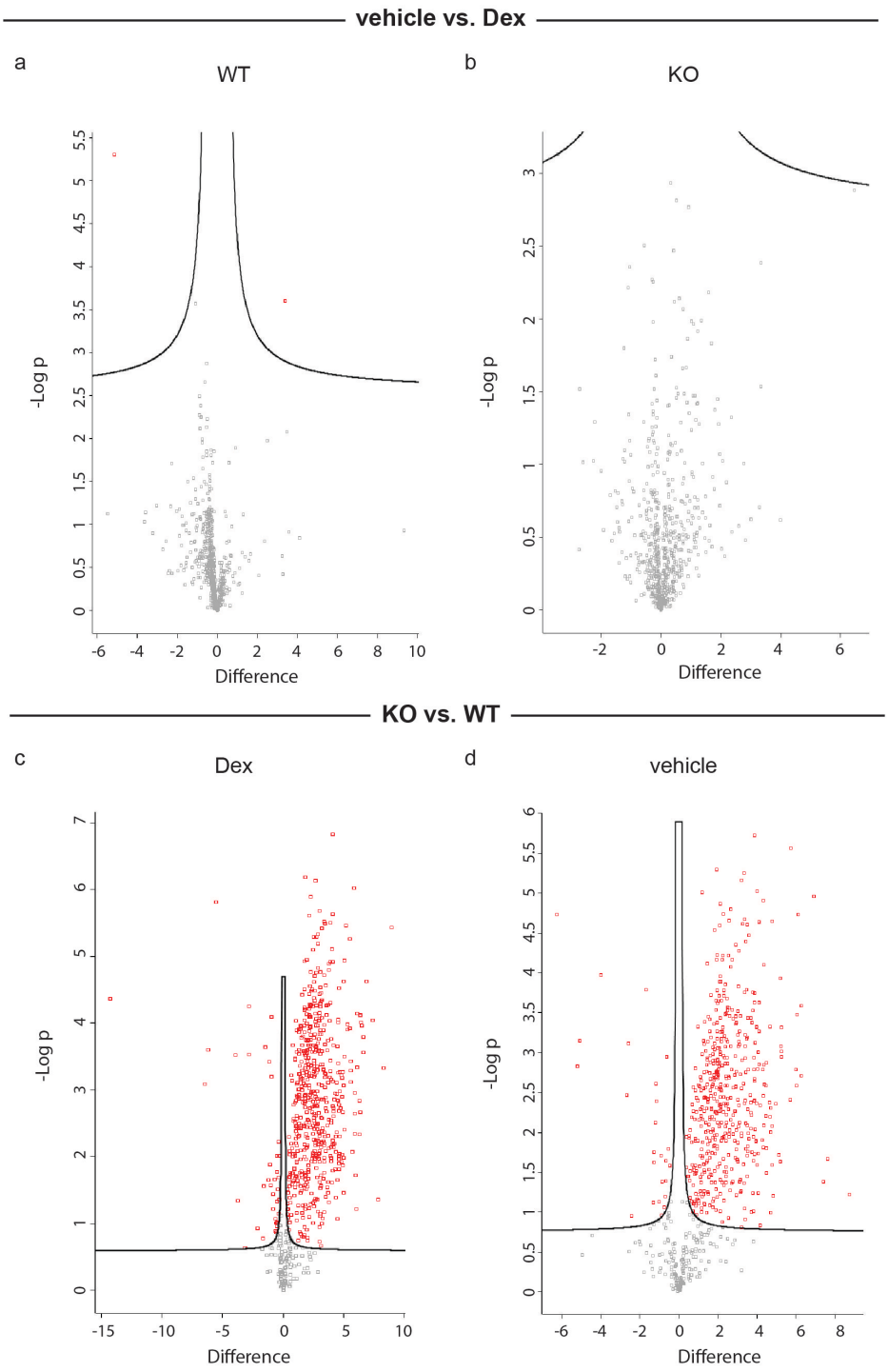

Figure 27 – Volcano plots of SIM-A9 secretome. a) Comparison between supernatants from WT SIM-A9 cells treated with 100 nM Dex or vehicle for 6 hours. **b)** Comparison between supernatants from Atg5 KO SIM-A9 cells treated with 100 nM Dex or vehicle for 6 hours. **c)** Comparison between supernatant from 6 hours 100 nM Dex treated WT and Atg5 KO SIM-A9 cells. **d)** Comparison between supernatants from 6 hours vehicle treated WT and Atg5 KO SIM-A9 cells. Significant proteins are represented in red. FDR = 0.01, s0 = 0.1

Unexpectedly, these results suggest that, secretory autophagy is highly active even under basal conditions, although Dex appears to have an enhancing effect (61 proteins more secreted than under basal condition). To explore the differences in secreted proteins under basal and Dex stimulated conditions, proteins that were modulated by Atg5 in vehicle and Dex treated samples were compared (fig. 28). Results displayed in the Venn diagram showed that the secretion of 79 proteins was increased specifically in response to Dex.

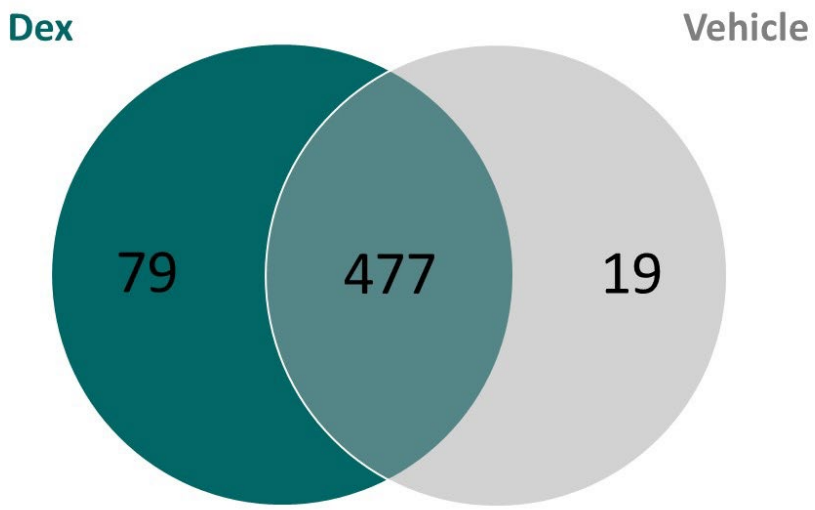

Figure 28 – Venn diagram of Atg5-dependent differentially secreted proteins. Comparison between significantly regulated proteins by CMA under 100 nM Dex and vehicle conditions in SH-SY5Y.

A gene onthology enrichment analysis was performed on the "Dex-specific" protein group. Interestingly, results showed that the most prominent fraction of proteins was enriched in the immune system-related signalling (fig. 29).

a

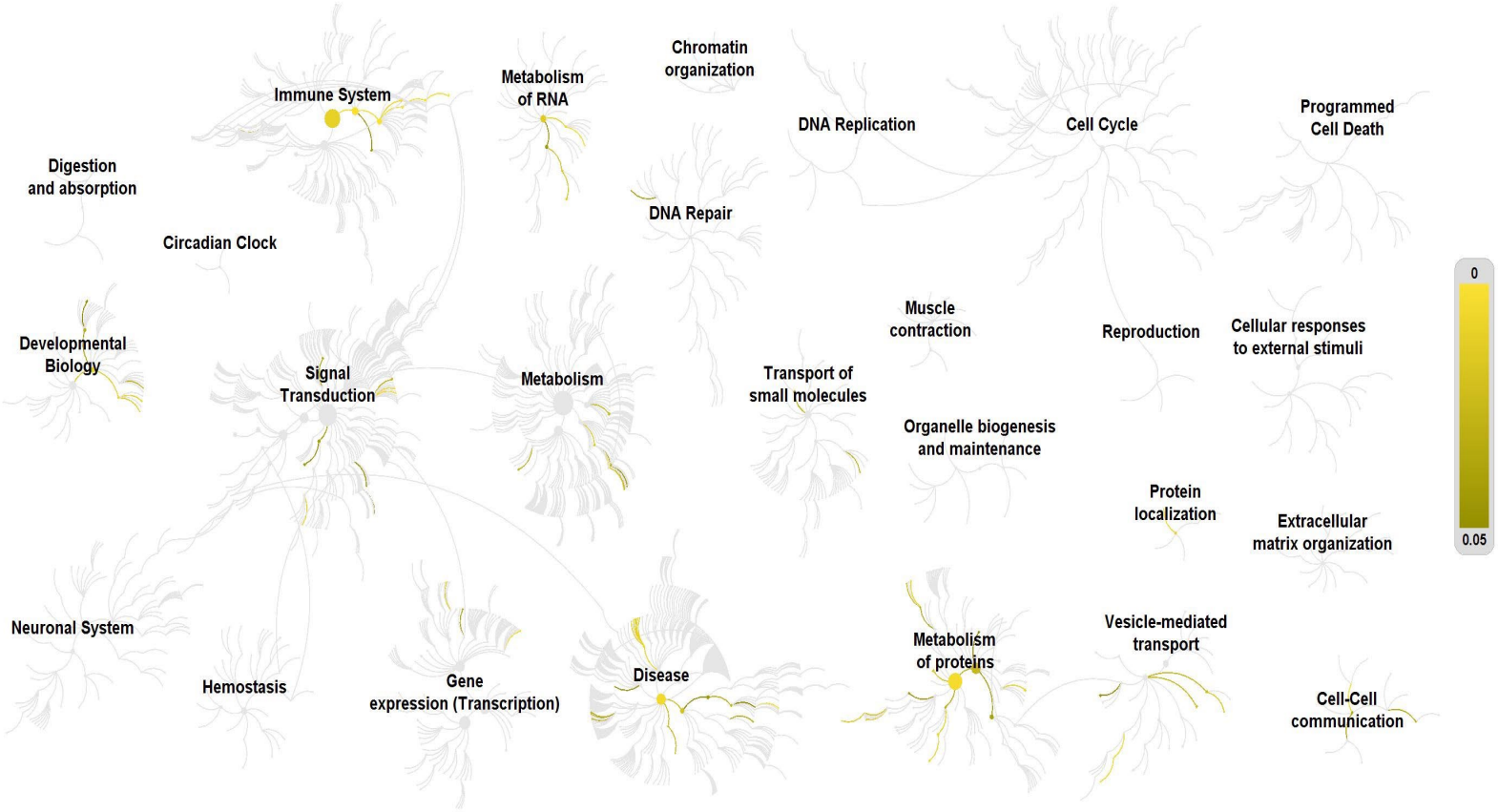
Immune System
Metabolism of RNA
Chromatin organization
DNA Replication
Cell Cycle
Programmed Cell Death
Digestion and absorption
DNA Repair
Circadian Clock
Developmental Biology
Signal Transduction
Metabolism
Transport of small molecules
Muscle contraction
Reproduction
Cellular responses to external stimuli
Organelle biogenesis and maintenance
Protein localization
Extracellular matrix organization
Neuronal System
Hemostasis
Gene expression (Transcription)
Disease
Metabolism of proteins
Vesicle-mediated transport
Cell-Cell communication
0
0.05

b

Pathway name	Entities				Reactions	
	found	ratio	p-value	FDR*	found	ratio
Gene and protein expression by JAK-STAT signaling after Interleukin-12 stimulation	8 / 73	0.005	8.95e-08	4.48e-05	4 / 36	0.003
Interleukin-12 signaling	8 / 84	0.006	2.57e-07	6.43e-05	4 / 56	0.005
Interleukin-12 family signaling	8 / 96	0.007	6.96e-07	1.16e-04	4 / 114	0.009
Signaling by Interleukins	17 / 641	0.045	5.09e-06	6.37e-04	9 / 492	0.041
Cell-extracellular matrix interactions	3 / 19	0.001	4.09e-04	0.035	2 / 10	8.25e-04
Vpr-mediated induction of apoptosis by mitochondrial outer membrane permeabilization	2 / 4	2.83e-04	4.28e-04	0.035	1 / 2	1.65e-04
Keratan sulfate/keratin metabolism	4 / 52	0.004	6.48e-04	0.046	5 / 16	0.001
Cytokine Signaling in Immune system	18 / 1,056	0.075	7.52e-04	0.047	14 / 640	0.053
AUF1 (hnRNP D0) binds and destabilizes mRNA	4 / 56	0.004	8.52e-04	0.047	4 / 4	3.30e-04
Mitochondrial protein import	4 / 69	0.005	0.002	0.087	7 / 14	0.001
TFAP2A acts as a transcriptional repressor during retinoic acid induced cell differentiation	2 / 9	6.36e-04	0.002	0.087	2 / 7	5.78e-04
Signaling by BRAF and RAF fusions	4 / 72	0.005	0.002	0.087	5 / 5	4.13e-04
RHO GTPases activate IQGAPs	3 / 36	0.003	0.003	0.097	5 / 5	4.13e-04
Formation of annular gap junctions	2 / 11	7.77e-04	0.003	0.105	2 / 2	1.65e-04
Metabolism of proteins	29 / 2,354	0.166	0.003	0.105	98 / 890	0.073
RHO GTPases Activate WASPs and WAVEs	3 / 41	0.003	0.004	0.107	7 / 10	8.25e-04
Gap junction degradation	2 / 12	8.48e-04	0.004	0.107	4 / 4	3.30e-04
Interleukin-10 signaling	4 / 86	0.006	0.004	0.107	2 / 15	0.001
Folding of actin by CCT/TriC	2 / 13	9.18e-04	0.004	0.107	2 / 2	1.65e-04
Disease	21 / 1,551	0.11	0.005	0.107	51 / 957	0.079
Oncogenic MAPK signaling	4 / 91	0.006	0.005	0.107	21 / 34	0.003
Signaling by high-kinase activity BRAF mutants	3 / 46	0.003	0.005	0.107	4 / 6	4.95e-04
Regulation of mRNA stability by proteins that bind AU-rich elements	4 / 93	0.007	0.005	0.107	4 / 26	0.002
MAP2K and MAPK activation	3 / 47	0.003	0.005	0.107	4 / 8	6.60e-04
XBP1(S) activates chaperone genes	4 / 95	0.007	0.006	0.113	2 / 47	0.004

Figure 29 – Gene onthology enrichment analysis. a) Visual representation of gene onthology enrichment analysis performed with Reactome (https://reactome.org/). Reactome pathways are arranged in hierarchies. Each center is the root of one toplevel pathway. In yellow the significantly enriched pathways (scale bar on the right). **b)** List of enriched pathways. Immune-related pathways are framed in orange.

4.2.6. Acute stress triggers Fkbp51-dependent secretion of Il-1b and Ctsd *in vivo*

Given the results obtained *in vitro*, an *in vivo* analysis of the stress effect on hippocampal cellular secretion was conducted. *In vivo* hippocampal microdyalisis was performed while animals were subjected to foot-shock. This procedure was performed with WT and Fkbp51 KO mice. Microdyalisate fractions were collected at baseline (three fractions), during footshock (FS; one fraction) and after footshock (post-FS; two fractions). As an established cargo of secretory autophagy, and in consistency with the previous experiments, Il1b was analyzed in the microdialysate fractions. Additionally, cathepsin d (Ctsd), another secretory autophagy cargo, described by Kimura and colleagues (Kimura et al., 2017), was measured.

Dialysate fractions were analyzed via capillary electrophoresis and subsequent UV-linking (Wes, ProteinSimple). Results revealed an increase in Il1b and Ctsd levels after footshock, which is in line with the *in vitro* data described previously (fig. 30 a, b). This increase was strongly diminished in the Fkbp51 KO animals (fig. 30 a, b), indicating that stress-induced secretion of Il1b and Ctsd is mediated by Fkbp51. To assess that secretion was dependent on the autophagic machinery, microdyalises were performed in animals treated with the autophagy inhibitor MRT 68921, an Ulk1-inhibitor confirmed to pass the blood brain barrier. Saline was applied to the control group. A significant increase in both Il1b and Ctsd was determined in the vehicle group after footshock (fig. 30 c, d). This enhancement was strongly impaired in mice treated with the autophagy inhibitor (AI; fig. 30 c, d). These data corroborated and reinforced the *in vitro* findings showing that, not only Dex, but also *in vivo* stress had a strong effect on autophagy-dependent secretion of Il1b and Ctsd.

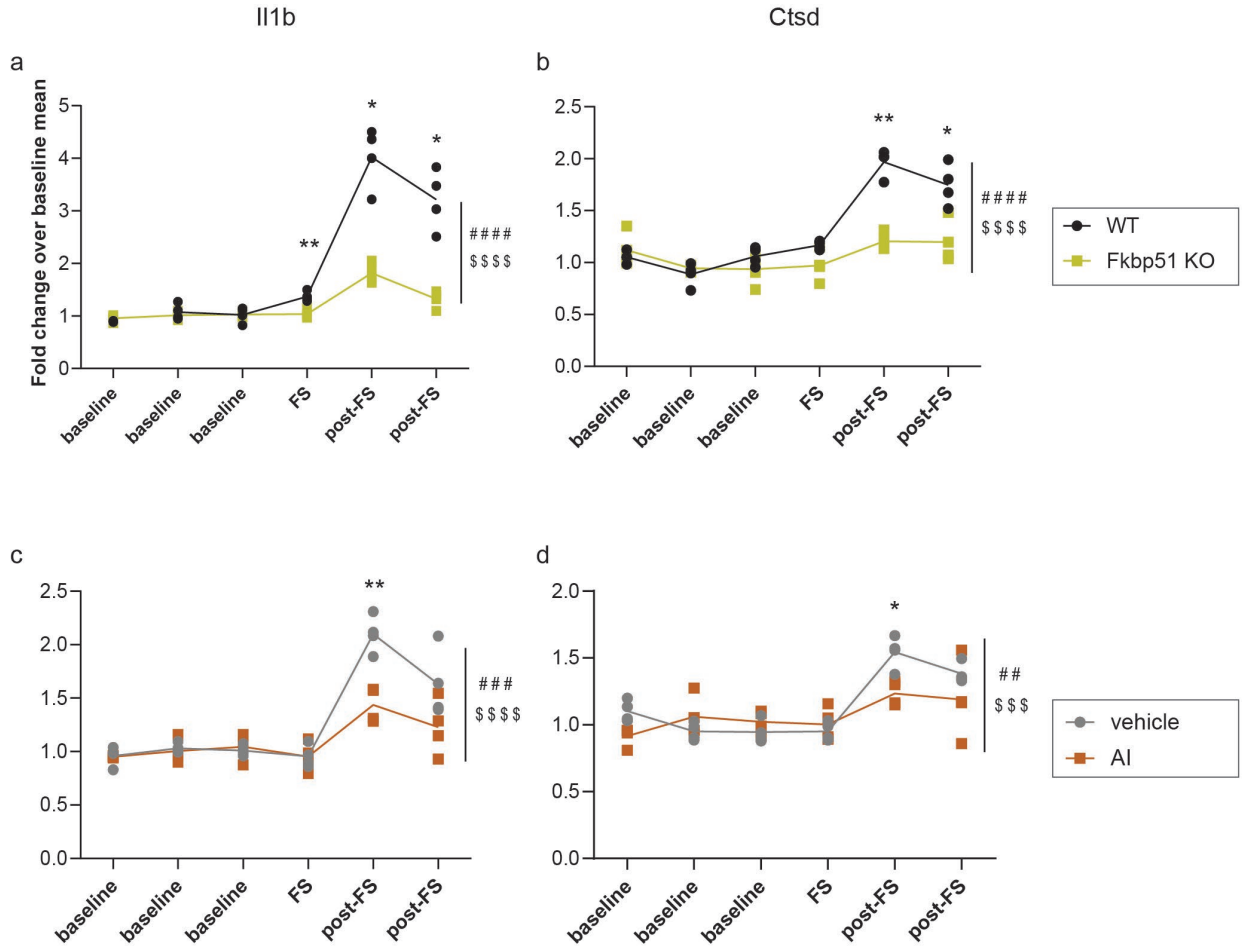

Figure 30 – Effect of stress on autophagy-dependent hippocampal secretion of Il1b and Ctsd. ProteinSimple quantifications of **a)** Il1b and **b)** Ctsd derived from in vivo hippocampal microdyalises of WT and Fkbp51 KO mice. ProteinSimple quantifications of **c)** Il1b and **d)** Ctsd derived from *in vivo* hippocampal microdyalises of vehicle and autophagy inhibitor MRT 68921 i.p. injected mice. *P < 0.05, **P < 0.01. Sidak's multiple comparison test. # and $ refer to time x genotype/treatment and time only factors respectively resulting from two-way ANOVA analyses. Error bars expressed in SEM.

4.2.7. Secretory autophagy as drug target

The obtained results reveal that psychological stress enhances secretory autophagy, and, thus, possibly neuroinflammation. Given the central role of Fkbp51 in the regulation and mediation of the effect of stress on secretory autophagy, pharmacological targeting of this protein was tested. For this purpose, the microglia cell line SIM-A9 was treated with the Fkbp51 ligand, SAFit1 or vehicle as control. In addition, cells were treated with Dex or vehicle for four hours. Il1b secreted in the media was analyzed via ELISA. Quantifications indicated that SAFit1 treatments impaired the Dex-induced Il1b secretion (fig. 31).

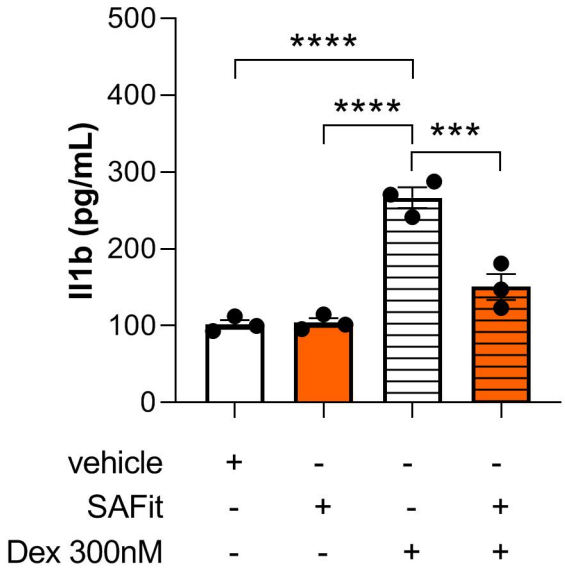

Figure 31 – Quantification of IL1B via ELISA assy. Il1b from supernatants was measured via ELISA after SIM-A9 cells were treated with veicle, SAFit, 100nM Dex and 300nM Dex + SAFit for 4 hours. ***P< 0.001; ****P< 0.0001. Tukey's multiple comparison test. Not displayed comparisons were not significant. Error bars expressed in SEM.

These results not only confirm that Fkbp51 is essential to mediate the effect of Dex on secretory autophagy, but also that Fkbp51 could be a potential target for anti-inflammatory therapy.

4.3. Characterization of FKBP51 isoforms and functions

The presented results, in accordance to the literature, highlight the large variety of cellular pathways in which FKBP51 is implicated and unravel the vastness of stress effect. Nevertheless, to date, very few studies have focused on the two isoforms of FKBP51 and their potentially different roles in the regulation of cellular functions. To fill this gap, I characterized *FKBP5*/51 splicing variants and the resulting isoforms.

4.3.1. Expression dynamics of *FKBP5* splicing variants in response to dexamethasone

In order to characterize the different transcriptional variants and protein isoforms of FKBP51, their expression levels were first determined via real time quantitative polymerase chain reaction (RT-qPCR), using material from HeLa cells (fig. 32).

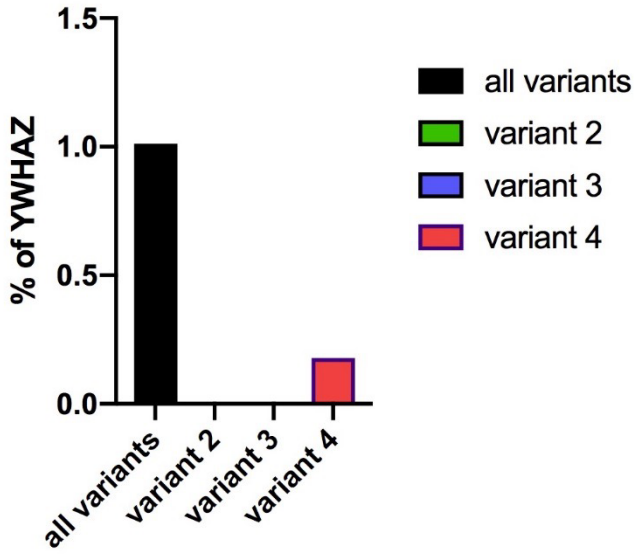

Figure 32 – RT-qPCR of FKBP51 variants at baseline. RT-qPCR quantification of FKBP51 variants expressed as percentage of the housekeeper YWHAZ in HeLa cells.

Results evidenced the absence of variants 2 and 3. Low but measurable levels of variant 4 could be detected. The highest signal was detected by using probes spanning all *FKBP5*-variants. This indicates that large part of this signal derives from variant 1 expression. These results are in line with online expression data (https://gtexportal.org).

At next, expression dynamics of the splicing variants were analyzed in response to Dex. For this purpose HeLa cells were exposed to 100 nM Dex or vehicle for 2, 4, 6, 12 and 24

hours, and transcription levels of the different variants were analyzed via RT-qPCR (fig. 33 a). Due to the lack of sequence unicity for variant 1, probes spanning variants 1, 2 and 3 were used. Considering the absence of variants 2 and 3, the observed signal was assumed to correspond to variant 1 and will be referred to as variant 1 from here on.

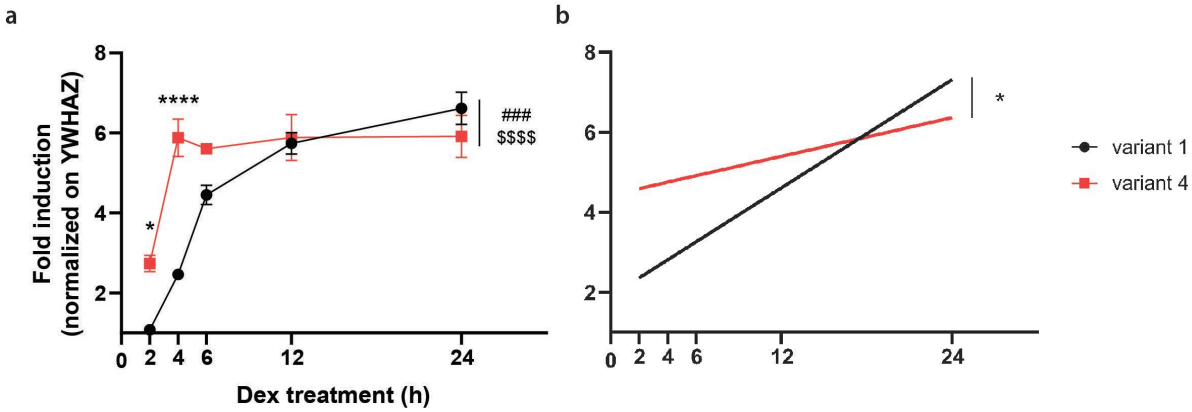

Figure 33 Expression dynamic of FKBP51 variants in response to Dex a) RT-qPCR quantification of FKBP51 variants, expressed as fold induction of Dex-treated over vehicle-treated, normalized on the housekeeper YWHAZ, of HeLa cells treated with 100nM Dex or vehicle for 24 hours. **b)** Linear regression of b. *P < 0.05 ***P < 0.001, ****P < 0.0001. Sidak's multiple comparisons test. # and $ refer to time by condition and time only factor respectively of two-way ANOVA test. Significance of the comparison between the linear regression lines resulted from the linear regression analysis.

The expression of both variant 1 and 4 was significantly increased in response to Dex across time. Interestingly, despite having lower expression at basal levels, variant 4 showed an increased response ratio over vehicle compared to variant 1 at early time points (significantly different at 2, 4 and 6 hours). Furthermore variant 4 showed a more immediate response to Dex than variant 1: variant 4 levels were significantly increased already after two hours of treatment while at the same time point variant 1 was still expressed at baseline levels. This faster dynamic could be observed throughout the measured time course. In fact, variant 4 showed an early peak at 4 hours and a following steady slope, while variant 1 expression was reflected in a slowly increasing curve up to 24 hours. This difference is visually summarized with the linear regression lines that show a significant difference (fig. 33 b).

4.3.2. Degradation of FKBP51 protein isoforms

With regard to the findings observed in expression dynamics, proteins half-lives were determined at next. To assess the protein stability of the two FKBP51 isoforms, a pulse-chase approach was used. HeLa cells were transfected with Halo-Tag (HT) plasmids coding

for either isoform 1 or 2. 24 hours later, cells were tagged with a cell permeable halogenated fluorophore 16, 8, 4 and 2 hours before harvesting. After harvesting the cells, proteins were extracted and subjected to western blot, and fluorescence intensity was measured on nitrocellulose membrane (fig. 34). Results indicated that isoform 2 was degraded faster with a half-live of four hours, while isoform 1 reached 50% of degradation only after 8 hours (fig. 34).

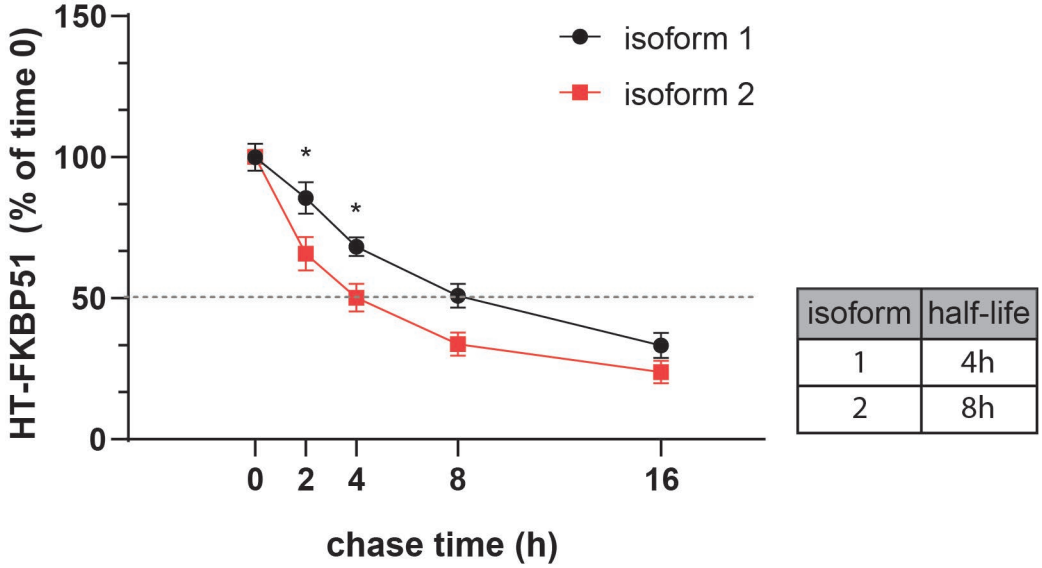

Figure 34 – Degradation dynamics of FKBP51 isoform 1 and 2 Pulse chase assay of FKBP51 isoform 1 and 2 of HeLa cells transfected with HT-isoform 1 or HT-isoform 2, pulsed with a fluorophore and chased for 2, 4, 8, and 16 hours. Quantifications were made from western blots. *P < 0.05. Sidak's multiple comparisons test.

Together with the expression dynamics, these data suggest a faster turnover of variant 4/isoform 2 compared to variant 1/isoform1.

4.3.3. Intracellular localization of isoform 1 and 2

The scarcity of information available regarding FKBP51 intracellular localization appears to be highly dependent on antibodies used for detection (https://www.proteinatlas.org), while no information is available for the different isoforms. To gain more insight about the cellular role of FKBP51, intracellular localization of both isoforms was analyzed. Due to the lack of commercially available or specific enough antibodies for FKBP51 isoform 2, and to avoid potential artifacts deriving from immunocytochemical processing, HeLa cells were transfected with plasmids coding for GFP-tagged isoforms 1 or 2. A plasmid expressing only GFP was used as control. Cells were live imaged with epifluorescent microscopy 24 hours

after transfection (fig. 34). Resulting images showed ubiquitous signal from the control-transfected cells. Isoform 1 presented a cytoplasmic accumulation, while isoform 2 showed a distinct subnuclear (probably nucleolar) localization.

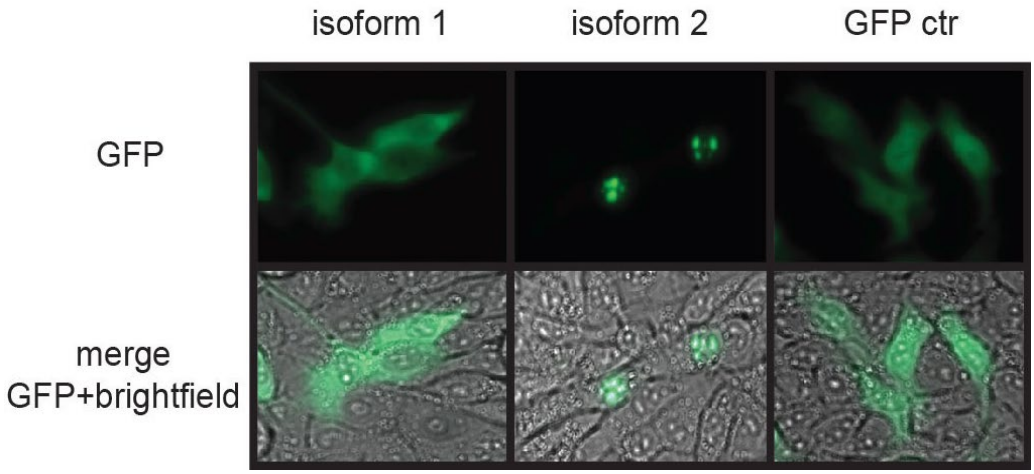

Figure 34 – Subcellular localization of FKBP51 isoform 1 and 2. Epifluorescent and bright field imaging of HeLa cells transfected with GFP-tagged FKBP51 isoform 1, GFP-tagged FKBP51 isoform 2, or GFP-control vector 24 hours prior to imaging.

In addition to the imaging approach, to determine cellular localization the transfected cells were harvested and subjected to subcellular fractionation to separate nuclear from cytoplasmic proteins. Fractionation was validated via western blot analyses and GFP signal was quantified in both nuclear and cytoplasmic fractions (fig 35 a, b). Results showed clean fraction separation and quantification analyses confirmed a large enrichment of isoform 2 in the nucleus. Surprisingly isoform 1 appeared slightly more enriched in the nucleus after fractionation.

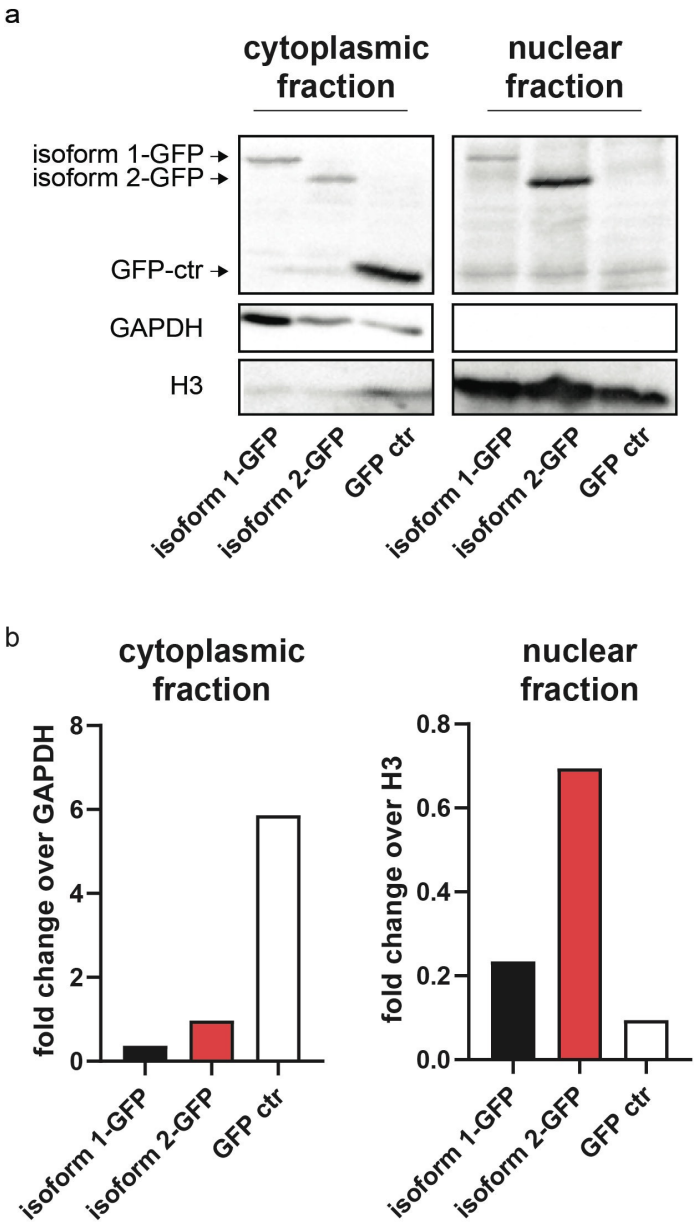

Figure 35 – Isoform 1 and 2 localization visualized by subcellular fractionation a) Subcellular fractionation of HeLa cells transfected with GFP-tagged FKBP51 isoform 1, GFP-tagged isoform 2 and GFP-vector as control followed by western blotting for GFP, GAPDH (cytoplasmic marker) and H3 (nuclear marker) in the cytoplasmic and nuclear fraction. **b)** Quantifications of western blots from a) normalized on GAPDH and H3 for cytoplasmic and nuclear fractions respectively.

4.3.4. Differential regulation of cellular pathways

The aim of the following part was to characterize the functional aspects of the two isoforms of FKBP51.

4.3.4.1. GR inhibition

In the previous parts I described that both *FKBP5* variants were responsive to Dex-dependent expression, which impacts the GR-FKBP51 interplay and can define a novel level of GR-regulation through FKBP51. In the following part I investigated whether the two isoforms possess a negative feedback function on GR.

Activity of the different isoforms on GR was assessed via GRE-driven reporter gene assays. HeLa cells were co-transfected with MMTV-Luc, a GRE-driven luciferase, and with a plasmid coding for either isoform 1, isoform 2 or an empty vector as a control. Cells were then treated with increasing concentrations of Dex, and luminescence was measured 48 hours after transfection (fig. 36). Cells overexpressing isoform 1 showed a significantly lower dose-response curve compared to cells overexpressing isoform 2 and controls, which, in turn, were perfectly overlapping. Isoform 1 desensitizes GR: higher concentrations of Dex were required to evoke GR activation.

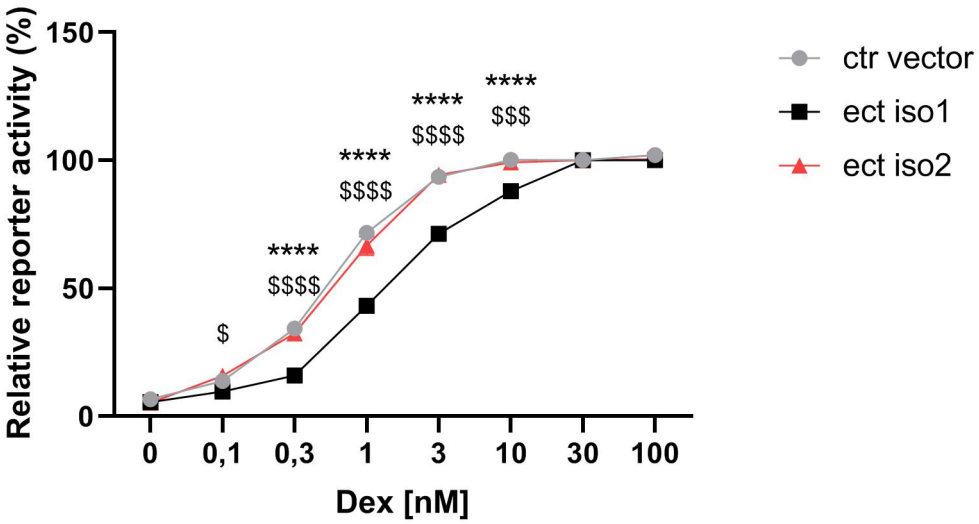

Figure 36 – Isoform 1- and 2-dependent effect of Dex on GRE activation. GRE-driven reporter gene assay performed in HeLa cells transfected with FKBP51 isoform 1 (ect iso1), FKBP51 isoform 2 (ect iso2) or an empty vector (ctr vector), treated with 0.1 nM, 0.3 nM, 1 nM, 3 nM, 10 nM, 30 nM, 100 nM or vehicle for 4 hours. *P < 0.05, ***P < 0.001, ****P < 0.0001. Turkey's multiple comparisons test. * and $ indicate comparisons between ctr vector and ect iso 1 and between ect iso1 and ect iso 2 respectively. Error bars expressed in SEM.

To confirm these findings, the reporter-gene assay was repeated with FKBP51 KO cells. CRISPR-Cas 9 approach was used to selectively ablate isoform 1 (iso 1 KO) or both isoforms (full KO) in HeLa cells using specific guide RNAs (fig.37).

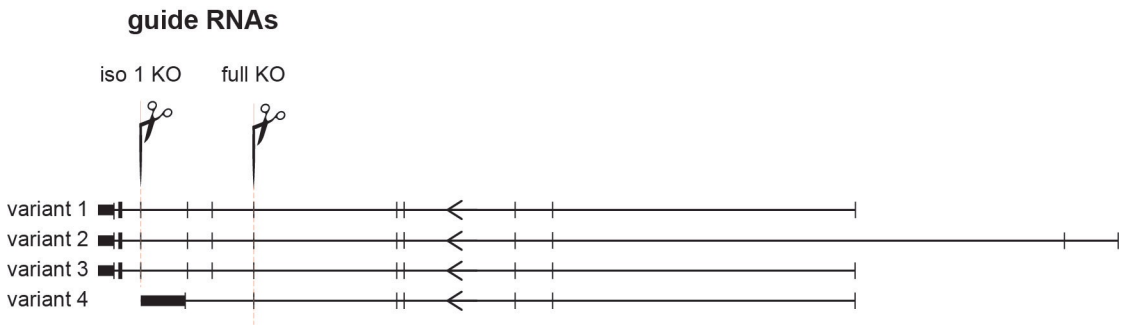

Figure 37 – Schematic visualization of gRNA targeting variants 1-3 or variants 1-4 of FKBP51. Target *loci* of gRNA targeting variants 1-3 and all variants used to generate HeLa FKBP51 full KO and isoform 1 KO respectively.

WT, full KO and isoform 1 KO cells were transfected with MMTV-Luc and, after 48 hours, treated with increasing concentrations of Dex. After 4 hours, luminescence intensity was measured (fig. 38). The resulting dose-response curve of the full KO and isoform 1-KO were overlapping and both showed increased activity compared to WT. This result suggests that the lack of isoform 1 allows lower concentration of Dex to activate GR, and that isoform 2 alone (isoform 1 KO) is not able to rescue this effect.

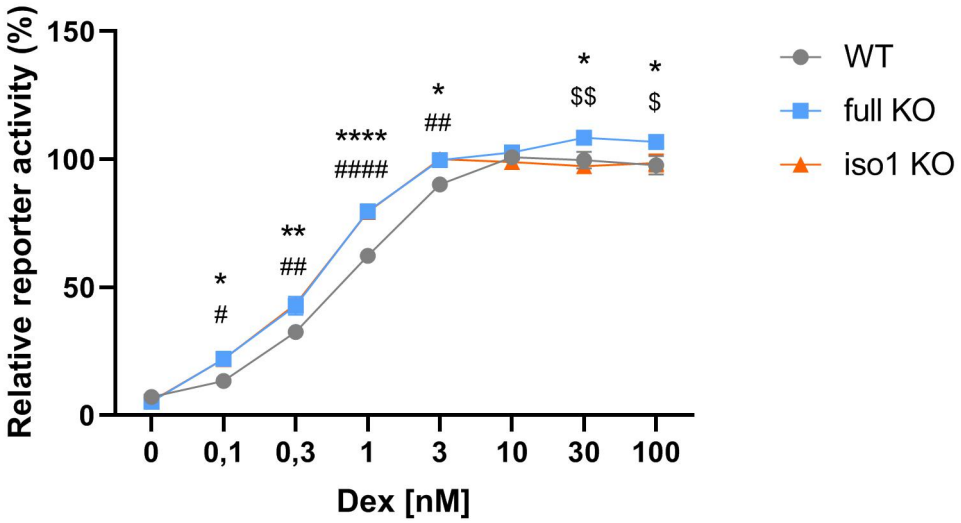

Figure 38 – Isoform 1- and 2-dependent effect of Dex on GRE activation. GRE-driven reporter gene assay performed in HeLa cells WT, lacking both isoforms of FKBP51 (full KO) or lacking isoform 1 only (iso 1 KO), treated with 0.1 nM, 0.3 nM, 1 nM, 3 nM, 10 nM, 30 nM, 100 nM or vehicle for 4 hours. *P < 0.05, **P < 0.01, ****P < 0.0001. Turkey's multiple comparisons test. * and # express comparison of WT with full KO and iso 1 KO respectively; $ refers to comparison between full KO and iso 1 KO. Error bars expressed in SEM.

Taken together, the results of both reporter-gene assays indicate that isoform 1 alone, and not isoform 2, has an inhibitory function on GR.

4.3.4.2. Macroautophagy regulation

As known from the literature, and seen in the previous results, another very important protein regulated by FKBP51 is AKT. As discussed throughout this thesis, autophagy is a major regulator of cellular homeostasis, and as demonstrated previously, it is responsive to GCs via FKBP51 (previous results for secretory autophagy and CMA; Gassen et al. 2014 for macroautophagy). In the following part, the role of the two isoforms of FKBP51 was analyzed on macroutophagy.

Upstream regulation of autophagy is tightly controlled by the kinase AKT. AKT (activated when phosphorylated) inactivates the autophagy initiator Beclin 1 via phosphorylation. In turn, AKT can be inactivated through dephosphorylation by the phosphatase PHLPP. This process is mediated by FKBP51.

Isoform 1, 2 or an empty vector as control was overexpressed in HeLa cells, and different actors and downstream effectors of the macroautophagy pathway were analyzed via western blot. Quantifications of the phosphorylated AKT showed that overexpression of both isoform 1 and 2 led to a decreased phosphorylation of AKT (pAKT) compared to control (fig. 39).

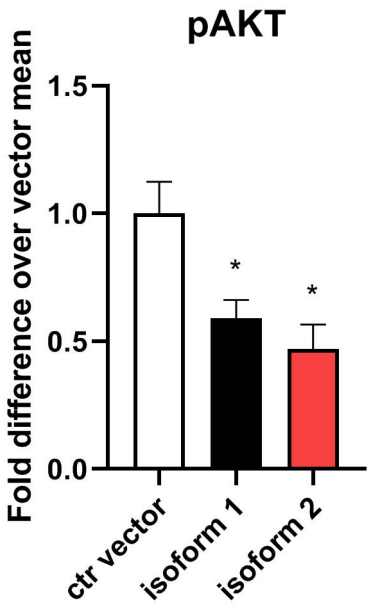

Figure 39 – Effect of FKBP51 isoforms on AKT phosphorylation. a) Quantification of western blots analyses for pAKT normalized on total AKT from HeLa cells transfected with FKBP51 isoform 1, FKBP51 isoform 2 or an empty vector. *P < 0.05. Mann-Whitney test. * indicates comparisons with ctr vector. Error bars expressed in SEM

Decreased pAKT leads to an enhanced autophagy. Therefore, the following autophagic markers were analyzed: Beclin1, upstream regulator of autophagy and modulated directly by AKT, ATG12, involved in expansion of autophagososmes, and LC3BII (lipidated form of LC3B-I), marker of autolysosome formation.

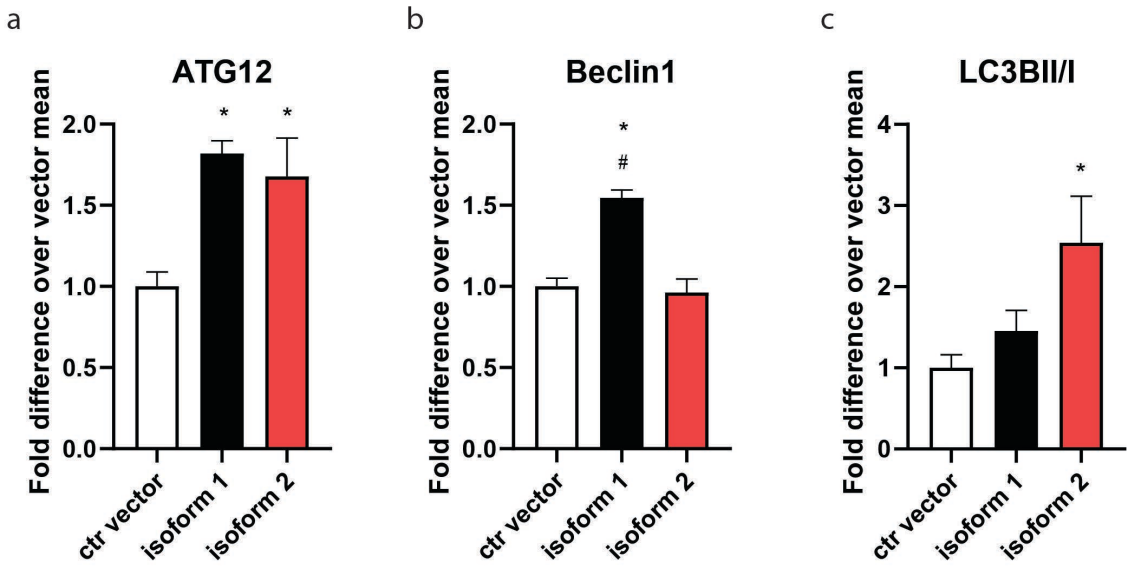

Figure 40 – Effect of FKBP51 isoforms on autophagy markers. Quantification of western blots analyses for **b)** Beclin1, **c)** ATG12 and **c)** LC3BII/I ratio from HeLa cells transfected with FKBP51 isoform 1, FKBP51 isoform 2 or an empty vector. *P < 0.05. Mann-Whitney test. * and # indicate comparisons with ctr vector and isoform 2 respectively. Error bars expressed in SEM.

Overexpression of isoform 1 led to an increase of Beclin1 and ATG12. Interestingly, overexpression of isoform 1 did not lead to an increase of LC3BII (normalized on LC3BI). Furthermore, overexpression of isoform 2 did not affect levels of Beclin1, but lead to increased ATG12 and LC3BII/I.

4.3.4.3. NFAT regulation

Data presented so far indicate the importance of the effect of stress on the immune function. A possible link via the regulation of secretory autophagy by FKBP51 was revealed. Another way to regulate the immune response through FKBP51, though, is the modulation of Calcineurin-NFAT signalling (T.-K. Li et al. 2002). FKBP51 isoform 1 overexpression leads to an increased phosphorylation and thus to inhibition of NFAT. The role of isoform 2 on this pathway was here analyzed.

For this purpose, the immortalized human T lymphocyte cell line Jurkat was used. Plasmids coding for isoforms 1 or 2 of FKBP51 were overexpressed and pNFAT levels were analyzed via western blot. As expected, quantifications revealed an increase of pNFAT when overexpressing isoform 1. Conversely, overexpression of isoform 2 did not affect pNFAT levels compared to control (fig. 41).

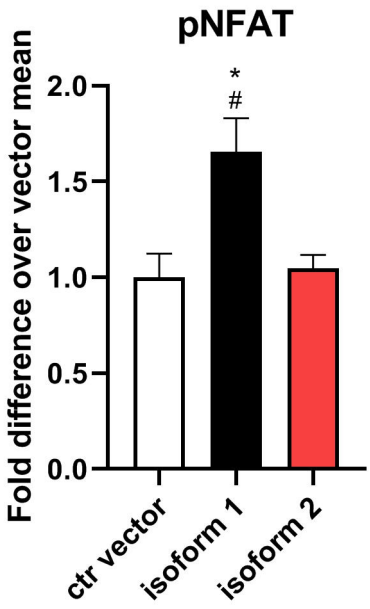

Figure 41 – Effect of FKBP51 isoforms on NFAT phosphorylation. Quantification of western blots analyses from HeLa cells transfected with FKBP51 isoform 1, FKBP51 isoform 2 or an empty vector, for pNFAT normalized on total NFAT. *P < 0.05. Mann-Whitney test. * and # indicate comparisons with ctr vector and isoform 2 respectively. Error bars expressed in SEM.

4.3.4.4. Regulation of DNA methylation

DNA methylation is a genome-wide mechanism to regulate gene expression that can be environmentally modulated. Gassen and colleagues found that FKBP51 modulates DNA methytransferase 1 (DNMT1) activity via phosphorylation in response to antidepressants, affecting genome-wide methylation levels.

To test the effect of the two FKBP51 isoforms on the phosphorylation (*i. e.* activation) levels of DNMT1 (pDNMT1), isoforms 1 or 2 of FKBP51 were overexpressed in HeLa cells. pDNMT1 was detected via western blot analysis and normalized to total DNMT1 (fig. 42). Quantifications indicated a large reduction of pDNMT1 in the presence of isoform 1 overexpression. Contrarily overexpression of isoform 2 did not affect DNMT1 phosphorylation compared to control.

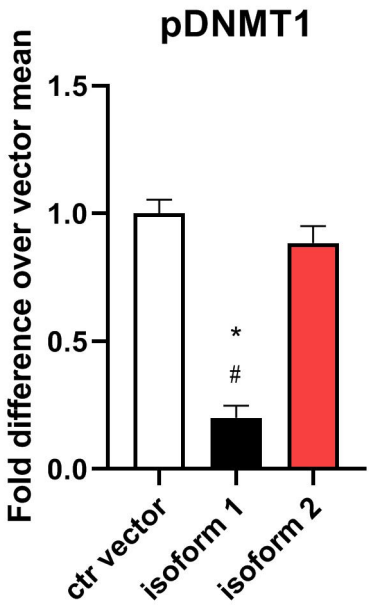

Figure 42 – Effect of FKBP51 isoforms on NFAT phosphorylation. Quantification of western blots analyses from HeLa cells transfected with FKBP51 isoform 1, FKBP51 isoform 2 or an empty vector, for pDNMT1 normalized on total DNMT. *P < 0.05. Mann-Whitney test. * and # indicate comparisons with ctr vector and isoform 2 respectively. Error bars expressed in SEM.

Overall, these data revealed that the two FKBP51 isoforms can have equivalent or opposite effects. The reasons behind this and the possible implications will be examined in the discussion part.

5. Discussion

Autophagy is one of the most evolutionarily conserved cellular mechanisms. It is a catabolic process that can be activated through cellular stressors like starvation or oxidative stress. The cell self-digests its components in order to maintain the correct homeostasis of proteins, protein complexes and organelles. Interestingly, Gassen and colleagues established a molecular link between stress signaling via the GR and autophagy activation (Gassen et al., 2014). In this study, the stress responsive protein FKBP51 is presented as a scaffolder and key driver of a regulatory protein heterocomplex essential for autophagy initiation. The possible link between stress signaling and homeostasis regulation mediated by FKBP51 motivated me to further explore the effect of stress on two more specialized types of autophagy: chaperone-mediated autophagy, a protein-selective lytic process, and secretory autophagy, a more recently described mechanism that leads to the secretion of cytosolic material. Interestingly, and in line with the study described above, my results could show that GR activation does enhance both analyzed pathways. This underlines the important role stress may play on cellular and protein homeostasis (proteostasis). My proposed model is in line with recent theories delineating that disbalanced proteostasis might underlie chronic mental illnesses (Bradshaw and Korth, 2018). These unraveled mechanisms also highlighted the need to further characterize FKBP51. For this reason I investigated the expression and degradation dynamics of *FKBP5*/51's splicing variants and protein isoforms, their intracellular localization and the differential roles they play in specific cellular pathways. The results revealed different kinetics, localization and domain-dependent roles of the two isoforms, highlighting the importance of a deeper investigation of FKBP51 to fully understand the molecular mechanisms underlying the regulation of stress response.

5.1. Effect of stress on Chaperone Mediated Autophagy (CMA)

CMA is characterized by its selectivity. Target proteins are identified by HSC70 through a specific amino acid sequence and are transported directly to the lysosome surface (Chiang et al., 1989). Here, the assembly of the multimeric complex, regulated by LAMP2A, leads to the translocation of the substrate protein into the lysosome lumen where it is degraded by

proteases. The activity of CMA is tightly controlled by AKT, which inhibits the translocation complex assembly via phosphorylation of GFAP. In turn, AKT is inhibited or activated respectively by PHLPP and mTORC2, which can be considered as the upstream regulators of CMA. CMA is constitutively active at low levels, but is enhanced upon cellular stress (hypoxia, starvation, oxidative stress). In this study, I could demonstrate that stress mediated by GR-signaling is able to enhance CMA, analogously to cellular stress. The first results obtained with pulse-chase experiments, show a great effect of the synthetic GR agonist Dex on the degradation of known CMA targets, which resulted to be both CMA (LAMP2A)- and FKBP51-dependent (fig. 1). A more attenuated effect of the LAMP2A KD (no significance between ctr Dex and KD Dex for MEF2D) might rely on the fact that the elimination of LAMP2A was not complete and low levels of CMA activity might have persisted. The co-IP experiments performed on extracted lysosomes could confirm the underlying hypothesized mechanism that presents FKBP51 as a scaffolder for the interaction between PHLPP and AKT, promoting CMA activation. A minor mitochondrial contamination in the lysosomal extracts, represented by the AIF signal, could have been a possible interference in the analysis of the results, but the enhanced AKT signal in the lysosomal fraction, indicates that this enrichment can only be attributed to lysosomes. Furthermore, FKBP51 has been described to localize in the mitochondria where it plays an anti-oxidative role in complex with GR and PKA, but no evidence suggest an involvement of AKT. This indicates that the AKT-FKBP51 interaction, observed with the co-IP, can be specifically attributed to lysosomes.

The successive analysis of the proteome-wide effect of GR activation on CMA-mediated protein degradation, revealed a surprisingly large degradation in response to stress. Almost 70% of the detected proteins resulted degraded in response to Dex via CMA. Yet, it needs to be considered that the observed results describe the degradation effect omitting novel synthesis. This approach reveals proteins that are regulated via CMA, but it overestimates the actual net effect. Additional examinations of the CMA net effect (including the protein synthesis and observing the total balance), might indicate more precise implications of this regulatory mechanism. Possibly, within this detected pool of proteins, subsets of targets are degraded in dependence of the cell type or the stress stimulus. This hypothesis is supported by the example of SNCA, a protein regulated via CMA and whose aberrant degradation specifically in the brain, is implicated in Parkinson´s disease (Cuervo et al., 2004; Ho et al.,

2019). Furthermore, stress-triggered regulation of CMA may not only unravel molecular mechanisms contributing to psychiatric or neurodegenerative disorders, but also constitute a possible target for novel medications. In fact, therapeutic activation of CMA has been considered as a possible treatment for Parkinson´s disease (Ho et al., 2019). Further functional enrichment analyses, performed on differentially regulated proteins, indicate a high enrichment of Dex-induced, CMA-regulated proteins in synaptic plasticity and neurotransmitter release signaling (fig. 9 and 10). These findings suggest a direct link between proteostasis, neuronal plasticity and synapse formation. Hakim and colleagues highlighted the importance of proteostasis in synaptic functions focusing on ubiquitin-proteasome system (UPS)-mediated degradation of synaptic proteins. Their findings implicate that the main driver for synaptic proteostasis must be a mechanism other than the UPS (Hakim et al., 2016). I suggest that such mechanism is, at least in part, CMA. For my study, the neuroblastoma SH-SY5Y cell line was chosen in order to have a background that was as neuronal as possible, with the advantage of an easy-to handle, human cell line. In fact, most of the studies conducted so far on CMA have used rodent models. For further investigations, human induced pluripotent stem cell (hiPSC)-derived neurons could better highlight human neuron-specific proteins regulated by CMA. In addition, investigation of the synaptic proteome, complemented by functional analysis methods such as electrophysiology, could unveil the suggested role of CMA in synaptic proteostasis and plasticity.

5.2. Stress affects secretory autophagy

Supporting the model that describes GR activation as a trigger of proteostasis regulation, the results of the here presented study indicate that stress enhances secretory autophagy. Via an unbiased proteomic approach, SEC22B, the main regulator of secretory autophagy (Kimura et al., 2017), was identified as novel binding partner of FKBP51 (fig. 12). *In vitro* experiments confirmed that FKBP51 is a component and essential player of the assembly of the SNARE complex regulating the membrane fusion in secretory autophagy. Furthermore, Dex treatment led to enhanced interactions within the SNARE complex (fig. 19). Even though FKBP51 was shown not to affect the interaction between TRIM16 and the cargo protein IL1B, and between TRIM16 and SEC22B, the Dex treatment resulted in a lower interaction between TRIM16 and IL1B. An explanation for this is an increased flow of

secretory autophagy, triggered by Dex, for which IL1B is secreted at higher rates, causing a detachment between IL1B and its receptor TRIM16.

Several studies suggest that macro- and secretory autophagy are triggered by lysosomal damage (Chauhan et al., 2016; Jia et al., 2018, 2019; Kimura et al., 2017; Maejima et al., 2013). Thus, lysosomal integrity and the related expression of galectins were tested. Galectins are cytosolic lectins, able to recognize lysosomal membrane damage by binding to luminal β-galactosides from glycoconjugates exposed to the cytosol upon membrane damage. GAL3 and GAL8 have been found to recruit autophagic receptors on the damaged site and transport the cargo to autophagosomes (Chauhan et al., 2016; Thurston et al., 2012). Using western blot analyses, I have found increased levels of GAL8 upon Dex treatment, which indicate increased lysosomal damage. Furthermore, co-IP experiments indicated that GAL8 interacts with FKBP51 and that this interaction is HSP90-dependent (fig. 21). These results suggest that FKBP51 is recruited on damaged lysosomes and bridges the fusion to autophagosomes via SEC22B. Experiments using the tfGal3 construct to monitor damaged lysosomes confirmed that Dex stimulation indeed leads to decreased lysosomal integrity (fig. 23). In line with these results, ELISA assays performed in murine microglia cells, analyzing the known cargo Il1b, showed that Dex treatment enhances Il1b secretion via secretory autophagy (fig. 25). Taken together these results indicate that Dex triggers secretory autophagy via FKBP51. To better understand the global impact of secretory autophagy activation, the secretome wide effect of Dex was tested with the use of Atg5 KO cells. Atg5 is an autophagy–related protein shown to be essential for secretory autophagy (Kimura et al., 2017). Comparisons between WT and Atg5 KO samples showed a surprisingly high amount of proteins secreted via secretory autophagy even at basal levels (70% of the total detected proteins), although Dex stimulation increased this regulation (78% of the total detected proteins). Surprisingly, Dex treatment did not significantly affect protein secretion in WT cells, although a trend was detected. Interestingly, though, within the Atg5 KO samples, the trend seen in the WT upon Dex stimulation disappeared. This suggests that the observed trend is indeed resulting from the Dex treatment. In fact by blocking secretory autophagy, Dex does not have any effect on protein secretion anymore. A plausible reason underlying the lack of significance might be a high basal activity. A technical aspect that might explain the high secretory autophagy levels is that the metabolic labeling used for protein enrichment can stress the cells if applied for a long time. I incubated the cells for 12

hours in order to label as many proteins as possible without having evident toxic effects. This could be a limiting factor, without which the differentially regulated proteins by secretory autophagy would have been more, and the Dex effect in the WT group would have probably been stronger. Furthermore, mass spectrometry is a potent tool for wide-scale analyses; nevertheless it is less sensitive than single protein analyses methods such as ELISA or western blot. In fact, Il1b was not detected in the secretome analysis, indicating insufficient sensitivity of the method. This limitation, however, suggests an underestimation of the observed effect, strengthening these results.

5.3. Secretory autophagy as mechanism underlying the interplay between stress and immune response

The microglia cell line SIM-A9 was chosen because several studies revealed that secretory autophagy plays an important role in the extracellular signaling of immune response. Microglia cells constitute between 5% and 10% of the total brain cells and are the main macrophages of the central nervous system (Aguzzi et al., 2013). Furthermore, the interplay between stress response and immune activation is of particular interest. Classically, stress has a suppressive effect on the immune system and it is known that this inhibitory effect is carried out by the HPA axis via GCs. Activation of GR can directly impair pro-inflammatory transcription by interacting with transcription factors NF-κB and AP-1 (Ratman et al., 2013), or, via GRE binding, enhancing or repressing transcription of anti- or pro-inflammatory genes respectively (Muzikar et al., 2009). Activation of the HPA axis, however, can also activate the immune system, enhancing the secretion of cytokines that promote different types of inflammatory responses (Takahashi et al., 2018). In fact, low doses of GCs can enhance the production of the macrophage migration inhibitory factor (MIF), a pro-inflammatory cytokine (Calandra et al., 1995). Moreover, the activation of inflammatory activity can be triggered by stress even in absence of infectious pathogens, via the HPA axis, as observed in case of depression (Audet et al., 2014). It has been shown that stressful experiences can increase levels of pro-inflammatory cytokines in the brain (Steptoe et al., 2007) either locally, secreted by activated microglia (Liu et al., 2014; Wohleb et al., 2015), or via systemic transport (Banks, 2006). To explain these opposite roles of GCs, Frank and colleagues (Frank et al., 2013) proposed a differential action of GCs depending

on timing and intensity of the stressor. During stress, when GC levels are increased, the resulting effect is anti-inflammatory, whereas during the recovery phase, when GC are decreasing to basal levels, there is a sensitization of the immune response. This model is supported by the observation of immune priming in microglia consequently to GC treatment (Frank et al., 2011). Along this line, further studies showed sensitization of the HPA axis and the immune response to subsequent LPS challenge greatly inducing central and peripheral pro-inflammatory activators after chronic and acute social disruptive stress (Gibb et al., 2013). This priming of the immune system by stress has also been suggested to mediate side effects such as allodynia (Loram et al., 2011) and drug abuse (Frank et al., 2011), and is proposed to be involved in major depression disorder (MDD) (Liu et al., 2014). It was therefore particularly interesting to find the Dex-triggered, autophagy-secreted proteins, resulting from the mass spectrometry analysis, to be highly enriched in the immune system pathways (fig. 29). These findings may unravel a global molecular mechanism underlying the link between stress and neuroimmune response. In particular, the effect of *in vivo* stress on hippocampal Il1b secretion highly supports this model. Further analyses analyzing inflammatory markers in the murine brains after stress exposure, would illustrate the hypothesized pathological effect of stress on neuroinflammation. Additionally, the treatment with the FKBP51 ligand SAFit not only reversed the effect of Dex, confirming FKBP51´s central role in stress-induced secretory autophagy, but also revealed itself as a promising, novel way to target neuroinflammation. The link between stress and immune system, however, is bidirectional. The immune system can, in fact, have a behavioral effect by modulating the HPA axis. Pro-inflammatory cytokines such as IL1B, interleukin 6 (IL6), and tumor necrosis factor α (TNFA) have been found to interfere directly with GR, inhibiting its negative feedback regulation on the HPA axis (Pace et al., 2007; Van Bogaert et al., 2010). Moreover, cytokines can also directly enhance the activity of the HPA axis by amplifying its feed forward signaling. IL1B and IL6 have been shown to amplify the stress effect on CRH and ACTH secretion respectively (Chover-Gonzalez et al., 1993; Mehet et al., 2012). Additionally, another study found that inhibition of IL1B receptor, decreases ACTH release in response to restraint stress, corroborating the proposition that cytokines may amplify stress-induced HPA axis activation (Gądek-Michalska et al., 2011). Therefore, not only psychological stress can lead to an increased immune activation, but also chronic inflammation can modify the HPA axis response and lead to psychiatric disorders

((Berkenbosch et al., 1987; Linthorst et al., 1994; Angeli et al., 1999). This suggests the existence of a possible positive feedback resulting from GR activation, via secretory autophagy. Further *in vivo* analysis investigating this circling effect might reveal additional information on this mechanism. In addition, analyses of inflammation markers in animal models or human post mortem tissues can deepen the understanding of downstream effects and clinical implications.

5.4. Effect of stress on proteostasis

As mentioned before, autophagy is one of the most evolutionarily conserved cellular responses to starvation. The cell self-digests its own components to provide nutrients in order to maintain essential cellular functions and to eliminate superfluous or damaged organelles, misfolded proteins, and invading micro-organisms (Levine and Kroemer, 2008). Here, I show that these energy-conservation and quality control processes can also be triggered by GR-mediated stress. A previous study showed that macroautophagy is triggered by GR activation (Gassen et al., 2014). Together with the current results showing the same effect on CMA and secretory autophagy, it can be implied that environmental stress has an effect on global proteostasis regulated by different autophagic pathways. As a transcription factor, GR has been in the focus for its role in transcriptional regulation. Here, however, an additional level of GR regulation was revealed: the activation of protein degradation and secretion. This dual function of GR might underlie a very sophisticated regulation process. Acute stress activates a complex machinery that triggers an appropriate response, and, in turn, holds the organism in its equilibrium state. My findings indicate that this regulatory mechanism is more complex than thought so far, and that proteostasis might be a central part of it. Enhanced transcription and translation of genes involved in stress response is counter-regulated by an increase in autophagy levels also triggered by GR activation itself. Numerous studies show that an inappropriate response to (chronic) stress can lead to psychiatric disorders for the development of which, a proportion of risk factors involve non-genetic causes. Bradshaw and colleagues summarize some evidences that lead to the hypothesis that aberrant proteostasis might underlie chronic mental illnesses in complement to the genetic causes (Bradshaw and Korth, 2018). My results are in line with this hypothesis: impaired stress response can lead to impaired proteostatic regulation, which could be complementary to or even resulting from genetic causes underlying

psychiatric disorders. In fact, an example of how a specific genotype could be strictly related to impaired stress response and homeostasis is *FKBP5*. The haplotype rs1360780 is associated with *FKBP5*'s expression levels and constitutes a risk factor for the development of different psychiatric disorders. Considering the role of FKBP51 in the different autophagic pathways, it appears clear that the *FKBP5* genotype can directly influence proteostasis. This constitutes a possible mechanism underlying the link between genetics and psychiatric disorders.

A very interesting and central aspect of the GR-induced regulatory mechanism is the dynamic between lytic and secretory autophagy, and the effect of stress on it. In fact, acute stress leads to activation of macroautophagy, CMA and secretory autophagy. Experiments with the tfGal3 construct, however, demonstrate that Dex stimulation induces lysosomal damage. Prolonged GR activation, as occurs in chronic stress and different psychiatric disorders, may cause a switch from lytic to secretory autophagy. In fact, damaged lysosomes are not functional for macroautophagy and CMA anymore, and are discarded via secretory autophagy. This process leads not only to an accumulation of cellular waste, because all the autophagic burden is derailed on the overloaded secretory autophagy, but also leads to a lack of recycling, since secretory autophagy only discards the collected material. As a consequence, protein aggregates and disrupted organelles accumulate in the cell, and building blocks for novel synthesis are at scarce causing a strong energetic imbalance. This imbalance, or impaired homeostasis, can lead to the development of several neurodegenerative and psychiatric disorders (fig. III).

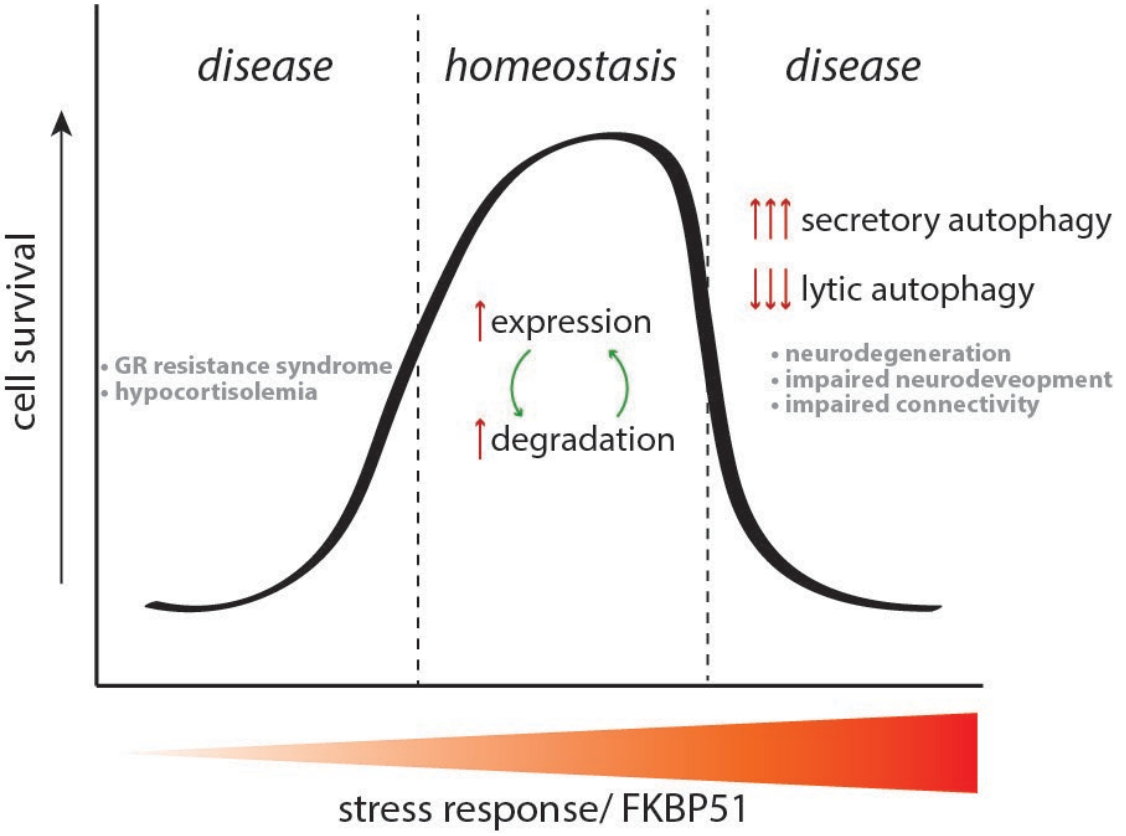

Figure III – Schematic representation of homeostasis in response to stress. Impaired levels of stress response and FKBP51 (either too low or to high) lead to impaired homeostasis and, consequently, to a diseased state.

5.5. Self-regulation of FKBP51

FKBP51 is the common denominator of the effect of stress on all these different levels. Interestingly, within the homeostatic regulation of GR, FKBP51 appears to have an autonomous self-regulating mechanism that counterbalances the effect of stress on this versatile protein on multiple levels. At the genetic level, FKBP51 indirectly regulates its own expression by inhibiting its activator GR (Davies et al., 2002). Furthermore, Klengel and colleagues unraveled the mechanism underlying the link between *FKBP5* polymorphisms and epigenetic regulation via DNA methylation (Klengel et al., 2013). In addition, FKBP51 was found to regulate DNMT1, one of the main DNA methyltrasferases, and, thus, indirectly regulate its own expression via epigenetic modifications (Gassen et al., 2015a). Another epigenetic mechanism through which *FKBP5* is regulated is via miRNA (Sun et al., 2018; Volk et al., 2016). Studies showed that FKBP51 interacts with and regulates argonaute proteins which together with miRNAs form the RNA-induced silencing complex (RISC) responsible for RNA silencing (Martinez et al., 2013; Taipale et al., 2014). Therefore, FKBP51 can also indirectly modulate its post-transcriptional regulation by modulating miRNA activity. In a

recently published study we demonstrated that, in immune cells, *FKBP5* expression can be regulated by NF-kB, which is known to be in turn enhanced by FKBP51, resulting in a positive feedback loop of *FKBP5* expression (Zannas et al., 2019). With the current study, I gained evidence that FKBP51 can regulate itself also on an additional level, via CMA. In fact, Dex-enhanced levels of FKBP51 elevate CMA activity of which FKBP51 itself is a target. Interestingly, genetic and epigenetic self-regulatory mechanisms of *FKBP5*/51 have all been linked to psychiatric or inflammatory disorders. These findings were collected from *in vitro* analyses performed in the neuroblastoma cell line SH-SY5Y, which allowed me to have a handy experimental approach (*e.g*. FKBP51 KO generation, SILAC labelling, good transfectability) and a neuronal-like background. However, to gain a better understanding of this regulatory mechanism, the use of more specific *in vitro* models, such as hiPSC-derived neurons or more complex models like cerebral organoids would be preferable. In addition, behavioral experiments and post-mortem brain analyses would allow a translation from a mechanistic to a functional and clinical investigation. The self-regulatory mechanism of FKBP51 also increases the interest of using this protein as drug target.

5.6. FKBP51 variants and isoforms: implications and future directions

All evidences highlight a central role for FKBP51 in stress response and its implication in numerous stress-related disorders. Furthermore, its self-regulation within the GR negative feedback mechanism, suggests a fine-tuning function for FKBP51. To better examine this potential role, expression and degradation dynamics of FKBP51 isoforms and their differential functions in known molecular pathways were analyzed in HeLa cells. The first experiments revealed that only variants 1 and 4, coding for isoform 1 and 2 respectively, were detected and that variant 1 is expressed at much higher levels than variant 4 (fig. 32), which is in line with online expression data (https://gtexportal.org). Interestingly, upon Dex stimulation, variant 4 showed a much higher increase than variant 1, compared to basal levels (fig 33). Furthermore, measurement of the protein degradation kinetics, via pulse chase-assay, showed a shorter half-life for isoform 2 (4 hours) compared to isoform 1 (8 hours) (fig. 34). The collected data suggest a different dynamic for the two different isoforms. In particular, isoform 2 appears to have a faster degradation rate, which might correspond to a more fine-tuning function. Furthermore, localization analyses showed a

strong nuclear (probably nucleolar) enrichment of isoform 2, while isoform 1 presented an equal distribution between cytoplasm and nucleus. This result not only suggests different roles for the two isoforms, but also indicates the existence of unknown functions of FKBP51 in the nucleus. To shed light on possible novel functions of isoform 2, the impact of isoform 1 and 2 onto known pathways was compared. The two isoforms were found to exert opposite regulatory effects on GR, NFAT and DNMT1 signaling (fig. 36, 38, 41, 42). Interestingly, the regulation of all these pathways depends on the interaction with HSP90. It is therefore not surprising that isoform 1 affects inhibition of GR and phosphorylation of NFAT and DNMT1, while isoform 2 does not have any effect on their function since it lacks the TPR domain responsible for the interaction with HSP90. On the other hand, pathways regulated via the interaction with AKT and PHLPP are modulated by both isoforms, since the interaction is dependent on the FK1 domain. The immediate consequence of FKBP51 interaction to AKT and PHLPP is dephosphorylation of AKT. Interestingly, while AKT dephosphorylation is equally regulated by the two isoforms, downstream effects, such as increase of autophagy markers, are not (fig. 39, 40). This finding suggests the existence of an additional mechanism for which isoform 2 has a decreased effect on autophagy activation. Presumably, isoform 2 has a lower binding affinity for Beclin1. Interestingly, though, isoform 2 appears to have a stronger effect in later stages of the autophagic pathway (autophagosome expansion and autolysosome formation), suggesting an alternative pathway, or a faster activity of isoform 2 compared to isoform 1. Once again, these results suggest different functional roles for the two isoforms. Considering the different functions related to the different domains, it would be of particular interest to explore the functions related to the unique sequence of 46 aa of isoform 2. *In silico* analyses performed with the Expasy Prosite database (https://prosite.expasy.org/) revealed the presence of a putative nuclear localization signal (NLS) inside the unique sequence, which might underlie the observed nuclear localization of isoform 2. Additionally, clinical observational and correlational analyses in case control cohorts can be used to broaden the clinical understanding of the two isoforms. In our lab, expression levels of *FKBP5* splicing variants (mRNA) and protein isoforms are being analyzed in post-mortem brain samples deriving from patients with schizophrenia, bipolar disorder, major depression disorder and healthy controls. Possible differential expression of FKBP51 variants in correlation with a diseased state would further clarify not only the splicing variant/isoform-specific function,

but also a possible specificity of the brain regions. However, these analyses remain observational and correlational. Complementary *in vivo* analyses would clarify the functional mechanisms.

Another important aspect, for which a better understanding of FKBP51 isoforms and their roles are important, is to use FKBP51 as a drug target. Given its involvement in numerous diseases, FKBP51 has gained visibility as therapeutic target. So far, SAFit appears to be the only candidate able to selectively target FKBP51 over its closest homologue FKBP52 in an efficient way. It binds to the FK pocket within the FK1-domain, which means it can theoretically regulate both isoforms of FKBP51. Pharmacological modulation with SAFit *in vivo* led to decreased chronic pain and increased stress-coping behaviors (Balsevich et al., 2017; Maiarù et al., 2016), while *in vitro* treatment of neuroblastoma cells with SAFit caused a downregulation of the isoform 2-specific downstream target PD-L1. My current study shows a potential use of SAFit for stress-induced neuroinflammation. *In vitro* experiments showed, in fact, the reversing effect of SAFit in stress-induced secretory autophagy in microglia cells (fig. 31). FKBP51´s regulation of a large set of different molecular pathways, however, increases the chance of undesired side effects. A solution to this problem could be a more selective targeting of specific functions. This selectivity could be achieved by targeting a single FKBP51 isoform. Targeting the TPR domain would guarantee selectivity for isoform 1. This would mean to impair all molecular functions modulated via HSP90, first among all, GR inhibition. To selectively target isoform 2 could be of particular interest, given the observed faster response dynamic to stress. A deeper characterization of isoform 2, however, would be necessary. Furthermore, from a stereochemical and pharmacological point of view, designing a ligand for a 46 aa unique sequence to selectively target isoform 2 might be extremely challenging. As mentioned in the beginning of this doctoral thesis, FKBP51 provides a more dynamic phenotype with an enhanced response to stress but also a stronger response to anti-depressants. Impairing this mechanism could, therefore, lead to an inefficient alteration and undesired side effects. For this reason, targeting downstream players of selective pathways modulated by FKBP51 could be an alternative option.

As summarized in figure IV, this work presents FKBP51 in a central stage of a novel level of homeostasis regulation in response to stress. The majority of evidence was gained with *in vitro* analyses using cell lines, which offered the advantage of being a fast and

manipulable system. As a next step, *in vivo* or more complex and specific *in vitro* tools (e.g. hiPSC induced specific cell types or organoids), might offer a better milieu for further investigations of these pathways and functions.

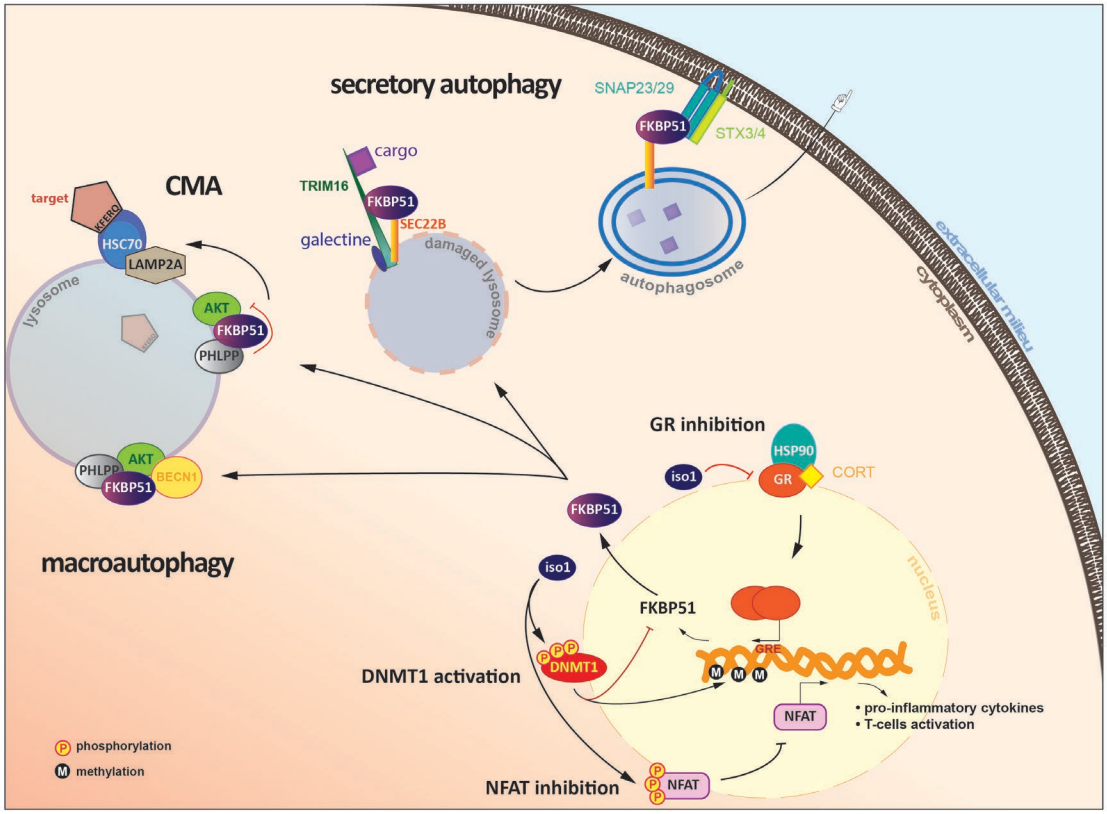

Figure IV – Schematic summary of the functions of FKBP51. Newly discovered role of FKBP51 in CMA and secretory autophagy. Mediation of AKT dephosphorylation and subsequent activation of macroautophagy by both FKBP51 isoforms (further clarifications regarding the extent of isoform 2 on this pathway still needed). Regulation of DNA methylation via DNMT1 and activation of the NFAT –mediated immune response by FKBP51 isoform 1 (iso 1) only.

6. Acronyms and abbreviations

3D	Three-dimensional
ACTH	adrenocorticotropic hormone
AGO	Argonaute protein
AIF	Apoptosis-inducing factor
AKT or PKB	Protein kinase B
AP-1	Activator protein 1
AR	Androgen receptor
AS160	Akt substrate 160
ATG protein	autophagy-related protein
BBB	blood brain barrier
BD	Bipolar disorder
ACN	Acetonitrile
C-terminal/ terminus	Carboxyl terminal/ terminus
CaN	Calcineurin
CBG	corticosteroid binding globulin
CDK4/5	Cyclin-dependent kinase
ChIP	chromatin immunoprecipitation experiments
CMA	Chaperone - mediated autophagy
CNS	Central nervous system
CORT	Cortisol/ corticosterone
CRH	corticotropin-releasing hormone
CRHR1	corticotropin-releasing hormone receptor 1
Cyp40	Cyclophilin 40
Dex	Dexamethasone
DLC1/2	Deleted in Liver Cancer ½
DNA	Deoxyribonucleic acid
DNMT1	DNA-methyltransferase 1
ELISA	Enzyme-linked Immunosorbent Assay
FA	Formic acid
FK1/2	FK506-binding (domain)

FKBP5/51/52	FK506-Binding Protein 5/51/52
GAL3/8	Galectin 3/8
GC	Glucocorticoid
GFAP	Glial fibrillary acidic protein
GR	glucocorticoid receptor
GRE	Glucocorticoid Response Element
gRNA	Guide RNA
GSK3b	Glycogen synthase kinase 3 beta
hiPSC	human induced Pluripotent Stem Cells
HPA	hypothalamic pituitary adrenal
HSC70	Heat shock cognate 70
HSP90	Heat shock protein 90
IkB	NF-kB inhibitor
IKK	IκB kinase
IL1B	Interleukin-1 beta
IL1B/2/6	Interleukin 1 beta/2/6
IP	Immunoprecipitation
i.p.	Intraperitoneal
ISOC	Store-operated calcium entry current
JAK	Janus kinase
KD	Knock down
KO	Knock out
LAMP2A	Lysosome-associated membrane protein type 2A
LE	ligand efficiency
LPS	Lipopolysaccharide
MC2-R	melanocortin type 2 receptor
MCM	minichromosome maintenance
MDD	Major depressive disorder
MIF	migration inhibitory factor
miRNA	micro RNA
MR	mineralocorticoid receptor
mRNA	messenger RNA

mTOR	Mechanistic (or mammalian) target of rapamycin
N-terminal/terminus	Amino-terminal/terminus
NFAT	Nuclear factor of activated T-cells
NF-kB	Nuclear factor kappa-light-chain-enhancer of activated B-cells
NLS	Nuclear localization signal
NUP155	Nuclear pore complex protein
PHLPP	PH domain and Leucine rich repeat Protein Phosphatases
PKA	protein kinase A
PP5	Protein Phosphatase 5
PPIase	peptidylprolyl isomerase
PR	Progesterone receptor
PTSD	Post traumatic stress disorder
PVN	paraventricular nucleus
RhoA	Ras homolog family member A
RISC	RNA-induced silencing complex
RNA	Ribonucleic acid
ROCK	Rho-associated protein kinase
RICTOR	Rapamycin-insensitive companion of mTOR
SAFit	Selective Antagonist of FKBP51 by induced fit
SEC22B	SEC22 Homolog B, Vesicle Trafficking Protein
siRNA	small interfering RNA
SNAP 23/29	Synaptosomal-associated protein 23/29
SNARE	soluble N-ethylmaleimide-sensitive-factor attachment receptor
SNCA	Alpha-synuclein
SNP	Single Nucleotide Polymorphism
STAT	Signal transducer and activator of transcription proteins
STX3/4	Syntaxin 3/4
TBP	TATA box-binding protein
TNFA	Tumor necrosis factor alpha
TPR	tetratricopeptide repeat (motif)
TRAF	TNF receptor associated factors
TRIM16	Tripartite motif-containing protein 16

TSS	Transcription start site
TSST	Trier social stress test
WCL	Whole cell lysate
WT	Wild Type

7. Bibliography

Aguzzi, A., Barres, B.A., and Bennett, M.L. (2013). Microglia: scapegoat, saboteur, or something else? Science *339*, 156–161.

Alfaro, I.E., Albornoz, A., Molina, A., Moreno, J., Cordero, K., Criollo, A., and Budini, M. (2019). Chaperone Mediated Autophagy in the Crosstalk of Neurodegenerative Diseases and Metabolic Disorders. Front. Endocrinol. *9*.

Aniento, F., Roche, E., Cuervo, A.M., and Knecht, E. (1993). Uptake and degradation of glyceraldehyde-3-phosphate dehydrogenase by rat liver lysosomes. J. Biol. Chem. *268*, 10463–10470.

Arias, E., Koga, H., Diaz, A., Mocholi, E., Patel, B., and Cuervo, A.M. (2015). Lysosomal mTORC2/PHLPP1/Akt regulate chaperone-mediated autophagy. Mol. Cell *59*, 270–284.

Attwood, B.K., Bourgognon, J.-M., Patel, S., Mucha, M., Schiavon, E., Skrzypiec, A.E., Young, K.W., Shiosaka, S., Korostynski, M., Piechota, M., et al. (2011). Neuropsin cleaves EphB2 in the amygdala to control anxiety. Nature *473*, 372–375.

Audet, M.-C., McQuaid, R.J., Merali, Z., and Anisman, H. (2014). Cytokine variations and mood disorders: influence of social stressors and social support. Front. Neurosci. *8*.

Avellino, R., Romano, S., Parasole, R., Bisogni, R., Lamberti, A., Poggi, V., Venuta, S., and Romano, M.F. (2005). Rapamycin stimulates apoptosis of childhood acute lymphoblastic leukemia cells. Blood *106*, 1400–1406.

Balsevich, G., Uribe, A., Wagner, K.V., Hartmann, J., Santarelli, S., Labermaier, C., and Schmidt, M.V. (2014). Interplay between diet-induced obesity and chronic stress in mice: potential role of FKBP51. J. Endocrinol. *222*, 15–26.

Balsevich, G., Häusl, A.S., Meyer, C.W., Karamihalev, S., Feng, X., Pöhlmann, M.L., Dournes, C., Uribe-Marino, A., Santarelli, S., Labermaier, C., et al. (2017). Stress-responsive FKBP51 regulates AKT2-AS160 signaling and metabolic function. Nat. Commun. *8*, 1725.

Bandyopadhyay, U., Kaushik, S., Varticovski, L., and Cuervo, A.M. (2008). The chaperone-mediated autophagy receptor organizes in dynamic protein complexes at the lysosomal membrane. Mol. Cell. Biol. *28*, 5747–5763.

Bandyopadhyay, U., Sridhar, S., Kaushik, S., Kiffin, R., and Cuervo, A.M. (2010). Identification of Regulators of Chaperone-Mediated Autophagy. Mol. Cell *39*, 535–547.

Banks, W.A. (2006). The Blood–Brain Barrier in Psychoneuroimmunology. Neurol. Clin. *24*, 413–419.

Barent, R.L., Nair, S.C., Carr, D.C., Ruan, Y., Rimerman, R.A., Fulton, J., Zhang, Y., and Smith, D.F. (1998). Analysis of FKBP51/FKBP52 Chimeras and Mutants for Hsp90 Binding and Association with Progesterone Receptor Complexes. *12*, 13.

Binder, E.B. (2009). The role of FKBP5, a co-chaperone of the glucocorticoid receptor in the pathogenesis and therapy of affective and anxiety disorders. Psychoneuroendocrinology *34*, S186–S195.

Binder, E.B., Salyakina, D., Lichtner, P., Wochnik, G.M., Ising, M., Pütz, B., Papiol, S., Seaman, S., Lucae, S., Kohli, M.A., et al. (2004). Polymorphisms in *FKBP5* are associated with increased recurrence of depressive episodes and rapid response to antidepressant treatment. Nat. Genet. *36*, 1319–1325.

Binder, E.B., Bradley, R.G., Liu, W., Epstein, M.P., Deveau, T.C., Mercer, K.B., Tang, Y., Gillespie, C.F., Heim, C.M., Nemeroff, C.B., et al. (2008). Association of FKBP5 Polymorphisms and Childhood Abuse With Risk of Posttraumatic Stress Disorder Symptoms in Adults. JAMA *299*, 1291–1305.

Blackburn, E.A., and Walkinshaw, M.D. (2011). Targeting FKBP isoforms with small-molecule ligands. Curr. Opin. Pharmacol. *11*, 365–371.

Bouwmeester, T., Bauch, A., Ruffner, H., Angrand, P.-O., Bergamini, G., Croughton, K., Cruciat, C., Eberhard, D., Gagneur, J., Ghidelli, S., et al. (2004). A physical and functional map of the human TNF-α/NF-κB signal transduction pathway. Nat. Cell Biol. *6*, 97–105.

Braak, H., and Braak, E. (1991). Neuropathological stageing of Alzheimer-related changes. Acta Neuropathol. (Berl.) *82*, 239–259.

Bradshaw, N.J., and Korth, C. (2018). Protein misassembly and aggregation as potential convergence points for non-genetic causes of chronic mental illness. Mol. Psychiatry.

Buchmann, A.F., Holz, N., Boecker, R., Blomeyer, D., Rietschel, M., Witt, S.H., Schmidt, M.H., Esser, G., Banaschewski, T., Brandeis, D., et al. (2014). Moderating role of FKBP5 genotype in the impact of childhood adversity on cortisol stress response during adulthood. Eur. Neuropsychopharmacol. *24*, 837–845.

Calandra, T., Bernhagen, J., Metz, C.N., Spiegel, L.A., Bacher, M., Donnelly, T., Cerami, A., and Bucala, R. (1995). MIF as a glucocorticoid-induced modulator of cytokine production. Nature *377*, 68.

de Calignon, A., Fox, L.M., Pitstick, R., Carlson, G.A., Bacskai, B.J., Spires-Jones, T.L., and Hyman, B.T. (2010). Caspase activation precedes and leads to tangles. Nature *464*, 1201–1204.

de Calignon, A., Polydoro, M., Suárez-Calvet, M., William, C., Adamowicz, D.H., Kopeikina, K.J., Pitstick, R., Sahara, N., Ashe, K.H., Carlson, G.A., et al. (2012). Propagation of tau pathology in a model of early Alzheimer's disease. Neuron *73*, 685–697.

Cannon, W.B. (1915). Bodily changes in pain, hunger, fear and rage, an account of recent researches into the function of emotional excitement (New York and London, D. Appleton and Co.).

Cannon, W.B. (1929). Organization for physiological homeostasis. Physiol. Rev. *9*, 399–431.

de Castro-Catala, M., Peña, E., Kwapil, T.R., Papiol, S., Sheinbaum, T., Cristóbal-Narváez, P., Ballespí, S., Barrantes-Vidal, N., and Rosa, A. (2017). Interaction between FKBP5 gene and childhood trauma on psychosis, depression and anxiety symptoms in a non-clinical sample. Psychoneuroendocrinology *85*, 200–209.

Chauhan, S., Kumar, S., Jain, A., Ponpuak, M., Mudd, M.H., Kimura, T., Choi, S.W., Peters, R., Mandell, M., Bruun, J.-A., et al. (2016). TRIMs and Galectins Globally Cooperate and TRIM16 and Galectin-3 Co-direct Autophagy in Endomembrane Damage Homeostasis. Dev. Cell *39*, 13–27.

Chen, H., Wang, N., Zhao, X., Ross, C.A., O'Shea, K.S., and McInnis, M.G. (2013). Gene expression alterations in bipolar disorder postmortem brains. Bipolar Disord. *15*, 177–187.

Chiang, H.L., Terlecky, S.R., Plant, C.P., and Dice, J.F. (1989). A role for a 70-kilodalton heat shock protein in lysosomal degradation of intracellular proteins. Science *246*, 382–385.

Cho, H., Mu, J., Kim, J.K., Thorvaldsen, J.L., Chu, Q., Crenshaw, E.B., Kaestner, K.H., Bartolomei, M.S., Shulman, G.I., and Birnbaum, M.J. (2001). Insulin resistance and a diabetes mellitus-like syndrome in mice lacking the protein kinase Akt2 (PKB beta). Science *292*, 1728–1731.

Chover-Gonzalez, A.J., Harbuz, M.S., and Lightmann, S.L. (1993). Effect of adrenalectomy and stress on interleukin-1β-mediated activation of hypothalamic corticotropin-releasing factor mRNA. J. Neuroimmunol. *42*, 155–160.

Chrousos, G.P. (2009). Stress and disorders of the stress system. Nat. Rev. Endocrinol. *5*, 374–381.

Cioffi, D.L., Hubler, T.R., and Scammell, J.G. (2011). Organization and function of the FKBP52 and FKBP51 genes. Curr. Opin. Pharmacol. *11*, 308–313.

Cuervo, A.M., and Dice, J.F. (1996). A receptor for the selective uptake and degradation of proteins by lysosomes. Science *273*, 501–503.

Cuervo, A.M., Stefanis, L., Fredenburg, R., Lansbury, P.T., and Sulzer, D. (2004). Impaired degradation of mutant alpha-synuclein by chaperone-mediated autophagy. Science *305*, 1292–1295.

Dallman, M.F. (2003). Stress by any other name …? Horm. Behav. *43*, 18–20.

Darby, M.M., Yolken, R.H., and Sabunciyan, S. (2016). Consistently altered expression of gene sets in postmortem brains of individuals with major psychiatric disorders. Transl. Psychiatry *6*, e890.

D'Arrigo, P., Russo, M., Rea, A., Tufano, M., Guadagno, E., Del Basso De Caro, M.L., Pacelli, R., Hausch, F., Staibano, S., Ilardi, G., et al. (2017). A regulatory role for the co-chaperone FKBP51s in PD-L1 expression in glioma. Oncotarget *8*, 68291–68304.

Davies, T.H., Ning, Y.-M., and Sánchez, E.R. (2002). A New First Step in Activation of Steroid Receptors HORMONE-INDUCED SWITCHING OF FKBP51 AND FKBP52 IMMUNOPHILINS. J. Biol. Chem. *277*, 4597–4600.

Denny, W.B., Valentine, D.L., Reynolds, P.D., Smith, D.F., and Scammell, J.G. (2000). Squirrel Monkey Immunophilin FKBP51 Is a Potent Inhibitor of Glucocorticoid Receptor Binding*This work was supported by Grants 13200 and 01254 from the National Center for Research Resources (to J.G.S.) and NIH Grant DK48218 (to D.F.S.). Endocrinology *141*, 4107–4113.

Dornan, J., and Walkinshaw, P.T. and M.D. (2003). Structures of Immunophilins and their Ligand Complexes.

Fichna, M., Krzyśko-Pieczka, I., Żurawek, M., Skowrońska, B., Januszkiewicz-Lewandowska, D., and Fichna, P. (2018). FKBP5 polymorphism is associated with insulin resistance in children and adolescents with obesity. Obes. Res. Clin. Pract. *12*, 62–70.

Frank, M.G., Watkins, L.R., and Maier, S.F. (2011). Stress- and glucocorticoid-induced priming of neuroinflammatory responses: Potential mechanisms of stress-induced vulnerability to drugs of abuse. Brain. Behav. Immun. *25*, S21–S28.

Frank, M.G., Watkins, L.R., and Maier, S.F. (2013). Stress-induced glucocorticoids as a neuroendocrine alarm signal of danger. Brain. Behav. Immun. *33*, 1–6.

Gaali, S., Kirschner, A., Cuboni, S., Hartmann, J., Kozany, C., Balsevich, G., Namendorf, C., Fernandez-Vizarra, P., Sippel, C., Zannas, A.S., et al. (2015). Selective inhibitors of the FK506-binding protein 51 by induced fit. Nat. Chem. Biol. *11*, 33–37.

Gaali, S., Feng, X., Hähle, A., Sippel, C., Bracher, A., and Hausch, F. (2016). Rapid, Structure-Based Exploration of Pipecolic Acid Amides as Novel Selective Antagonists of the FK506-Binding Protein 51. J. Med. Chem. *59*, 2410–2422.

Gądek-Michalska, A., Tadeusz, J., Rachwalska, P., Spyrka, J., and Bugajski, J. (2011). Effect of prior stress on interleukin-1β and HPA axis responses to acute stress. Pharmacol. Rep. PR *63*, 1393–1403.

Galigniana, M.D., Harrell, J.M., Housley, P.R., Patterson, C., Fisher, S.K., and Pratt, W.B. (2004). Retrograde transport of the glucocorticoid receptor in neurites requires dynamic assembly of complexes with the protein chaperone hsp90 and is linked to the CHIP component of the machinery for proteasomal degradation. Brain Res. Mol. Brain Res. *123*, 27–36.

Gassen, N.C., Hartmann, J., Zschocke, J., Stepan, J., Hafner, K., Zellner, A., Kirmeier, T., Kollmannsberger, L., Wagner, K.V., Dedic, N., et al. (2014). Association of FKBP51 with Priming of Autophagy Pathways and Mediation of Antidepressant Treatment Response: Evidence in Cells, Mice, and Humans. PLOS Med. *11*, e1001755.

Gassen, N.C., Fries, G.R., Zannas, A.S., Hartmann, J., Zschocke, J., Hafner, K., Carrillo-Roa, T., Steinbacher, J., Preißinger, S.N., Hoeijmakers, L., et al. (2015a). Chaperoning epigenetics: FKBP51 decreases the activity of DNMT1 and mediates epigenetic effects of the antidepressant paroxetine. Sci. Signal. *8*, ra119.

Gassen, N.C., Hartmann, J., Schmidt, M.V., and Rein, T. (2015b). FKBP5/FKBP51 enhances autophagy to synergize with antidepressant action. Autophagy *11*, 578–580.

Gassen, N.C., Hartmann, J., Zannas, A.S., Kretzschmar, A., Zschocke, J., Maccarrone, G., Hafner, K., Zellner, A., Kollmannsberger, L.K., Wagner, K.V., et al. (2016). FKBP51 inhibits GSK3β and augments the effects of distinct psychotropic medications. Mol. Psychiatry *21*, 277–289.

Gibb, J., Al-Yawer, F., and Anisman, H. (2013). Synergistic and antagonistic actions of acute or chronic social stressors and an endotoxin challenge vary over time following the challenge. Brain. Behav. Immun. *28*, 149–158.

Gillespie, C.F., and Ressler, K.J. (2005). Emotional Learning and Glutamate: Translational Perspectives. CNS Spectr. *10*, 831–839.

Gotlib, I.H., Joormann, J., Minor, K.L., and Hallmayer, J. (2008). HPA Axis Reactivity: A Mechanism Underlying the Associations Among 5-HTTLPR, Stress, and Depression. Biol. Psychiatry *63*, 847–851.

Guarnieri, D.J., Brayton, C.E., Richards, S.M., Maldonado-Aviles, J., Trinko, J.R., Nelson, J., Taylor, J.R., Gourley, S.L., and DiLeone, R.J. (2012). Gene profiling reveals a role for stress hormones in the molecular and behavioral response to food restriction. Biol. Psychiatry *71*, 358–365.

Hakim, V., Cohen, L.D., Zuchman, R., Ziv, T., and Ziv, N.E. (2016). The effects of proteasomal inhibition on synaptic proteostasis. EMBO J. *35*, 2238–2262.

Hamilton, C.L., Abney, K.A., Vasauskas, A.A., Alexeyev, M., Li, N., Honkanen, R.E., Scammell, J.G., and Cioffi, D.L. (2018). Serine/threonine phosphatase 5 (PP5C/PPP5C) regulates the ISOC channel through a PP5C-FKBP51 axis. Pulm. Circ. *8*, 2045893217753156.

Harrell, J.M., Murphy, P.J.M., Morishima, Y., Chen, H., Mansfield, J.F., Galigniana, M.D., and Pratt, W.B. (2004). Evidence for Glucocorticoid Receptor Transport on Microtubules by Dynein. J. Biol. Chem. *279*, 54647–54654.

Hartmann, J., Wagner, K.V., Liebl, C., Scharf, S.H., Wang, X.-D., Wolf, M., Hausch, F., Rein, T., Schmidt, U., Touma, C., et al. (2012). The involvement of FK506-binding protein 51 (FKBP5) in the behavioral and neuroendocrine effects of chronic social defeat stress. Neuropharmacology *62*, 332–339.

Hausch, F., Kozany, C., Theodoropoulou, M., and Fabian, A.-K. (2013). FKBPs and the Akt/mTOR pathway. Cell Cycle *12*, 2366–2370.

Hawn, S.E., Sheerin, C.M., Lind, M.J., Hicks, T.A., Marraccini, M.E., Bountress, K., Bacanu, S.-A., Nugent, N.R., and Amstadter, A.B. (2019). GxE effects of FKBP5 and traumatic life events on PTSD: A meta-analysis. J. Affect. Disord. *243*, 455–462.

Heim, C., and Nemeroff, C.B. (2002). Neurobiology of early life stress: clinical studies. Semin. Clin. Neuropsychiatry *7*, 147–159.

Ho, P.W.-L., Leung, C.-T., Liu, H., Pang, S.Y.-Y., Lam, C.S.-C., Xian, J., Li, L., Kung, M.H.-W., Ramsden, D.B., and Ho, S.-L. (2019). Age-dependent accumulation of oligomeric SNCA/α-synuclein from impaired degradation in mutant LRRK2 knockin mouse model of Parkinson

disease: role for therapeutic activation of chaperone-mediated autophagy (CMA). Autophagy 1–24.

Höhne, N., Poidinger, M., Merz, F., Pfister, H., Brückl, T., Zimmermann, P., Uhr, M., Holsboer, F., and Ising, M. (2015). FKBP5 Genotype-Dependent DNA Methylation and mRNA Regulation After Psychosocial Stress in Remitted Depression and Healthy Controls. Int. J. Neuropsychopharmacol. *18*.

Ising, M., Depping, A.-M., Siebertz, A., Lucae, S., Unschuld, P.G., Kloiber, S., Horstmann, S., Uhr, M., Müller-Myhsok, B., and Holsboer, F. (2008). Polymorphisms in the FKBP5 gene region modulate recovery from psychosocial stress in healthy controls. Eur. J. Neurosci. *28*, 389–398.

Jääskeläinen, T., Makkonen, H., and Palvimo, J.J. (2011). Steroid up-regulation of FKBP51 and its role in hormone signaling. Curr. Opin. Pharmacol. *11*, 326–331.

Jia, J., Abudu, Y.P., Claude-Taupin, A., Gu, Y., Kumar, S., Choi, S.W., Peters, R., Mudd, M.H., Allers, L., Salemi, M., et al. (2018). Galectins Control mTOR in Response to Endomembrane Damage. Mol. Cell *70*, 120-135.e8.

Jia, J., Abudu, Y.P., Claude-Taupin, A., Gu, Y., Kumar, S., Choi, S.W., Peters, R., Mudd, M.H., Allers, L., Salemi, M., et al. (2019). Galectins control MTOR and AMPK in response to lysosomal damage to induce autophagy. Autophagy *15*, 169–171.

Jinwal, U.K., Koren, J., Borysov, S.I., Schmid, A.B., Abisambra, J.F., Blair, L.J., Johnson, A.G., Jones, J.R., Shults, C.L., O'Leary, J.C., et al. (2010). The Hsp90 cochaperone, FKBP51, increases Tau stability and polymerizes microtubules. J. Neurosci. Off. J. Soc. Neurosci. *30*, 591–599.

Jirawatnotai, S., Sharma, S., Michowski, W., Suktitipat, B., Geng, Y., Quackenbush, J., Elias, J.E., Gygi, S.P., Wang, Y.E., and Sicinski, P. (2014). The cyclin D1-CDK4 oncogenic interactome enables identification of potential novel oncogenes and clinical prognosis. Cell Cycle *13*, 2889–2900.

Joëls, M., and Baram, T.Z. (2009). The neuro-symphony of stress. Nat. Rev. Neurosci. *10*, 459–466.

Juruena, M.F. (2014). Early-life stress and HPA axis trigger recurrent adulthood depression. Epilepsy Behav. *38*, 148–159.

Kimura, T., Jia, J., Kumar, S., Choi, S.W., Gu, Y., Mudd, M., Dupont, N., Jiang, S., Peters, R., Farzam, F., et al. (2017). Dedicated SNAREs and specialized TRIM cargo receptors mediate secretory autophagy. EMBO J. *36*, 42–60.

Klengel, T., Mehta, D., Anacker, C., Rex-Haffner, M., Pruessner, J.C., Pariante, C.M., Pace, T.W.W., Mercer, K.B., Mayberg, H.S., Bradley, B., et al. (2013). Allele-specific FKBP5 DNA demethylation mediates gene-childhood trauma interactions. Nat. Neurosci. *16*, 33–41.

Klionsky, D.J. (2005). The molecular machinery of autophagy: unanswered questions. J Cell Sci *118*, 7–18.

de Kloet, C.S., Vermetten, E., Geuze, E., Kavelaars, A., Heijnen, C.J., and Westenberg, H.G.M. (2006). Assessment of HPA-axis function in posttraumatic stress disorder: Pharmacological and non-pharmacological challenge tests, a review. J. Psychiatr. Res. *40*, 550–567.

de Kloet, E.R., Joëls, M., and Holsboer, F. (2005). Stress and the brain: from adaptation to disease. Nat. Rev. Neurosci. *6*, 463–475.

Komura, E., Chagraoui, H., Mansat de Mas, V., Blanchet, B., de Sepulveda, P., Larbret, F., Larghero, J., Tulliez, M., Debili, N., Vainchenker, W., et al. (2003). Spontaneous STAT5 activation induces growth factor independence in idiopathic myelofibrosis: possible relationship with FKBP51 overexpression. Exp. Hematol. *31*, 622–630.

Krugers, H.J., Arp, J.M., Xiong, H., Kanatsou, S., Lesuis, S.L., Korosi, A., Joels, M., and Lucassen, P.J. (2017). Early life adversity: Lasting consequences for emotional learning. Neurobiol. Stress *6*, 14–21.

Lasagna-Reeves, C.A., Castillo-Carranza, D.L., Sengupta, U., Sarmiento, J., Troncoso, J., Jackson, G.R., and Kayed, R. (2012). Identification of oligomers at early stages of tau aggregation in Alzheimer's disease. FASEB J. Off. Publ. Fed. Am. Soc. Exp. Biol. *26*, 1946–1959.

Lee, R.S., Tamashiro, K.L.K., Yang, X., Purcell, R.H., Harvey, A., Willour, V.L., Huo, Y., Rongione, M., Wand, G.S., and Potash, J.B. (2010). Chronic corticosterone exposure increases expression and decreases deoxyribonucleic acid methylation of Fkbp5 in mice. Endocrinology *151*, 4332–4343.

Levine, B., and Kroemer, G. (2008). Autophagy in the Pathogenesis of Disease. Cell *132*, 27–42.

Li, T.-K., Baksh, S., Cristillo, A.D., and Bierer, B.E. (2002). Calcium- and FK506-independent interaction between the immunophilin FKBP51 and calcineurin. J. Cell. Biochem. *84*, 460–471.

Li, W., Li, J., and Bao, J. (2012). Microautophagy: lesser-known self-eating. Cell. Mol. Life Sci. *69*, 1125–1136.

Lippmann, M., Bress, A., Nemeroff, C.B., Plotsky, P.M., and Monteggia, L.M. (2007). Long-term behavioural and molecular alterations associated with maternal separation in rats. Eur. J. Neurosci. *25*, 3091–3098.

Liu, J., Buisman-Pijlman, F., and Hutchinson, M.R. (2014). Toll-like receptor 4: innate immune regulator of neuroimmune and neuroendocrine interactions in stress and major depressive disorder. Front. Neurosci. *8*.

Loram, L.C., Taylor, F.R., Strand, K.A., Frank, M.G., Sholar, P., Harrison, J.A., Maier, S.F., and Watkins, L.R. (2011). Prior exposure to glucocorticoids potentiates lipopolysaccharide induced mechanical allodynia and spinal neuroinflammation. Brain. Behav. Immun. *25*, 1408–1415.

Lucassen, P.J., Naninck, E.F.G., van Goudoever, J.B., Fitzsimons, C., Joels, M., and Korosi, A. (2013). Perinatal programming of adult hippocampal structure and function; emerging roles of stress, nutrition and epigenetics. Trends Neurosci. *36*, 621–631.

Lupien, S.J., McEwen, B.S., Gunnar, M.R., and Heim, C. (2009). Effects of stress throughout the lifespan on the brain, behaviour and cognition. Nat. Rev. Neurosci. *10*, 434–445.

Macfarlane, D.P., Forbes, S., and Walker, B.R. (2008). Glucocorticoids and fatty acid metabolism in humans: fuelling fat redistribution in the metabolic syndrome. J. Endocrinol. *197*, 189–204.

Maejima, I., Takahashi, A., Omori, H., Kimura, T., Takabatake, Y., Saitoh, T., Yamamoto, A., Hamasaki, M., Noda, T., Isaka, Y., et al. (2013). Autophagy sequesters damaged lysosomes to control lysosomal biogenesis and kidney injury. EMBO J. *32*, 2336–2347.

Maiarù, M., Tochiki, K.K., Cox, M.B., Annan, L.V., Bell, C.G., Feng, X., Hausch, F., and Géranton, S.M. (2016). The stress regulator FKBP51 drives chronic pain by modulating spinal glucocorticoid signaling. Sci. Transl. Med. *8*, 325ra19-325ra19.

Maiarù, M., Morgan, O., Mao, T., Breitsamer, M., Bamber, H., Pöhlmann, M., Schmidt, M., Winter, G., Hausch, F., and Géranton, S. (2018). The stress regulator FKBP51. Pain *159*, 1224–1234.

Mamdani, F., Rollins, B., Morgan, L., Myers, R.M., Barchas, J.D., Schatzberg, A.F., Watson, S.J., Akil, H., Potkin, S.G., Bunney, W.E., et al. (2015). Variable telomere length across post-mortem human brain regions and specific reduction in the hippocampus of major depressive disorder. Transl. Psychiatry *5*, e636.

Martinez, N.J., Chang, H.-M., Borrajo, J. de R., and Gregory, R.I. (2013). The co-chaperones Fkbp4/5 control Argonaute2 expression and facilitate RISC assembly. RNA N. Y. N *19*, 1583–1593.

Matosin, N., Halldorsdottir, T., and Binder, E.B. (2018). Understanding the Molecular Mechanisms Underpinning Gene by Environment Interactions in Psychiatric Disorders: The FKBP5 Model. Biol. Psychiatry *83*, 821–830.

Mehet, D.K., Philip, J., Solito, E., Buckingham, J.C., and John, C.D. (2012). Evidence From In Vitro and In Vivo Studies Showing that Nuclear Factor-Kappa B Within the Pituitary Folliculostellate Cells and Corticotrophs Regulates Adrenocorticotrophic Hormone Secretion in Experimental Endotoxaemia. J. Neuroendocrinol. *24*, 862–873.

Mehta, D., Gonik, M., Klengel, T., Rex-Haffner, M., Menke, A., Rubel, J., Mercer, K.B., Pütz, B., Bradley, B., Holsboer, F., et al. (2011). Using Polymorphisms in FKBP5 to Define Biologically Distinct Subtypes of Posttraumatic Stress Disorder. Arch. Gen. Psychiatry *68*, 901–910.

Mifsud, K.R., and Reul, J.M.H.M. (2016). Acute stress enhances heterodimerization and binding of corticosteroid receptors at glucocorticoid target genes in the hippocampus. Proc. Natl. Acad. Sci. *113*, 11336–11341.

Mifsud, K.R., and Reul, J.M.H.M. (2018). Mineralocorticoid and glucocorticoid receptor-mediated control of genomic responses to stress in the brain. Stress *21*, 389–402.

Mizushima, N., and Komatsu, M. (2011). Autophagy: renovation of cells and tissues. Cell *147*, 728–741.

Mizushima, N., Levine, B., Cuervo, A.M., and Klionsky, D.J. (2008). Autophagy fights disease through cellular self-digestion. Nature *451*, 1069–1075.

Muzikar, K.A., Nickols, N.G., and Dervan, P.B. (2009). Repression of DNA-binding dependent glucocorticoid receptor-mediated gene expression. Proc. Natl. Acad. Sci. *106*, 16598–16603.

Ni, L., Yang, C.-S., Gioeli, D., Frierson, H., Toft, D.O., and Paschal, B.M. (2010). FKBP51 Promotes Assembly of the Hsp90 Chaperone Complex and Regulates Androgen Receptor Signaling in Prostate Cancer Cells. Mol. Cell. Biol. *30*, 1243–1253.

Nicolaides, N.C., Charmandari, E., Chrousos, G.P., and Kino, T. (2014). Recent advances in the molecular mechanisms determining tissue sensitivity to glucocorticoids: novel mutations, circadian rhythm and ligand-induced repression of the human glucocorticoid receptor. BMC Endocr. Disord. *14*, 71.

Okamoto, K. (2014). Organellophagy: Eliminating cellular building blocks via selective autophagy. J. Cell Biol. *205*, 435–445.

O'Leary, J.C., Dharia, S., Blair, L.J., Brady, S., Johnson, A.G., Peters, M., Cheung-Flynn, J., Cox, M.B., Erausquin, G. de, Weeber, E.J., et al. (2011). A New Anti-Depressive Strategy for the Elderly: Ablation of FKBP5/FKBP51. PLOS ONE *6*, e24840.

Paakinaho, V., Makkonen, H., Jääskeläinen, T., and Palvimo, J.J. (2010). Glucocorticoid Receptor Activates Poised *FKBP51* Locus through Long-Distance Interactions. Mol. Endocrinol. *24*, 511–525.

Pace, T.W., Hu, F., and Miller, A.H. (2007). Cytokine-effects on glucocorticoid receptor function: relevance to glucocorticoid resistance and the pathophysiology and treatment of major depression. Brain. Behav. Immun. *21*, 9–19.

Pariante, C.M., and Lightman, S.L. (2008). The HPA axis in major depression: classical theories and new developments. Trends Neurosci. *31*, 464–468.

Paz, I., Sachse, M., Dupont, N., Mounier, J., Cederfur, C., Enninga, J., Leffler, H., Poirier, F., Prevost, M.-C., Lafont, F., et al. (2010). Galectin-3, a marker for vacuole lysis by invasive pathogens. Cell. Microbiol. *12*, 530–544.

Pei, H., Li, L., Fridley, B.L., Jenkins, G.D., Kalari, K.R., Lingle, W., Petersen, G., Lou, Z., and Wang, L. (2009). FKBP51 Affects Cancer Cell Response to Chemotherapy by Negatively Regulating Akt. Cancer Cell *16*, 259–266.

Pereira, M.J., Palming, J., Svensson, M.K., Rizell, M., Dalenbäck, J., Hammar, M., Fall, T., Sidibeh, C.O., Svensson, P.-A., and Eriksson, J.W. (2014). FKBP5 expression in human

adipose tissue increases following dexamethasone exposure and is associated with insulin resistance. Metabolism. *63*, 1198–1208.

Periyasamy, S., Hinds Jr, T., Shemshedini, L., Shou, W., and Sanchez, E.R. (2010). FKBP51 and Cyp40 are positive regulators of androgen-dependent prostate cancer cell growth and the targets of FK506 and cyclosporin A. Oncogene *29*, 1691–1701.

Pitman, R.K., and Delahanty, D.L. (2005). Conceptually Driven Pharmacologic Approaches to Acute Trauma. CNS Spectr. *10*, 99–106.

Ratman, D., Vanden Berghe, W., Dejager, L., Libert, C., Tavernier, J., Beck, I.M., and De Bosscher, K. (2013). How glucocorticoid receptors modulate the activity of other transcription factors: A scope beyond tethering. Mol. Cell. Endocrinol. *380*, 41–54.

Reul, J.M., and de Kloet, E.R. (1985). Two receptor systems for corticosterone in rat brain: microdistribution and differential occupation. Endocrinology *117*, 2505–2511.

Romano, M.F., Avellino, R., Petrella, A., Bisogni, R., Romano, S., and Venuta, S. (2004). Rapamycin inhibits doxorubicin-induced NF-kappaB/Rel nuclear activity and enhances the apoptosis of melanoma cells. Eur. J. Cancer Oxf. Engl. 1990 *40*, 2829–2836.

Romano, S., Sorrentino, A., L. Di Pace, A., Nappo, G., Mercogliano, C., and F. Romano, M. (2011). The Emerging Role of Large Immunophilin FK506 Binding Protein 51 in Cancer. Curr. Med. Chem. *18*, 5424–5429.

Romano, S., Xiao, Y., Nakaya, M., D'Angelillo, A., Chang, M., Jin, J., Hausch, F., Masullo, M., Feng, X., Romano, M.F., et al. (2015a). FKBP51 employs both scaffold and isomerase functions to promote NF-κB activation in melanoma. Nucleic Acids Res. *43*, 6983–6993.

Romano, S., D'Angelillo, A., Staibano, S., Simeone, E., D'Arrigo, P., Ascierto, P.A., Scalvenzi, M., Mascolo, M., Ilardi, G., Merolla, F., et al. (2015b). Immunomodulatory pathways regulate expression of a spliced FKBP51 isoform in lymphocytes of melanoma patients. Pigment Cell Melanoma Res. *28*, 442–452.

Rosmond, R. (2003). Stress induced disturbances of the HPA axis: a pathway to Type 2 diabetes? Med. Sci. Monit. Int. Med. J. Exp. Clin. Res. *9*, RA35-39.

Rothbaum, B.O., and Davis, M. (2003). Applying learning principles to the treatment of post-trauma reactions. Ann. N. Y. Acad. Sci. *1008*, 112–121.

Russell, G.M., Henley, D.E., Leendertz, J., Douthwaite, J.A., Wood, S.A., Stevens, A., Woltersdorf, W.W., Peeters, B.W.M.M., Ruigt, G.S.F., White, A., et al. (2010). Rapid Glucocorticoid Receptor-Mediated Inhibition of Hypothalamic–Pituitary–Adrenal Ultradian Activity in Healthy Males. J. Neurosci. *30*, 6106–6115.

Russell, L.C., Whitt, S.R., Chen, M.-S., and Chinkers, M. (1999). Identification of Conserved Residues Required for the Binding of a Tetratricopeptide Repeat Domain to Heat Shock Protein 90. J. Biol. Chem. *274*, 20060–20063.

Sabatini, D.M. (2006). mTOR and cancer: insights into a complex relationship. Nat. Rev. Cancer *6*, 729–734.

Sanchez, E.R. (2012). Chaperoning steroidal physiology: Lessons from mouse genetic models of Hsp90 and its cochaperones. Biochim. Biophys. Acta BBA - Mol. Cell Res. *1823*, 722–729.

SantaCruz, K., Lewis, J., Spires, T., Paulson, J., Kotilinek, L., Ingelsson, M., Guimaraes, A., DeTure, M., Ramsden, M., McGowan, E., et al. (2005). Tau Suppression in a Neurodegenerative Mouse Model Improves Memory Function. Science *309*, 476–481.

Scharf, S.H., Liebl, C., Binder, E.B., Schmidt, M.V., and Müller, M.B. (2011). Expression and regulation of the Fkbp5 gene in the adult mouse brain. PloS One *6*, e16883.

Schiene, C., and Fischer, G. (2000). Enzymes that catalyse the restructuring of proteins. Curr. Opin. Struct. Biol. *10*, 40–45.

Schmidt, M.V., Paez-Pereda, M., Holsboer, F., and Hausch, F. (2012). The Prospect of FKBP51 as a Drug Target. ChemMedChem *7*, 1351–1359.

Schreiber, S.L. (1991). Chemistry and biology of the immunophilins and their immunosuppressive ligands. Science *251*, 283–287.

Shea, A., Walsh, C., MacMillan, H., and Steiner, M. (2005). Child maltreatment and HPA axis dysregulation: relationship to major depressive disorder and post traumatic stress disorder in females. Psychoneuroendocrinology *30*, 162–178.

Sinars, C.R., Cheung-Flynn, J., Rimerman, R.A., Scammell, J.G., Smith, D.F., and Clardy, J. (2003). Structure of the large FK506-binding protein FKBP51, an Hsp90-binding protein and a component of steroid receptor complexes. Proc. Natl. Acad. Sci. *100*, 868–873.

Sinclair, D., Fillman, S.G., Webster, M.J., and Weickert, C.S. (2013). Dysregulation of glucocorticoid receptor co-factors FKBP5, BAG1 and PTGES3 in prefrontal cortex in psychotic illness. Sci. Rep. *3*.

Somarelli, J.A., S.Y., L., J., S., and R. J., H. (2008). Structure-based classification of 45 FK506-binding proteins. Proteins *72*, 197–208.

Spencer, R.L., Miller, A.H., Moday, H., Stein, M., and McEwen, B.S. (1993). Diurnal differences in basal and acute stress levels of type I and type II adrenal steroid receptor activation in neural and immune tissues. Endocrinology *133*, 1941–1950.

Stechschulte, L.A., Qiu, B., Warrier, M., Hinds, T.D., Zhang, M., Gu, H., Xu, Y., Khuder, S.S., Russo, L., Najjar, S.M., et al. (2016). FKBP51 Null Mice Are Resistant to Diet-Induced Obesity and the PPARγ Agonist Rosiglitazone. Endocrinology *157*, 3888–3900.

Steptoe, A., Hamer, M., and Chida, Y. (2007). The effects of acute psychological stress on circulating inflammatory factors in humans: A review and meta-analysis. Brain. Behav. Immun. *21*, 901–912.

Sun, T., Du, S.-Y., Armenia, J., Qu, F., Fan, J., Wang, X., Fei, T., Komura, K., Liu, S.X., Lee, G.-S.M., et al. (2018). Expression of lncRNA MIR222HG co-transcribed from the miR-221/222 gene promoter facilitates the development of castration-resistant prostate cancer. Oncogenesis *7*, 30.

Taipale, M., Tucker, G., Peng, J., Krykbaeva, I., Lin, Z.-Y., Larsen, B., Choi, H., Berger, B., Gingras, A.-C., and Lindquist, S. (2014). A Quantitative Chaperone Interaction Network Reveals the Architecture of Cellular Protein Homeostasis Pathways. Cell *158*, 434–448.

Takahashi, A., Flanigan, M.E., McEwen, B.S., and Russo, S.J. (2018). Aggression, Social Stress, and the Immune System in Humans and Animal Models. Front. Behav. Neurosci. *12*.

Takaoka, M., Ito, S., Miki, Y., and Nakanishi, A. (2017). FKBP51 regulates cell motility and invasion via RhoA signaling. Cancer Sci. *108*, 380–389.

Tatro, E.T., Everall, I.P., Masliah, E., Hult, B.J., Lucero, G., Chana, G., Soontornniyomkij, V., Achim, C.L., and HNRC (2009). Differential Expression of Immunophilins FKBP51 and FKBP52 in the Frontal Cortex of HIV-Infected Patients with Major Depressive Disorder. J. Neuroimmune Pharmacol. *4*, 218–226.

Thurston, T.L.M., Wandel, M.P., von Muhlinen, N., Foeglein, A., and Randow, F. (2012). Galectin 8 targets damaged vesicles for autophagy to defend cells against bacterial invasion. Nature *482*, 414–418.

Touma, C., Gassen, N.C., Herrmann, L., Cheung-Flynn, J., Büll, D.R., Ionescu, I.A., Heinzmann, J.-M., Knapman, A., Siebertz, A., Depping, A.-M., et al. (2011). FK506 Binding Protein 5 Shapes Stress Responsiveness: Modulation of Neuroendocrine Reactivity and Coping Behavior. Biol. Psychiatry *70*, 928–936.

Toyama, B.H., Savas, J.N., Park, S.K., Harris, M.S., Ingolia, N.T., Yates, J.R., and Hetzer, M.W. (2013). Identification of long-lived proteins reveals exceptional stability of essential cellular structures. Cell *154*, 971–982.

Trandinh, C.C., Pao, G.M., and Saier, M.H. (1992). Structural and evolutionary relationships among the immunophilins: two ubiquitous families of peptidyl-prolyl cis-trans isomerases. FASEB J. Off. Publ. Fed. Am. Soc. Exp. Biol. *6*, 3410–3420.

Van Bogaert, T., De Bosscher, K., and Libert, C. (2010). Crosstalk between TNF and glucocorticoid receptor signaling pathways. Cytokine Growth Factor Rev. *21*, 275–286.

Volk, N., Pape, J.C., Engel, M., Zannas, A.S., Cattane, N., Cattaneo, A., Binder, E.B., and Chen, A. (2016). Amygdalar MicroRNA-15a Is Essential for Coping with Chronic Stress. Cell Rep. *17*, 1882–1891.

Wager, T.T., Chandrasekaran, R.Y., Hou, X., Troutman, M.D., Verhoest, P.R., Villalobos, A., and Will, Y. (2010). Defining Desirable Central Nervous System Drug Space through the Alignment of Molecular Properties, in Vitro ADME, and Safety Attributes. ACS Chem. Neurosci. *1*, 420–434.

Watts, A.G. (2005). Glucocorticoid regulation of peptide genes in neuroendocrine CRH neurons: A complexity beyond negative feedback. Front. Neuroendocrinol. *26*, 109–130.

Willour, V., Chen, H., Toolan, J., Belmonte, P., Cutler, D., Goes, F., Zandi, P., Lee, R., MacKinnon, D., Mondimore, F., et al. (2009). Family-based association of FKBP5 in bipolar disorder. Mol. Psychiatry *14*, 261–268.

Wochnik, G.M., Rüegg, J., Abel, G.A., Schmidt, U., Holsboer, F., and Rein, T. (2005). FK506-binding Proteins 51 and 52 Differentially Regulate Dynein Interaction and Nuclear Translocation of the Glucocorticoid Receptor in Mammalian Cells. J. Biol. Chem. *280*, 4609–4616.

Wohleb, E.S., McKim, D.B., Sheridan, J.F., and Godbout, J.P. (2015). Monocyte trafficking to the brain with stress and inflammation: a novel axis of immune-to-brain communication that influences mood and behavior. Front. Neurosci. *8*.

Yang, Q., She, H., Gearing, M., Colla, E., Lee, M., Shacka, J.J., and Mao, Z. (2009). Regulation of neuronal survival factor MEF2D by chaperone-mediated autophagy. Science *323*, 124–127.

Yehuda, R., Cai, G., Golier, J.A., Sarapas, C., Galea, S., Ising, M., Rein, T., Schmeidler, J., Müller-Myhsok, B., Holsboer, F., et al. (2009). Gene Expression Patterns Associated with Posttraumatic Stress Disorder Following Exposure to the World Trade Center Attacks. Biol. Psychiatry *66*, 708–711.

Young, K.A., Thompson, P.M., Cruz, D.A., Williamson, D.E., and Selemon, L.D. (2015). BA11 FKBP5 expression levels correlate with dendritic spine density in postmortem PTSD and controls. Neurobiol. Stress *2*, 67–72.

Zannas, A.S., and Binder, E.B. (2014). Gene–environment interactions at the FKBP5 locus: sensitive periods, mechanisms and pleiotropism. Genes Brain Behav. *13*, 25–37.

Zannas, A.S., Wiechmann, T., Gassen, N.C., and Binder, E.B. (2016). Gene–Stress–Epigenetic Regulation of FKBP5: Clinical and Translational Implications. Neuropsychopharmacology *41*, 261–274.

Zannas, A.S., Jia, M., Hafner, K., Baumert, J., Wiechmann, T., Pape, J.C., Arloth, J., Ködel, M., Martinelli, S., Roitman, M., et al. (2019). Epigenetic upregulation of FKBP5 by aging and stress contributes to NF-κB–driven inflammation and cardiovascular risk. Proc. Natl. Acad. Sci. 201816847.